2015-09-28

A Modeling Framework to Investigate the Impact of Climate and Land-Use/Cover Change on Hydrological Processes in the Elbow River Watershed in Southern Alberta

Farjad, Babak

UNIVERSITY OF CALGARY

A Modeling Framework to Investigate the Impact of Climate and Land-Use/Cover Change on Hydrological Processes in the Elbow River Watershed in Southern Alberta

by

Babak Farjad

A THESIS

SUBMITTED TO THE FACULTY OF GRADUATE STUDIES

IN PARTIAL FULFILMENT OF THE REQUIREMENTS FOR THE

DEGREE OF DOCTOR OF PHILOSOPHY

GRADUATE PROGRAM IN GEOMATICS ENGINEERING

CALGARY, ALBERTA

SEPTEMBER, 2015

Abstract

Complex dynamical and physical interactions exist between climate, land use/cover (LULC), and hydrology. In fact, each of these systems is considered complex because they possess the following characteristics. They consist of a large number of components that interact in a non-linear way. They interchange information with their surroundings and constantly modify their self-organized structure. They are far-from-equilibrium and display instability, sensitivity to initial conditions, sudden changes, and a behavior that cannot be captured by simple models. Understanding how hydrological processes respond to climate and LULC change requires knowledge about how these complex systems interact in the present and how they might in the future. The objective of this research is to understand the responses of hydrological processes to climate and LULC change in the Elbow River watershed using an integrated modeling framework that can address the complexity of these interrelated systems. To achieve this goal, the physically-based, distributed MIKE SHE/MIKE 11 model was coupled with a LULC cellular automata to simulate hydrological processes up to the year 2070 under five GCM-scenarios (NCARPCM-A1B, CGCM2-B2(3), HadCM3-A2(a), CCSRNIES-A1FI, and HadCM3-B2(b)). Results reveal that most scenarios generate an increase in overland flow, baseflow, and evapotranspiration in the winter/spring, and a decrease in the summer/fall. The highest increase in streamflow occurs in mid-late spring due to an increase in snowmelt and rain-on-snow events that may enhance the risk of flooding. In addition, LULC change substantially modifies the river regime in the east sub-catchment, where urbanization occurs. The separated impacts of climate and LULC change on streamflow are positively correlated in winter and spring, which intensifies their

influence and leads to a rise in streamflow, which in turn increases the vulnerability of the watershed to floods, particularly in spring. Flow duration curves indicate that LULC change has a greater contribution to peak flows than climate change in both the 2020s and 2050s. The integrated modeling framework used in this research is a powerful analytical tool that can help scientists and decision makers for the planning of sustainable water resources and infrastructure management.

Acknowledgements

I would like to express my deepest gratitude to Dr. Danielle Marceau for her trust, patient guidance and encouragement. I would not have accomplished this without her support. Also, I'm very thankful to other members of my advisory committee, Dr. Shawn Marshall and Dr. Anil Gupta for their invaluable advices, assistance, and intellectual feedback. I am also very grateful for my Colleagues at the Geocoumputing lab: Majeed, Fang, Nishad, Omar, Faezeh, Mahsa, Mohammad, Ken, Habib, Christina, and David for their intellectual support during my studies.

I would like to thank my great uncles; Rahim and David, also my great friends; Giampiero, Sara, and Aryanna for being there for me through hard times.

I am grateful to the University of Calgary, Alberta Innovates Technology Futures, Alberta Environment and Sustainable Resource Development (AESRD), and Tecterra for their support to complete this thesis.

To Canada and its wonderful people who made my PhD studies a joyful experience.

Many thanks to my family, my brother and sisters: I could not ask for a better family.

And finally I have been blessed with the greatest parents in the world: Touba and Mahmoud; their unconditional love and endless support made this possible.

Dedication

To my mother

Table of Contents

List of Tables

List of Figures and Illustrations

List of Abbreviations

Symbol	Definition
AESRD	Alberta Environment and Sustainable Resource Development
BF	Baseflow
CA	Cellular Automata
CC	Correlation Coefficient
DHI	Danish Hydraulic institute
ET	Evapotranspiration
FDC	Flow duration curves
GCM	General Circulation Model
INF	Infiltration
LAI	Leaf Area Index
LULC	Land use/cover
OL	Overland flow
PET	Potential evapotranspiration
Q	Discharge
RE	Recharge
RD	Root Depth
SRES	Special Report on Emissions Scenarios
SZ	Saturated Zone
UZ	Unsaturated Zone
WPP	Western Prairie Provinces

Chapter 1 : Introduction

There is a global growing imbalance between water supply and demand. Water resources are expected to decrease due to climate change and human activities in this century while water demand is expected to rise by 35–60% and possibly double by 2025 and 2050, respectively (Garnier et al., 2015). This clearly underlines the need for knowledge about the future impacts of drivers that are responsible for creating pressure on water supply. Climate and land-use/cover (LULC) change are the two main factors that might negatively impact water resources (Wagner et al., 2013; Garnier et al., 2015). A realistic projection of climate and LULC change impacts on water resources depends on the ability to adequately capture the complex interaction between climate, LULC, and hydrology.

1.1 Impact of climate change on hydrology

The hydrological cycle is linked with the Earth's radiation balance. Changes in radiation balance due to increasing amounts of greenhouse gases tend to increase atmospheric and oceanic temperatures. An increase in temperature can result in a change in the air humidity and facilitate the evaporation process with water-holding capacity that is crucially important to hydrological processes. In addition, a rise in temperature increases rain in proportion to snow in areas where precipitation is a combination of snow and rain in the winter season. The melting of snow and ice and the rising of global sea levels are also caused by the increased temperature. Changes in precipitation patterns can cause a

change in runoff and consequently influence soil moisture and infiltration. An increase in precipitation augments the amount of water stored in the soil, which influences groundwater recharge, actual evapotranspiration, and surface runoff. Spatial and temporal changes in precipitation likely result in variation in the timing and duration of the recharge season(s), and also in the amount of water that ends up in aquifers. Changes in flood frequency are very much influenced by the timing and duration of the precipitation events, and changes in drought frequency might occur as a result of lack of precipitation.

These relationships between climate and hydrology have begun to be studied in the early 1940s (Noora, 2012) and were greatly limited by the available computer technology. In the 1980s, with drastic advances in the knowledge of climate scenarios and hydrological models, a major step was taken in the study of climate systems and their interaction with hydrology; however there was still a considerable uncertainty in calculations due to unreliable scenarios and low model resolution (Noora, 2012). In the 1990s, as many comprehensive and complex climate and hydrological models were developed and as computers became more powerful, studies began to probe into different aspects of climate and hydrology.

Several studies have been conducted to understand climate change influence on hydrology (Kienzle et al., 2012; Barron et al., 2012) focusing on aspects such as responses of streamflow and sub-surface hydrology to climate change, and extreme events frequency related to climate change. For example, Saha (2015) investigated climate change effects on hydrology of the Peace Region of British Columbia, Canada

using the Gridded Surface Subsurface Hydrologic Analysis (GSSHA) modeling system under A2 and B1 climate scenarios for the period of 2020 to 2040 compared to 2000–2011. They indicated that the mean annual stream flow increases by 15.5% and 12.1% under the A2 and B1 scenarios respectively from 2020 to 2040. They also found that stream flow increases in all seasons under both scenarios. Viola et al., 2015 evaluated the hydrology of the Upper Grande River Basin, in Southeast Brazil under HadCM3 A1B climate scenario using the LASH (Lavras Simulation of Hydrology) hydrological model for the period of 2011-2099. They found a slight decrease and strong increase in the annual surface flow for the period of 2011-2040 and 2041-2099, respectively. They also found an increase in summer (the rainy season of the region) surface flow, which can alter the flood river regimes of the region.

Chang and Jung (2010) assessed the effects of climate change on annual, seasonal, and high and low runoff in the 218 sub-basins of the Willamette River basin of Oregon. The study showed that snowmelt-dominated basins exhibit large reductions in summer flow in response to increased temperature, while rainfall-dominated basins show large increases in winter flow in response to precipitation change. Campbell et al. (2011) found that 7% increase in precipitation and 3% increase in evapotranspiration (based on PCM-B1 climate change scenario) cause 10% increase in streamflow for the period 2055-2099.

Studies have focused on climate change effects on extreme events such as floods and droughts. For example, Yulianti and Burn (1998) investigated the influence of air temperature on low flow frequency due to climate change in the Prairies region of

Canada. They found that the frequency of low flow events increased due to a considerable rise in temperature over the past century, and that there was a relationship between an increase in regional air temperature and low flow in the Prairies.

Most previous studies have focused mainly on surface hydrological processes, and little attention has been paid to climate change impacts on sub-surface processes. Any change in climate can influence directly the initial sub-surface layers such as soil water, and/or indirectly the deeper zones such as saturated zone; however, feedbacks between soil water and unsaturated zones with climate change occur over short periods of time compared to saturated zones, which might take decades (Green et al., 2011). Goderniaux et al. (2009) estimated the potential climate impacts on groundwater in the Geer basin in eastern Belgium. They applied a physically-based, surface-subsurface flow model combined with six climate change scenarios. They found that groundwater level is expected to decrease by up to 8 m by 2080.

1.2 Impact of LULC change on hydrology

In addition to climate, LULC change can also considerably influence hydrological processes. LULC change alters water balance, causing modifications in infiltration, evapotranspiration, and interception. LULC change results from anthropogenic activities such as urbanization, agriculture, deforestation, and afforestation. These activities modify the physical properties of the surface, such as vegetation and soil, which in turn alter the hydrological regime. Modifications in LULC can lead to changes in surface and groundwater balance, and might even influence high and low flow frequency and

magnitude (Arnell, 1994). For instance, the conversion of natural vegetation into agricultural land decreases evapotranspiration, and hence increases water storage (Gordon et al., 2003) while the conversion of soil and natural vegetation into impervious surfaces decreases infiltration, evapotranspiration, and groundwater recharge, and increases the rate of surface runoff (Arnold and Gibbons, 1996). Arnold and Gibbons (1996) reported that the conversion of forest into 10–20%, 35–50%, and 75–100% impervious surfaces increases runoff two times, three times, and five times, respectively. Consequently, urbanization affects many of the processes that control streamflow by replacing vegetation and soil with impervious surfaces. Rose and Peters (2001) identified five major impacts of urbanization on hydrology: (1) a higher proportion of precipitation converts to surface runoff with the increase of impervious surfaces, (2) the catchment response to precipitation is accelerated and the lag time between precipitation and runoff is decreased, (3) peak flow magnitudes are increased, (4) low flow is decreased due to reduced contributions from groundwater storage, and (5) water quality is degraded by effluent discharges.

Numerous studies have indicated the relationships between LULC properties and runoff, water yield, and infiltration. They revealed a large effect of vegetation (especially caused by deforestation) on runoff, with an inverse relation between forest and runoff demonstrated in many forested landscapes (Wang et al., 2008). Vegetation helps attenuating the impact of raindrops, thereby reducing the water to be left on the land surface for surface runoff while soil pores made by root systems permit the infiltration of water. Bosch and Hewlett (1982) concluded that changing annual and perennial

herbaceous vegetated land by establishing forest cover decreased water yield. In this order, coniferous hardwood, brush, and grass cover have the highest consumptive use of water, with the implication that conversions from these respective cover types to annual crops will increase water yield accordingly. Bruijnzeel (1990) indicated that vegetation type, plant maturation stage, and management affect the change in water yield.

Calder (1998) reported that vegetation after clear-cutting, depending on the species, may consume more water than very old forests. Loss of water through interception is higher from forests than from shorter crops. Therefore, forest decreases runoff as compared to shorter vegetation (Bosch and Hewlett, 1982). Transpiration from forests is also greater due to greater access to soil water from increased rooting depth. Other studies indicate that deforestation increases runoff (Benito et al., 2003; Gentry and Lopez-Parodi, 1980; Coe et al., 2011), water yield (Bosch and Hewlett, 1982), and flood peaks (Hornbeck et al., 1970; Harr et al., 1975; Harr, 1981, 1986).

Peak flow is highly related to the infiltration capacity of soil and soil water storage. Verry et al. (1983) and Bruijnzeel (1990) found that peak flows can increase after cutting trees. Also, Brooks et al. (1989) and Bruijnzeel (1990) report that when the magnitude of storm precipitation becomes very large, the impact that soil can have on stormflow peaks is reduced. In large watersheds, the effects of LULC changes on peak flows could not be seen at the watershed outlet due to the time lag between different tributaries and variations in rainfall (Bruijnzeel, 1990); however, overall stormflow increase due to LULC changes can be considerable in individual sub-watersheds (Brooks et al., 2003).

According to Calder (1998) increasing transpiration in dry periods increases soil moisture deficits and reduces dry season flows. It is widely reported that a rise in high streamflow, decrease in low streamflow, and an increased variability in streamflow are usually associated with an increase of urban lands because the increased impervious surface caused by urbanization decreases infiltration of precipitation and increases runoff (White and Greer, 2006; Tu, 2009; He and Hogue, 2012).

1.3 Impact of climate and LULC change on hydrology

Few studies in the literature have focused on both the climate and LULC impacts on hydrology. Tu (2009) investigated the impact of climate and LULC change on streamflow in watersheds of eastern Massachusetts, USA. The ArcView Generalized Watershed Loading Function (AVGWLF) hydrological model was integrated with a simple regression-based LULC model along with GCM-scenarios to predict streamflow up to 2024. The author found that streamflow increases in late fall and winter, while it decreases in summer. Wang et al. (2014) assessed the combined effects of climate and LULC change on streamflow in the Wolf Bay watershed in southern Alabama. They employed the SWAT model integrated with a LULC change model (that incorporates GIS, artificial neural network, and an agent-based model) along with GCM-scenarios. They found that monthly average streamflow and surface flow increase in spring, winter, and fall due to climate change whereas LULC change does not have a considerable effect on monthly average streamflow, however, it causes an increase in surface flow and a decrease in lower baseflow.

These studies are among the first in which an integrated modeling framework is used to capture the three-way interaction between climate, LULC, and hydrology. Climate, LULC, and hydrological processes are explicitly interconnected with complex interactions occurring between them (Wang et al., 2012). Uncertainty can arise if an integrated modeling framework is naively applied without consideration of the level of system complexity. This inherent complexity ranges from low to high according to a system characteristic. For example, a rain-dominant watershed with gentle topographic, geology, and LULC variations is less complex than a hybrid (snow-rain) watershed with heterogeneous LULC, geology, and topography. The main challenge therefore is to design an integrated modeling framework able to deal with the complexity of the systems being investigated. However, yet there is no clearly established classification of model structure and capability to study the interaction between climate, LULC, and hydrology.

1.3.1 Integrated modeling framework

In this section, the requirements of models to adequately deal with the complexity of climate, LULC and hydrology within an integrated framework are described.

1.3.1.1 Hydrology models

Numerous hydrological models exist to simulate and characterize watershed hydrology, with different levels of complexity that reflects the level of details of the hydrological system that is captured by the model. For example, a groundwater system can be modeled with low complexity as one reservoir, with uniform characteristics, or it can be modeled with high complexity as several aquifers, each having different hydraulic conductivities and resistances.

In Figure 1.1, hydrological models are classified based on the level of complexity in a three-dimensional framework. The system process and spatial distribution dimensions identity the degree of being physically (dimension Z) and spatially distributed (dimension X) based models, respectively, while the dynamic simulation dimension identifies the simulation time interval (dimension Y). These dimensions are described as follows.

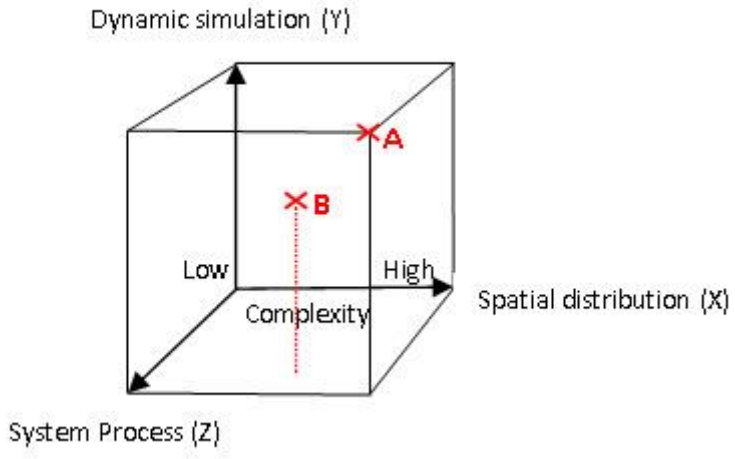

Figure 1.1 A three-dimensional framework representing hydrological modeling complexity. A and B show two levels of complexity that could be captured by two different hydrological models

(i) System process: hydrological models with a high level of complexity in system process are mainly based on physical principles and provide a more detailed description of the processes that occur in a watershed. They use a set of mathematical equations to solve physical processes (physically-based models). Models with a moderate level of complexity in component-based process provide a simplified description of the system (conceptual models). Models with a low level of complexity include few component-based processes and are based on the system inputs and outputs relationship (data-driven models) (Table 1.1).

Table 1.1 Three levels of system process complexity in hydrological models

ID	Level of complexity	Description
H(SPL)	Low level	Data-driven model
H(SPM)	Moderate level	Conceptual model
H(SPH)	High level	Physically-based model

H(SPL) (Hydrology- system process complexity, low level)
H(SPM) (Hydrology- system process complexity, moderate level)
H(SPH) (Hydrology- system process complexity, high level)

(ii) Spatial distribution: models with a high level of spatial complexity consider the catchment as finite geo-referenced computational units with different responses to forcing inputs (fully distributed models). Models with a moderate level of spatial complexity consider the conceptual functional relationships for homogeneous sub-catchment (semi-distributed models). Hydrological models with a low level of spatial complexity consider the watershed as one computational unit, with state variables that represent average values of watershed characteristics such as the total rainfall, soil characteristics, and overland flow conditions (lumped models) (Table 1.2).

Table 1.2 Three levels of spatial complexity in hydrological models text

ID	Level of complexity	Description
H(SL)	Low level	Lumped model
H(SM)	Moderate level	Semi-distributed model
H(SH)	High level	Distributed model

H(SL) (Hydrology-spatial complexity, low level)
H(SM) (Hydrology-spatial complexity, moderate level)
H(SH) (Hydrology-spatial complexity, high level)

(iii) Dynamic simulation: hydrological models with a high level of dynamic simulation complexity are those that can employ both a short- and longer-time step along with either a detailed or coarse drainage network schematization of the watershed (continuous

models and single-event models). Models with a moderate level for dynamic simulation complexity are the ones that include a coarse schematization of the watershed (continuous models). Models with a low level of dynamic simulation complexity include a short-time step along with a detailed watershed schematization and drainage network (single-event models) (Table 1.3).

Table 1.3 Three levels of dynamic simulation complexity in hydrological models

ID	Level of complexity	Description
H(DL)	Low level	Single-event model
H(DM)	Moderate level	Continuous model
H(DH)	High level	Continuous and single-event models

H(DL) (Hydrology-dynamic simulation complexity, low level)
H(DM) (Hydrology-dynamic simulation complexity, moderate level)
H(DH) (Hydrology-dynamic simulation complexity, high level)

In order to model a complex hydrological system at the "A" level (Fig. 1.1), a fully physically-based hydrological distributed model is needed to simulate hydrological processes at different time steps. MIKE SHE/MIKE 11, a distributed physically-based model, is a good example of a "A" level complexity model while a suitable "B" level of complexity is given by a hydrological model like SWAT, which is a semi-distributed model that simulates hydrological processes in a coarse schematization of the watershed in a continuous way.

1.3.1.2 LULC models

A LULC model can help understand and interpret the complexity and the interactions between the bio-physical and human systems, both of which being at the basis of land

dynamics. LULC models have also different levels of complexity with respect to spatial, temporal scales, and interactions between system components. These dimensions are selected to indicate the complexity of LULC models (Fig. 1.2).

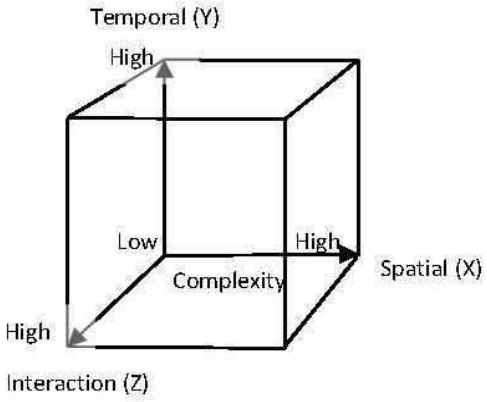

Figure 1.2 A three-dimensional framework representing LULC modeling complexity

(i) Spatial complexity: LULC models with a low spatial complexity have a low ability to deal with data spatially. Models with a moderate level of complexity are fully spatially based models, and models with a high level of complexity are spatially interactive in several dimensions (Table 1.4).

Table 1.4 Three levels of spatial complexity in LULC models

ID	Level of complexity
L(SL)	Low level
L(SM)	Moderate level
L(SH)	High level

L(SL) (Land use-spatial complexity, low level)
L(SM) (Land use- spatial complexity, moderate level)
L(SH) (Land use- spatial complexity, high level)

(ii) Temporal complexity: LULC models with a low temporal complexity have few time steps and time phases. Models with a moderate complexity have many time steps, and

longer time phases while high level complexity models have the capacity to deal with a large number of time steps and time lags in long time phases (Table 1.5).

Table 1.5 Three levels of temporal complexity in LULC models

ID	Level of complexity
L(TL)	Low level
L(TM)	Moderate level
L(TH)	High level

L(TL) (Land use-temporal scale complexity, low level)
L(TM) (Land use- temporal scale complexity, moderate level)
L(TH) (Land use- temporal scale complexity, high level)

(iii) Interaction complexity of LULC models: LULC models with a low complexity are not rule-based, but only consider a rate of trend in historical LULC changes over a certain period of time to project future LULC changes. Models with a moderate level of interaction complexity are rule-based and consider both external (e.g., socio-economical) and internal (e.g., distance from river, city center) driving factors. However, they do not consider the interaction between LULC classes. LULC models with a high interaction complexity are rule-based, and not only consider both internal and external driving factors among LULC classes, but also the interaction between LULC classes (Table 1.6).

Table 1.6 Three levels of interaction complexity in LULC models

ID	Level of complexity
L(IL)	Low level
L(IM)	Moderate level
L(IH)	High level

L(IL) (Land use-temporal interaction complexity, low level)
L(IM) (Land use- temporal interaction complexity, moderate level)
L(IH) (Land use- temporal interaction complexity, high level)

1.3.1.3 Climate models

Inherent uncertainty in future climate decreases the confidence in climate models projection. Therefore, climate models are run against future emissions scenarios to project climate variables such as temperature, precipitation, and cloudiness. The major sources of uncertainty in projections of climate variables are related to the different ways in which climate models represent physical processes and feedbacks in the climate system along with uncertainty in future scenarios of greenhouse gas emissions, which affects the radiative forcing (Carter et al., 2003). Three dimensions are considered to assign different levels of complexity to climate change models (Figure 1.3).

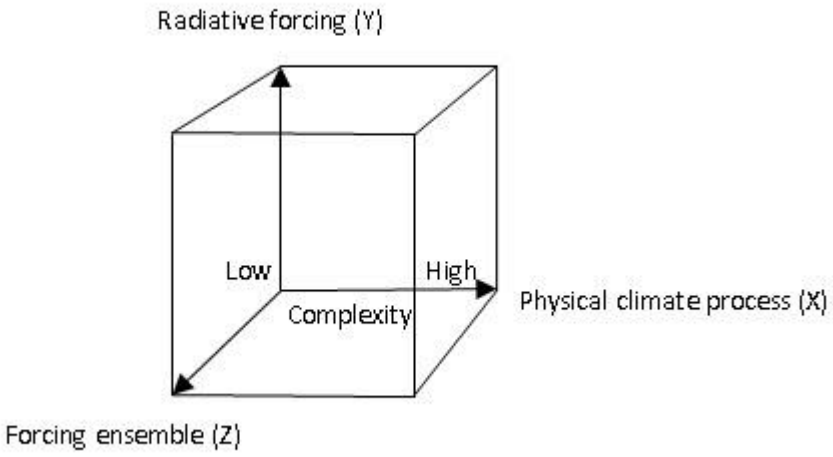

Figure 1.3 A three-dimensional framework representing climate modeling complexity

(i) Physical climate process: climate models range from the simple zero-dimensional or one-box model (discussed by Lashof 1989) to 3D general circulation models (GCMs), which represent low and high complexity, respectively (Table 1.7).

Table 1.7 Two levels of physical climate process complexity in climate models

ID	Level of complexity
C(PL)	Low level
C(PH)	High level

C(PL) (Climate- climate model complexity, Low level)
C(PH) (Climate- climate model complexity, High level)

(ii) Radiative forcing: A change in the radiative energy budget, which can lead to a change in climate parameters and consequently result in a new equilibrium state of the climate system can be represented in a range varying from synthetic (referred to incremental changes in climatic variables) to IPCC SRES (Special Report on Emissions Scenarios) emission scenarios; that represents low and high complexity, respectively (Table 1.8).

Table 1.8 Two levels of radiative forcing complexity in climate models

ID	Level of complexity
C(RL)	Low level
C(RH)	High level

C(RL) (Climate- climate scenario complexity, Low level)
C(RH) (Climate- climate scenario complexity, High level)

(iii) Forcing ensemble: a climate model is subjected to different forcings to generate the possible future states of the system. This can range from a single GCM-scenario to a combination of as many GCM and greenhouse gas emission scenarios as possible to better cover the uncertainty associated with climate projections; they represent low and high forcing ensemble complexity, respectively (Table 1.9).

Table 1.9 Two levels of forcing ensemble complexity in climate models

ID	Level of complexity
C(FL)	Low level
C(FH)	High level

C(FL) (Climate- forcing ensemble complexity, Low level)
C(FH) (Climate- forcing ensemble complexity, High level)

1.3.1.4 3-dimensional modeling framework

Figure 1.4 shows a 3-D modeling framework that indicates the degree of ability of a model to deal with the corresponding degree of complexity of the system it represents. It can be used either to integrate two components or all three components. It is assumed that the higher the level of complexity of the model in the framework, the better is its ability to address the complexity of the system. The framework is divided in different levels with a particular degree of complexity. The levels are identified using capital letters from A to I, which reflects the levels of complexity defined in Table 1.10. For example, the integrated modeling framework employed by Wang et al. (2012) and Tu (2009) belong to B-G-E and C-G-D levels, respectively, in Table 1.10 and Figure 1.4. The detailed characteristics of the integrated modeling framework used in these studies are described in Table 1.11.

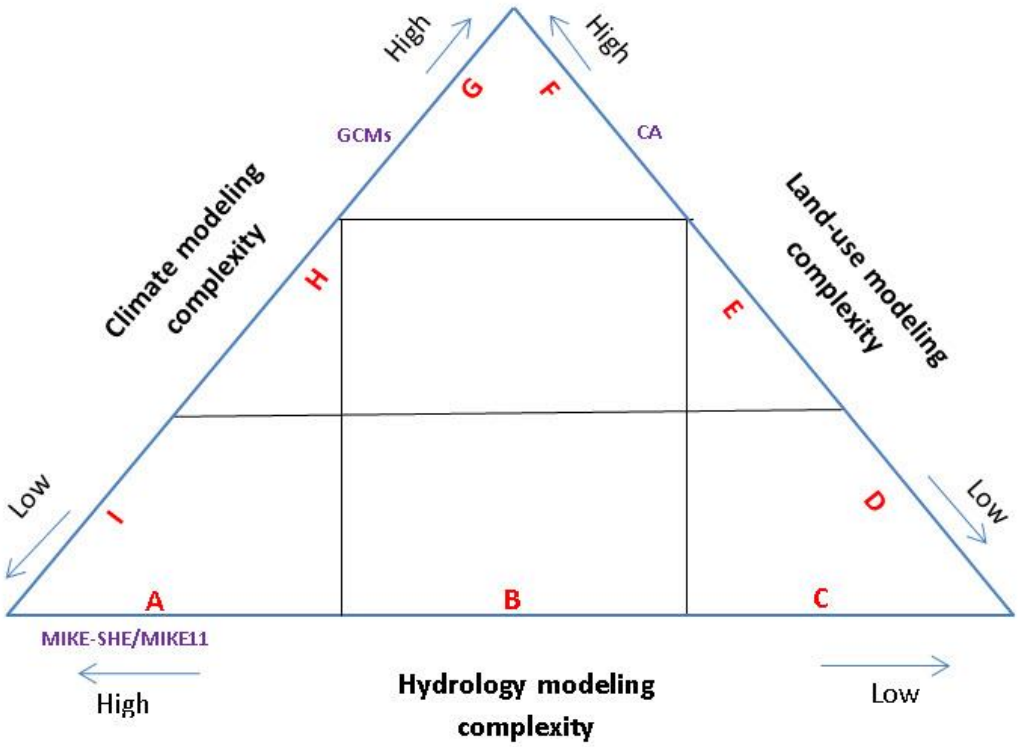

Figure 1.4 Levels of complexity defined on the 3-dimensional modeling framework

Table 1.10 Levels of complexity determined by different combinations of the components of the integrated modeling framework

Level	Characteristics	Level of complexity
A-G-F	[C(PH)+C(RH)+C(FH)]+[L(SH)+L(TH)+L(IH)]+ [H(SPH)+H(SL)+H(DH)]	Extremely high
B-G-F	[C(PH)+C(RH)+C(FH)]+[L(SH)+L(TH)+L(IH)]+[H(SPH)+H(SM)+H(DH)]	Very high
B-G-E	[C(PH)+C(RH)+C(FH)]+[L(SH)+L(TM)+L(IH)]+ [H(SPH)+H(SM)+H(DM)]	High
B-G-D	[C(PH)+C(RH)+C(FH)]+[L(SM)+L(TM)+L(IM)]+ [H(SPH)+H(SM)+H(DM)]	Moderately high
B-G-E	[C(PH)+C(RH)+C(FH)] +[L(SM)+L(TM)+L(IM)]+ [H(SPM)+H(SM)+H(DM)]	Moderate
C-G-D	[C(PH)+C(RH)+C(FH)]+ [L(SL)+L(TL)+L(IL)]+ [H(SPM)+H(SL)+H(DM)]	Moderately low
C-I-D	[C(PL)+C(RL)+C(FL)]+ [L(SL)+L(TL)+L(IL)]+[H(SPL)+H(SL)+H(DL)]	Low
C-I-D	[C(PL)+C(RL)+C(FL)]+ [L(SL)+L(TL)+L(IL)]+[H(SPL)+H(SL)+H(DL)]	Very low

Table 1.11 Complexity of the integrated modeling framework applied by Tu (2009) and Wang et al. (2012)

Study	Level of component complexity	Description
Tu (2009)	H(SPM)	Moderate level of complexity in component-based process provides a simplified description of the system; conceptual models (Table 1)
	H(SL)	Low level of spatial complexity; considers the watershed as one computational unit, with state variables that represent average values of watershed characteristics; Lumped model (Table 2)
	H(DM)	Moderate level in dynamic simulation complexity that includes a coarse schematization of the watershed; continuous model (Table 3)
	L(SL)	Low level in spatial LULC complexity that has a low ability to deal with data spatially (Table 4)
	L(TL)	Low level in temporal LULC complexity that has few time steps and time phases (Table 5)
	L(IL)	Low level in interaction of LULC complexity; is not rule-based, but considers a rate of trend in historical LULC changes over a certain period of time to project future LULC changes (Table 6)
	C(PH)	High level in complexity of climate model; GCM (Table 7)
	C(RH)	High level in complexity of climate change scenarios; IPCC SRES (Table 8)
	C(FH)	High level in complexity of forcing ensemble that uses a combination of several GCMs and greenhouse gas emission scenarios (Table 9)
Wang et al. (2012)	H(SPH)	High level of complexity in system process mainly based on physical principles; physically-based model (Table 1)
	H(SM)	Moderate level of spatial complexity; considers the conceptual functional relationships for homogeneous sub-catchment; semi-distributed model (Table 2)
	H(DM)	Moderate level in dynamic simulation complexity that includes a coarse schematization of the watershed; continuous model (Table 3)
	L(SH)	High level in spatial LULC complexity; is spatially interactive in several dimensions (Table 4)
	L(TM)	Moderate level in temporal complexity; has many simulation time steps (Table 5)
	L(IH)	High level in interaction of LULC complexity that considers both internal and external driving factors and the interaction between LULC classes (Table 6)
	C(PH)	High level in complexity of climate model; GCM (Table 7)
	C(RH)	High level in complexity of climate change scenarios; IPCC SRES (Table 8)
	C(FH)	High level in complexity of forcing ensemble that uses a combination of several GCMs and greenhouse gas emission scenarios (Table 9)

The integrated modeling framework applied by Tu (2009) has some limitations. First, the system process is conceptual and climate sequence dependent, which can increase the uncertainty related to the calibration of the hydrological model (H(SPM)). Second, it considers the conceptual functional relationships for homogeneous sub-catchments,

which increases the uncertainty when capturing surface and subsurface flows in heterogeneous watersheds (H(SM)). Third, the model used for simulating LULC change has limitations in dealing with data spatially (is not spatially interactive) (L(SL)) and in reproducing LULC change at different time steps (L(TL)). Finally, it is not a rule-based system and does not consider socio-economical factors. The integrated modeling framework applied by Wang et al. (2012) address these limitations, however, not at the H(SM), H(DM), and L(TM) complexity levels. The contributions of these studies can be enhanced by using a combination of models that capture a higher level of complexity for the three components in the A-G-F level (Figure 1.4). An example of an integrated modeling framework that belongs to the A-G-F level is the MIKE SHE/MIKE 11 hydrological model, a LULC CA model, and a combination of GCM-scenarios.

1.4 Objective of this research

The objective of this research is to understand the responses of hydrological processes to climate and land-use/cover (LULC) change in the Elbow River watershed using an integrated modeling framework that can address the complexity of these systems. This modeling framework consists of a LULC change cellular automata (CA) model, the distributed physically-based, MIKE SHE/MIKE 11 model, and GCM-scenarios, which are used to:

1- Investigate hydrological responses due to climate change in the 2020s and 2050s, relative to the period of 1961-1990

2- Predict LULC changes in the watershed for the period of 2020s and 2050s.

3- Investigate the combined and separate impact of climate and LULC change on hydrological processes.

The majority of studies on hydrological responses have considered either the impact of climate change-only (described in section 1.1) or LULC change-only (described in section 1.2), referring to only two sides of the 3D framework (Fig. 1.4). Furthermore, to the best of our knowledge, no studies have been conducted yet at the A-G-F level that encompasses the following components:

a) A physically-based distributed model able to simulate major hydrological processes by considering both short- and long-time steps along with a detailed dynamic land surface and sub-surface of the watershed.

b) A LULC simulation model that replicates spatial patterns and real-world dynamics with the following characteristics: i) being able to predict LULC changes at different time intervals in a spatially explicit context, ii) being able to incorporate socio-economical factors.

c) GCMs models and SRES (Special Report on Emissions Scenarios) greenhouse gas emission scenarios that represent a plausible range of future climate conditions of the watershed.

This integrated modeling framework is designed to address the limitation of previous studies, which can lead to a greater understanding of hydrology, LULC, and climate interactions especially in watersheds with complex characteristics.

1.5 Thesis overview, publications, and authorship

In the second chapter of this thesis, the importance of studying the hydrology of the Elbow River watershed and its main characteristics including meteorology, river regime, geomorphology, geology, and hydrogeology are described. The third chapter focuses on the hydrological responses to climate change in the west and east sub-catchments, and the entire watershed in the 2020s and 2050s, relative to the baseline period 1961-1990. A temperature-based ET model was used to predict potential evapotranspiration along with the physically-based, distributed MIKE SHE/MIKE 11 model to simulate hydrological processes under a range of plausible GCM-scenarios up to 2070. In Chapter 4, the separate and combined impact of climate and LULC change on the hydrology of the watershed are investigated for the period of 2020s and 2050s. Two selected GCM-scenarios (identified in Chapter 3) along with two LULC scenarios (determined with the CA model) are employed to investigate the climate and LULC effects on the hydrology of the watershed up to 2070. Chapter 5 provides an overview of the results and highlights the contributions of this research and recommendations for future studies.

This document is prepared as a manuscript-based thesis.

Chapter Two includes a portion of a book chapter (which has been adapted to suit thesis structure) that was published in 2015. The reference is: Farjad, B., Gupta, A., & Marceau, D. J. (2015). *Hydrological Regime Responses to Climate Change for the 2020s and 2050s Periods in the Elbow River Watershed in Southern Alberta, Canada*. In Environmental Management of River Basin Ecosystems (pp. 65-89). Springer International Publishing.

Chapter Three includes an article submitted in April 2015 for publication that is under review: Farjad, B., Gupta, A., & Marceau, D. J. (in review). Annual and seasonal responses of hydrological processes to scenarios of climate change in the Elbow River watershed in southern Alberta, Canada.

Chapter Four includes an article submitted for publication in July 2015 that is under review: Farjad, B., & Marceau, D. J. (in review). A modeling framework to forecast hydrological regime under scenarios of climate and land-use/cover change.

I drafted the above three manuscripts, and I am responsible for collecting data, calibrating and validating the models, running simulations, and interpreting the results. However, I have received comments and suggestions from Dr. Danielle Marceau and Dr. Anil Gupta throughout all these steps.

1.6 References

Arnell, N.W., (1994). *Hydrological impacts of climate change*. In: The Rivers Handbook, Calow, P. and G.E. Petts (eds.), Blackwell, vol. 2, pp, 173-185.

Arnold, Jr, C. L., & Gibbons, C. J. (1996). Impervious surface coverage: the emergence of a key environmental indicator. *Journal of the American planning Association*, 62(2), 243-258.

Barron, O., Silberstein, R., Ali, R., Donohue, R., McFarlane, D. J., Davies, P., ... & Donn, M. (2012). Climate change effects on water-dependent ecosystems in south-western Australia. *Journal of Hydrology*, 434, 95-109.

Benito, E., Santiago, J. L., De Blas, E., & Varela, M. E. (2003). Deforestation of water-repellent soils in Galicia (NW Spain): effects on surface runoff and erosion under simulated rainfall. *Earth Surface Processes and Landforms*, 28(2), 145-155.

Bosch, J. M., & Hewlett, J. D. (1982). A review of catchment experiments to determine the effect of vegetation changes on water yield and evapotranspiration. *Journal of Hydrology*, 55(1), 3-23.

Bruijnzeel, L.A. (1990). *Hydrology of most tropical forests and effects of conversion: a state of knowledge review*. (Book) Published with support of National Committee of the Netherlands for the International Hydrological Programme of UNESCO, The International Institute for Aerospace Survey and Earth Sciences Programme on Geo-information for Environmentally Sound Management of Tropical Resources (Hydrology). and The International Association of Hydrological Sciences, 224 pp.

Campbell, J. L., Driscoll, C. T., Pourmokhtarian, A., & Hayhoe, K. (2011). Streamflow responses to past and projected future changes in climate at the Hubbard Brook

Experimental Forest, New Hampshire, United States. *Water Resources Research*, 47(2).

Calder R. Lan (1998). *Water-Resource and Land-use Issues*. ISSN: 1028-6705. International Water Management Institute (IWMI). Research report, 24 pp.

Carter, T. R., Jylhä, K., & Tuomenvirta, H. (2003). *Future climate in world regions: an intercomparison of model-based projections for the new IPCC emissions scenarios* Finnish Environment Institute, ISNN 1238-7312, Research report, Publication series 644, 83 pp.

Chang, H., & Jung, I. W. (2010). Spatial and temporal changes in runoff caused by climate change in a complex large river basin in Oregon. *Journal of Hydrology*, 388(3), 186-207.

Chen, J., Brissette, F. P., & Leconte, R. (2011). Uncertainty of downscaling method in quantifying the impact of climate change on hydrology. *Journal of Hydrology*, 401(3), 190-202.

Cherkauer, D. S., (2004). Quantifying ground water recharge at multiple scales using PRMS and GIS. *Groundwater*, 42(1): 97-110.

Coe, M. T., Latrubesse, E. M., Ferreira, M. E., & Amsler, M. L. (2011). The effects of deforestation and climate variability on the streamflow of the Araguaia River, Brazil. *Biogeochemistry*, 105(1-3), 119-131.

Gardner, L. R. (2009). Assessing the effect of climate change on mean annual runoff. *Journal of Hydrology*, 379(3), 351-359.

Garnier, M., Harper, D. M., Blaskovicova, L., Hancz, G., Janauer, G. A., Jolánkai, Z., ... & Jolánkai, G. (2015). Climate Change and European Water Bodies, a Review of

Existing Gaps and Future Research Needs: Findings of the Climate Water Project. *Environmental Management*, 56(2), 271-285.

Gentry, A. H., & Lopez-Parodi, J. (1980). Deforestation and increased flooding of the upper Amazon. *Science*, 210(4476), 1354-1356.

Goderniaux, P., Brouyère, S., Fowler, H. J., Blenkinsop, S., Therrien, R., Orban, P., & Dassargues, A. (2009). Large scale surface–subsurface hydrological model to assess climate change impacts on groundwater reserves. *Journal of Hydrology*, 373(1), 122-138.

Gordon, L., Dunlop, M., & Foran, B. (2003). Land cover change and water vapour flows: learning from Australia. *Philosophical Transactions of the Royal Society B: Biological Sciences*, 358(1440), 1973-1984.

Green, T. R., Taniguchi, M., Kooi, H., Gurdak, J. J., Allen, D. M., Hiscock, K. M., ... & Aureli, A. (2011). Beneath the surface of global change: Impacts of climate change on groundwater. *Journal of Hydrology*, 405(3), 532-560.

Harr RD. 1981. Some characteristics and consequences of snowmelt during rainfall in western Oregon. *Journal of Hydrology* 53: 277–304.

Harr RD. 1986. Effects of clear-cut logging on rain-on-snow runoff in western Oregon: a new look at old studies. *Water Resources Research* 22: 1095–1100.

Harr RD, Harper WC, Krygier JT, Hsieh FS. 1975. Changes in storm hydrographs after road building and clear-cutting in the Oregon Coast Range. *Water Resources Research* 11: 436–444.

He, M., & Hogue, T. S. (2012). Integrating hydrologic modeling and land use projections for evaluation of hydrologic response and regional water supply impacts in semi-arid environments. *Environmental Earth Sciences*, 65(6), 1671-1685.

Hornbeck, J. W., Pierce, R. S., & Federer, C. A. (1970). Streamflow changes after forest clearing in New England. *Water Resources Research*, 6(4), 1124-1132.

Hugo, K., (2015) *Bow River floods and groundwater*. http://www.esaa.org/

Jiang, C., Xiong, L., Wang, D., Liu, P., Guo, S., & Xu, C. Y. (2015). Separating the impacts of climate change and human activities on runoff using the Budyko-type equations with time-varying parameters. *Journal of Hydrology*, 522, 326-338.

Jones, R. N., Chiew, F. H., Boughton, W. C., & Zhang, L. (2006). Estimating the sensitivity of mean annual runoff to climate change using selected hydrological models. *Advances in Water Resources*, 29(10), 1419-1429.

Kankaanpää, S., Carter, T. R. (2004) *Construction of European forest land use scenarios for the 21st century*. In: The Finnish Environment 707, Finnish Environment Institute Helsinki, 57 pp.

Kienzle, S. W., Nemeth, M. W., Byrne, J. M., & MacDonald, R. J. (2012). Simulating the hydrological impacts of climate change in the upper North Saskatchewan River basin, Alberta, Canada. *Journal of Hydrology*, 412, 76-89.

Lashof, D. A. (1989). The dynamic greenhouse: feedback processes that may influence future concentrations of atmospheric trace gases and climatic change. *Climatic Change*, 14(3), 213-242.

Meyer, W. B., & BL Turner, I. I. (1994). *Changes in land use and land cover: a global perspective*, Vol. 4, Cambridge University Press.

Mkankam Kamga, F. (2001). Impact of greenhouse gas induced climate change on the runoff of the Upper Benue River (Cameroon). *Journal of Hydrology*, 252(1), 145-156.

Montenegro S, Ragab R (2012) Impact of possible climate and land use changes in the semi arid regions: A case study from North Eastern Brazil. *Journal of Hydrology* 434:55–68.

Prudhomme, C., Jakob, D., & Svensson, C. (2003). Uncertainty and climate change impact on the flood regime of small UK catchments. *Journal of hydrology*, 277(1), 1-23.

Prudhomme, C., Davies, HN. (2008) Assessing uncertainties in climate change impact analyses on river flow regimes in the UK. Part 2: future climate. *Climatic Change*. doi:10.1007/s10584-008-9461-6.

Rose, S., & Peters, N. E. (2001). Effects of urbanization on streamflow in the Atlanta area (Georgia, USA): a comparative hydrological approach. *Hydrological Processes*, 15(8), 1441-1457.

Saha, G. C. (2015). Climate Change Induced Precipitation Effects on Water Resources in the Peace Region of British Columbia, Canada. *Climate*, 3(2), 264-282.

Sleeter, B. M., Sohl, T. L., Bouchard, M. A., Reker, R. R., Soulard, C. E., Acevedo, W, ... Zhu, Z. (2012) Scenarios of land use and land cover change in the conterminous United States: utilizing the special report on emission scenarios at ecoregional scales. *Global Environmental Change* 22(4): 896–914.

Solecki, W. D., Oliveri, C. (2004) Downscaling climate change scenarios in an urban land use change model. *Journal of Environmental Management* 72(1):105–115.

Tong S T, Sun Y, Ranatunga T, He J, Yang Y J (2012) Predicting plausible impacts of sets of climate and land use change scenarios on water resources. *Applied Geography* 32(2), 477–489.

Tu, J. (2009). Combined impact of climate and land use changes on streamflow and water quality in eastern Massachusetts, USA. *Journal of Hydrology*, 379(3), 268-283.

Verburg, P.H., Schulp, C.J.E., Witte, N., Veldkamp, A. (2006) Downscaling of land use change scenarios to assess the dynamics of European landscapes. *Agriculture, Ecosystems & Environment* 114(1): 39–56.

Verry, E. S., Lewis, J. R., & Brooks, K. N. (1983). Aspen clearcutting increases snowmelt and storm flow peaks in north central Minnesota. *Water Resources Bulletin*, 19(1), 59-67.

Viola, M. R., de Mello, C. R., Chou, S. C., Yanagi, S. N., & Gomes, J. L. (2015). Assessing climate change impacts on Upper Grande River Basin hydrology, Southeast Brazil. *International Journal of Climatology*, 35(6), 1054-1068.

Wang, S., Kang, S., Zhang, L., & Li, F. (2008). Modelling hydrological response to different land-use and climate change scenarios in the Zamu River basin of northwest China. *Hydrological Processes*, 22(14), 2502-2510.

Wang, L., Liu, J., Sun, G., Wei, X., Liu, S., & Dong, Q. (2012). Water, climate, and vegetation: ecohydrology in a changing world. *Hydrology and Earth System Sciences*, 16, 4633-4636.

Wang R, Kalin L, Kuang W, Tian H (2014) Individual and combined effects of land use/cover and climate change on Wolf Bay watershed streamflow in southern Alabama. *Hydrological Processes,* 28(22), 5530–5546.

Wagner PD, Kumar S, Schneider K (2013) An assessment of land use change impacts on the water resources of the Mula and Mutha Rivers catchment upstream of Pune, India. *Hydrology and Earth System Sciences*, 17:2233–2246.

White, M. D., & Greer, K. A. (2006). The effects of watershed urbanization on the stream hydrology and riparian vegetation of Los Penasquitos Creek, California. *Landscape and Urban Planning*, 74(2), 125-138.

Wilby, R.L., Wigley, T.M.L., (1997). Downscaling general circulation model output: a review of methods and limitations. *Progress in Physical Geography* 214, 530–548.

Wijesekara, G.N., Farjad, B., Gupta, A., Qiao, Y., Delaney, P., Marceau, D.J. (2014) A Comprehensive Land-Use/Hydrological Modeling System for Scenario Simulations in the Elbow River Watershed, Alberta, Canada. *Environmental Management* 53(2): 357-381.

Yulianti, J. S., & Burn, D. H. (1998). Investigating links between climatic warming and low streamflow in the Prairies region of Canada. *Canadian Water Resources Journal*, 23(1), 45-60.

Chapter 2 : The Elbow River Watershed

The Elbow River watershed, located in southern Alberta, drains approximately 1235 km^2 (Fig. 2.1). It belongs to the Canada's Western Prairie Provinces (WPP), which lie in the rain shadow of the Rocky Mountains and are the driest of southern Canada (Schindler and Donahue, 2006). This area has experienced several severe droughts in the 20th century. In one of the worst events in the 1930s, referred to as the "dirty thirties", 7.3 million hectares of agricultural land were damaged and 250,000 people left the Canadian prairies (Gan, 2000).

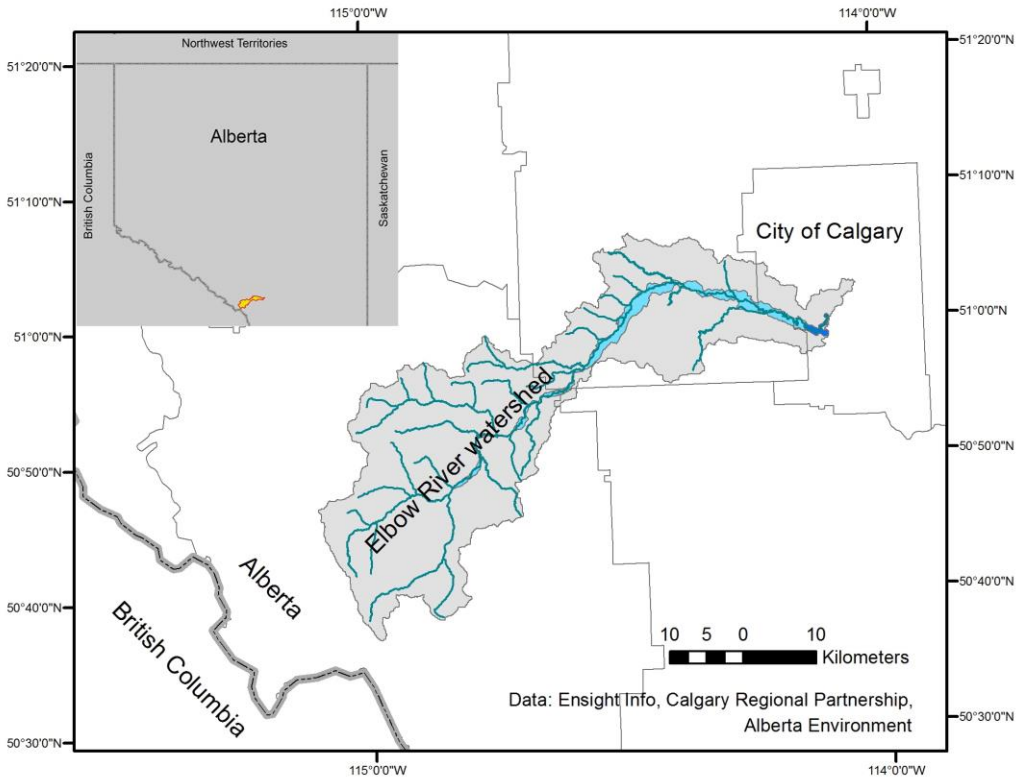

Figure 2.1 Location of the Elbow River watershed

The Elbow River watershed is one of the regions in the WPP that is most affected by climate change. Valeo et al. (2007) performed statistical analysis on historical data in the watershed and found that the annual average temperature has increased by 0.056°C/yr between 1965 and 2004 in the west part of the watershed and by 0.007°C/yr between 1885 and 2004 in the east part. Future projected data (provided by Alberta Environment and Sustainable Resource Development) for the CCSRNIES A1FI climate model project that the temperature may increase by approximately 4°C by 2050, relative to 1990, in the watershed. This considerable change can lead to extreme hydrological events in the future, such as droughts (Schindler and Donahue, 2006) and floods (Valeo et al., 2007).

Chen et al. (2006) investigated future climate trends and river water resources availability based on historical climate, streamflow, and population data in the Calgary region. They indicated that Calgary might face significant water supply challenges in the future. For this city to maintain a sustainable water supply, it will require water conservation efforts to reduce the per-capita water consumption to less than 50% of the current level by 2064. Even then, in the hot and dry projected periods, water demand could exceed the supply allotments (Chen et al., 2006). As a result, the Province of Alberta has stopped accepting new applications for the allocation of water since August 2006 in the Bow River basin of which the Elbow River is an important multi-use tributary (Pernitsky and Guy, 2010).

Flooding is the other great stress endured in the Elbow River. In June 2013, the Elbow River was flowing through Calgary at 12 times the regular rate causing $400 million of damages, and the evacuation of 110,000 people (City of Calgary, 2013). Two other

floods of less magnitude occurred in 1995 and 2005. These floods happened in the month of June, which coincided with Albertans experiencing the driest years in climate history (Valeo et al., 2007). This is an indication of how climate change can alter the frequency and severity of extreme events in a watershed, which depend not only on the magnitude of the change but also on the watershed characteristics, and its vulnerability to climate change. To better understand the vulnerability of the Elbow River watershed to climate change, its main characteristics are presented in the next section.

2.1 Characteristics of the Elbow River watershed

The Elbow River originates at Elbow Lake at an elevation of 2095 m above sea level and flows 120 km eastward through the alpine, subalpine, boreal foothill, and aspen parkland before joining the Bow River at 1033 m above sea level in downtown Calgary (Beers and Sosiak, 1993). In terms of LULC (Fig. 2.2), the watershed is comprised of urban area (5.9%), agricultural land (16.7%), rangeland/parkland (6.2%), evergreen forest (34%), deciduous forest (10%), and clear-cut (1.8%), (Wijesekara et al., 2012).

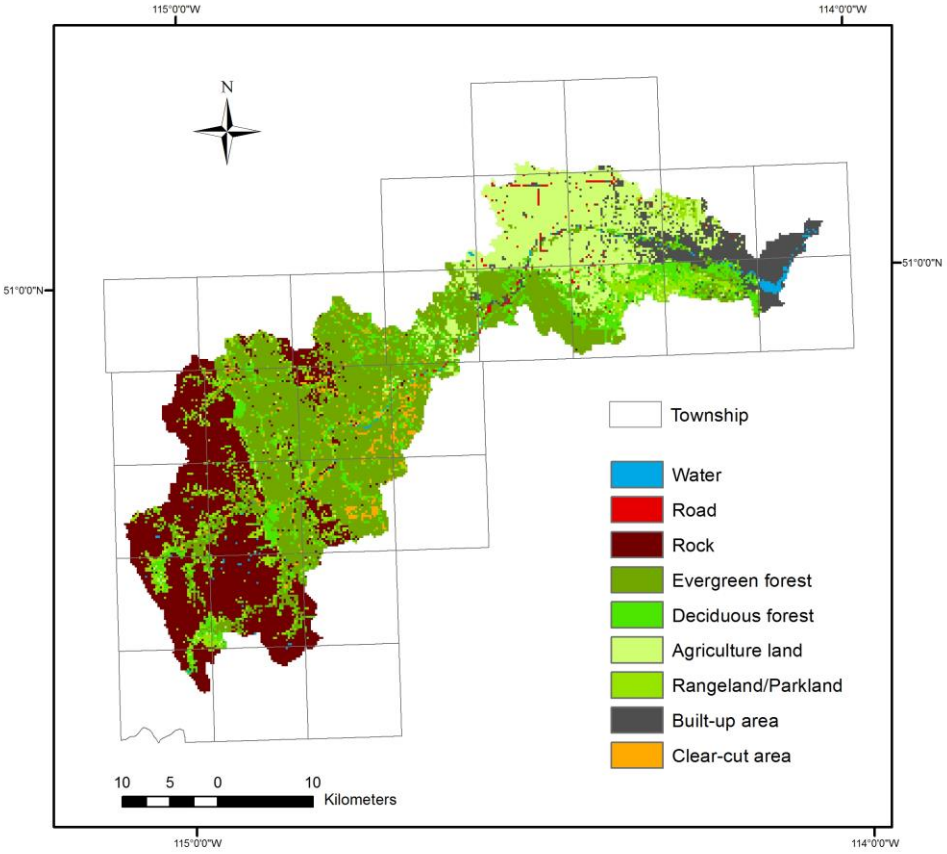

Figure 2.2 LULC map of the Elbow River watershed for the year 2010 (Data: Geocomputing Laboratory, University of Calgary)

2.1.1 Meteorological characteristics of the watershed

Climate data (obtained from Alberta Environment and Sustainable Resource Development (AESRD)) indicate that the average annual air temperature is 2.5 °C in the watershed. The warmest month is July with an average temperature of 13.2 °C, while the coldest month is January with an average temperature of -9 °C. The average total annual precipitation is 690 mm, of which almost 67% falls between the months of April to September. The month of June is the wettest month with an average precipitation of 99.6

mm. The average annual potential evaporation is 552.5 mm, with the highest rate of evaporation (101 mm) recorded in July.

There is a considerable difference in climate between the east and west portions of the watershed, since it lies between almost 2100 m difference in elevation. To take this difference into consideration, the watershed was delineated into two sub-catchments (based on a digital elevation model): the west sub-catchment which is upstream of the 05BJ004 station (Bragg Creek), and the east sub-catchment which is downstream of that station (Fig. 2.3).

To estimate the average precipitation for the east and west sub-catchments, two precipitation gauges were selected for each sub-catchment in different locations; since precipitation varies spatially, it was necessary to use the data from gauges located at different locations. For the east sub-catchment, the temperature index station is Calgary, and the precipitation index stations are 3031875 and 3031090 (Fig. 2.3). For the west sub-catchment, the temperature index station is Nakiska, and the precipitation index stations are 305LRKB and 353602 (Fig. 2.3).

In the east sub-catchment, the annual average temperature is 4.1 °C at the Calgary station while in the west sub-catchment the annual average temperature is -1.9 °C at the Nakiska station. From April to September, precipitation reaches 399 mm in the west sub-catchment and 332 mm in the east sub-catchment (Fig. 2.4 and 2.5). The west sub-

catchment gets considerably higher precipitation (272 mm) than the east sub-catchment (98 mm) between the months of October and March.

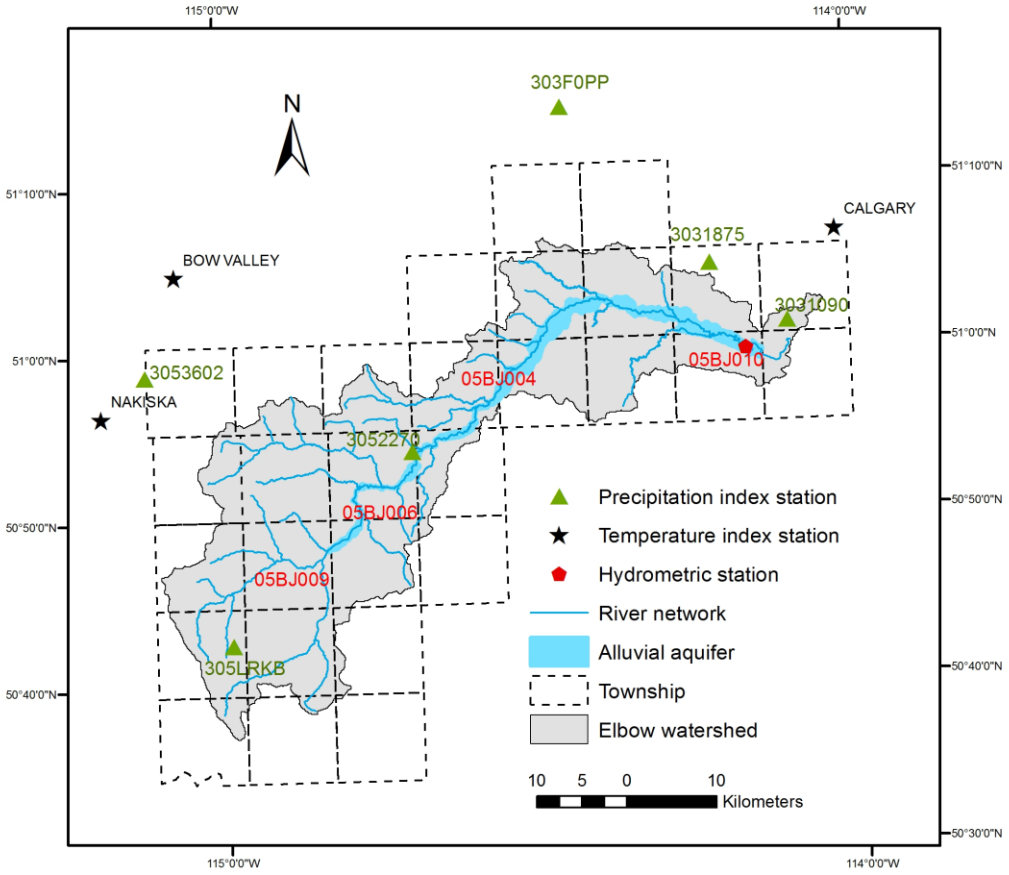

Figure 2.3 Location of the climate index and hydrometric stations in the Elbow River watershed

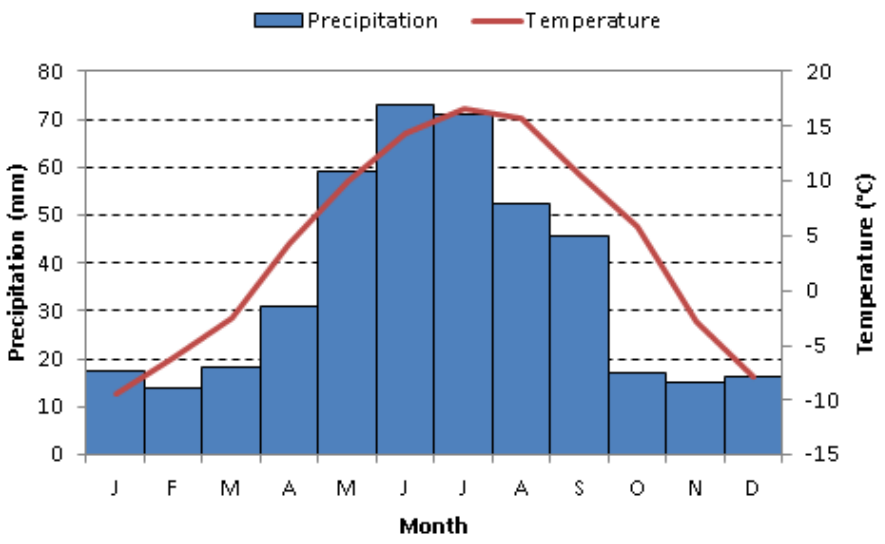

Figure 2.4 Average monthly precipitation and temperature distribution in the east sub-catchment of the Elbow River watershed

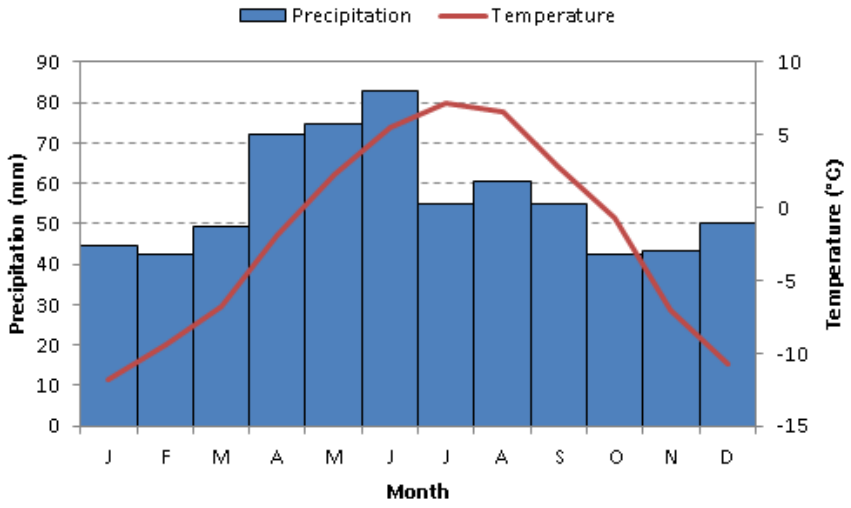

Figure 2.5 Average monthly precipitation and temperature distribution in the west sub-catchment of the Elbow River watershed

2.1.2 River regime

Four hydrometric stations, 05BJ009, 05BJ006, 05BJ004, and 05BJ010 (Fig. 2.3), measure discharge rates along the river. From west to east, the 05BJ009 and 05BJ006 stations cover 129 km^2 and 437 km^2 drainage areas in the front ranges of the Rocky Mountains in the west sub-catchment. The average annual discharge is respectively 3.33 m^3/s and 6.44 m^3/s at these stations. The volume of water flowing down the river increases at the 05BJ004 station with the average annual discharge of 8.13 m^3/s. This station represents the outlet of the west sub-catchment and measures discharge rates of 791 km^2 drainage area upstream of the hamlet of Bragg Creek. The river flows to the lowlands areas in the east sub-catchment and drains a cumulative area of almost 1200 km^2 at the 05BJ010 station upstream of the outlet of the watershed. The average annual discharge rate at this hydrometric station, which can be considered as the river flow volume discharging into the Glenmore reservoir, is 10 m^3/s.

The discharge rates differ, especially for peak flows, from month to month, and year to year. Figure 2.6 displays a typical average daily hydrograph of the Elbow River that was created based on 72-year average daily discharge in the watershed. Generally, the flow of the river starts rising between the 100th and the 130th days from the beginning of the year, and reaches its peak flow between the 150th and the 180th days and then gradually starts decreasing between the 181th and the 210th days. In fact, overland flow and through flow are the major contributors to the river flow in the days between rising and falling limbs of the hydrograph and the baseflow is the main contributor in the remaining of the days during a year. In terms of monthly discharge variability (Fig. 2.7), the high

flow period occurs in May, June, and July. The average peak flow for these months are 30 m^3/s, 63.1 m^3/s, and 35 m^3/s while the low flow are 4.83 m^3/s, 8.51 m^3/s, and 6.27 m^3/s for the period of 1978 to 2011, respectively.

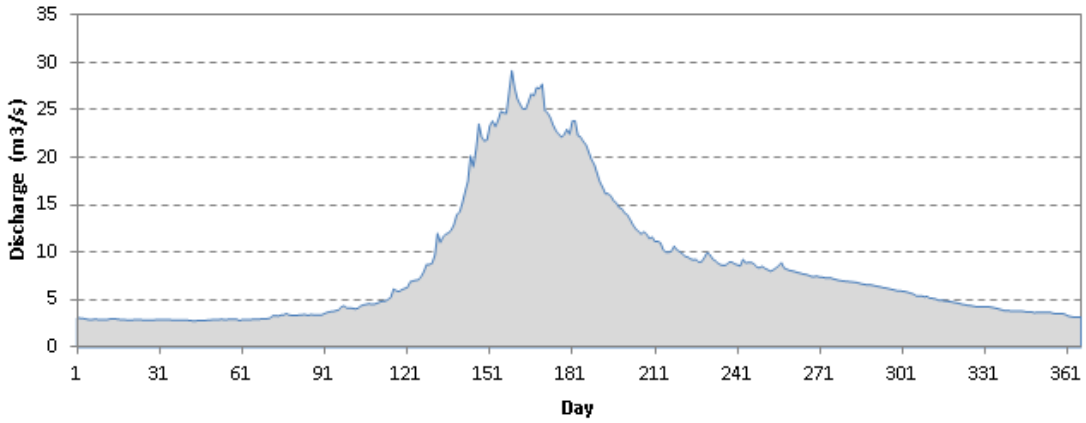

Figure 2.6 72-year average daily hydrograph at the 05BJ004 station

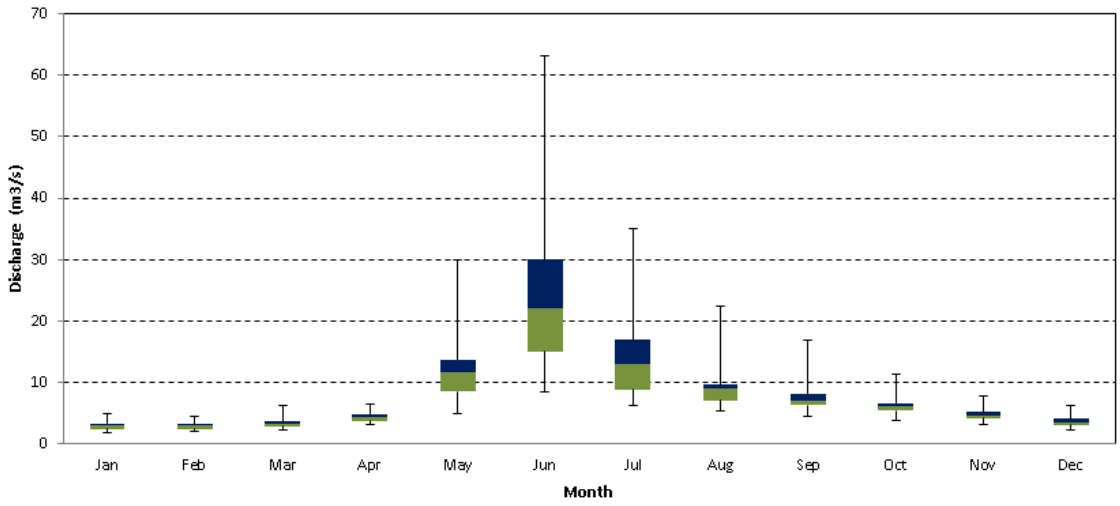

Figure 2.7 Box plot of average monthly discharge illustrating the minimum, the 25 percentile, the median, the 75 percentile, and the maximum discharge values

The highest peak flows of the watershed that have been recorded in history (at the 05BJ004 station) occurred in 1879 (Waterline, 2011) and in 2013 with discharge values of 980 and 959 m^3/s, respectively. Other high peak flows of lesser magnitude are 836 m^3/s in 1932 and 489 m^3/s in 1929 while the recurrence of 20 and 100-year of flood events are 340 and 758 m^3/s, respectively (Waterline, 2011). It is not possible to directly relate the flood events (such as the recent ones of 1995, 2005, and 2013) to climate change. However, observed trends in increased peak flows and temperature (which results in increased snow melting) are signs of increasing vulnerability to floods of higher magnitudes and frequencies.

2.1.3 Geomorphological characteristics of the watershed

The geomorphological characteristics of the watershed can influence the flow regime, especially during flooding. For example, the time of concentration, which describes the speed and intensity of the watershed response to storms, changes with the different morphological characteristics. The geomorphological characteristics of the Elbow River watershed, namely the stream patterns, shape, drainage density, stream order, and topography vary considerably from west to east (Fig. 2.8). The west sub-catchment mostly lies in the highland areas with less recession time of overland flow. The stream patterns of the west sub-catchment are similar to trellis patterns that are characterized by long main streams intercepted by numerous shorter right-angle tributaries. Trellis patterns are commonly found in regions of folded or tilted strata. However, the stream pattern of

the east-sub catchment is dendritic, which is characterized by gentle regional slope, and relatively uniform lithology (Mejía and Niemann, 2008).

The above mentioned physical characteristics in the west sub-catchment along with the orographic precipitation and snowmelt are the major factors explaining that about 80-90% of streamflow originates upstream of the station 05BJ004.

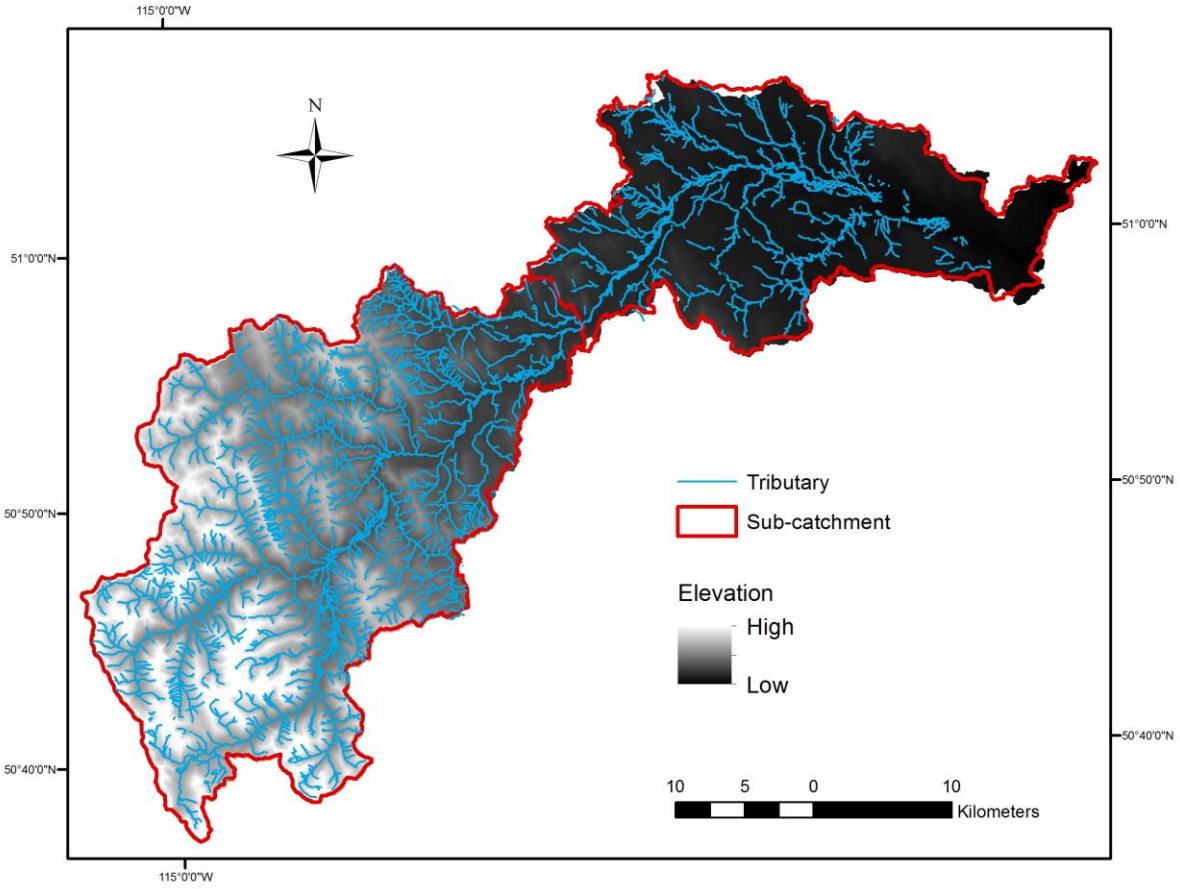

Figure 2.8 Geomorphological characteristics of the Elbow River watershed (Data source Alberta Environment and Sustainable Resource Development)

2.1.4 Geological and hydrogeological characteristics of the watershed

The surficial geology of the Elbow River watershed is dominated by glacial deposits and recent alluvial deposits (Manwell et al., 2006). The watershed contains the following aquifers (Waterline, 2011): Unconsolidated Glacial Overburden aquifers, Elbow River alluvial aquifer, Porcupine Hills Formation aquifers (multiple aquifers with depth), Coalspur Formation aquifer, Brazeau Formation aquifer, and the karstic Paleozoic carbonate aquifer(s).

The alluvial aquifer plays an important role in the hydrological regime of the watershed since it is generally very permeable and hydraulically connected to the Elbow River. The aquifer lies along the Elbow River for approximately 5% of the watershed (61 km^2) which extends from the near headwaters in the west to the Glenmore reservoir in the east (Waterline, 2011).

The hydraulic conductivity of the aquifer is on the order of 1×10^{-3} m^{s-1} (Manwell et al., 2006; Meyboom, 1961), and the direction of groundwater flow is generally from the west to the east along the axis of the watershed (Waterline, 2011).

Different geological settings and the alluvial aquifer along the river create complex interactions between surface water and groundwater. This complexity can be enhanced when there are different climate conditions in the watershed. Furthermore, the watershed is typical of snow dominated basins, with a spring freshet driven by snow melt and rainfall in late spring and early summer. Along with the morphological characteristics of

the basin, this creates favorable conditions for springtime flooding, which resulted in extensive damage in 2005 and 2013. Therefore, understanding how future climate change might influence the hydrological regime of the Elbow River watershed is of critical importance.

2.3 References

Beers C. and Sosiak A. (1993). Water quality of the Elbow River. Environmental Quality Monitoring Branch, Alberta Environmental Protection.

Buytaert, W., Célleri, R., and Timbe, L. (2009). Predicting climate change impacts on water resources in the tropical Andes: Effects of GCM uncertainty. *Geophysical Research Letters*, 36(7).

Buytaert, W., Vuille, M., Dewulf, A., Urrutia, R., Karmalkar, A., and Celleri, R. (2010). Uncertainties in climate change projections and regional downscaling in the tropical Andes: implications for water resources management. *Hydrology and Earth System Sciences*, 14(7), 1247-1258.

Chen, D., and Chen, H. W. (2013). Using the Köppen classification to quantify climate variation and change: an example for 1901–2010. *Environmental Development*, 6, 69-79.

Chen, Z., Grasby, S. E., Osadetz, K. G., and Fesko, P. (2006). Historical climate and stream flow trends and future water demand analysis in the Calgary region, Canada. *Water Science and Technology*, 53(10), 1-12.

City of Calgary (2013). *Calgary flood 2013*. http://www.calgary.ca/General/flood-recovery/Pages/Calgary-flood-2013-infographic-recap.aspx.

De Wit, M. J. M., Van Den Hurk, B. J. J. M., Warmerdam, P. M. M., Torfs, P. J. J. F., Roulin, E., and Van Deursen, W. P. A. (2007). Impact of climate change on low-flows in the river Meuse. *Climatic Change*, 82(3-4), 351-372.

DHI (2009) MIKE SHE. User Manual Volume 2: Reference Guide

DHI Water and Environment (2010). Elbow River watershed hydrology modeling. Report submitted to Alberta Environment.

Espadafor, M., Lorite, I. J., Gavilán, P., and Berengena, J. (2011). An analysis of the tendency of reference evapotranspiration estimates and other climate variables during the last 45 years in Southern Spain. *Agricultural Water Management*, 98(6), 1045-1061.

Gan, T. Y. (2000). Reducing vulnerability of water resources of Canadian prairies to potential droughts and possible climatic warming. *Water Resources Management*, 14(2), 111-135.

Gan, T. Y. (1998). Hydroclimatic trends and possible climatic warming in the Canadian Prairies. *Water Resources Research*, 34(11), 3009-3015.

Golder Associates. (2010). Hydro-Climate Modeling of Alberta South Saskatchewan Regional Planning Area. 09-1326-1006, Report submitted to Alberta Environment, 82 pp.

Hargreaves, G. H., and Allen, R. G. (2003). History and evaluation of Hargreaves evapotranspiration equation. *Journal of Irrigation and Drainage Engineering*, 129(1), 53-63.

Hay, L. E., Wilby, R. L., and Leavesley, G. H. (2000). A comparison of delta and downscaled GCM scenarios for three Mountainous basins in the United States. JAWRA Journal of the American Water Resources Association, 36(2), 387-397.

Hendriks, M. R. (2010). *Introduction to Physical Hydrology*. Oxford University Press.

Kottek, M., Grieser, J., Beck, C., Rudolf, B., and Rubel, F. (2006). World map of the Koppen-Geiger climate classification updated. *Meteorologische Zeitschrift*, 15(3), 259-264.

Manwell, B. R., and Ryan, M. C. (2006). Chloride as an indicator of non-point source contaminant migration in a shallow alluvial aquifer. *Water Quality Research Journal of Canada*, 41(4), 383-397.

Mareuil, A., Leconte, R., Brissette, F., and Minville, M. (2007). Impacts of climate change on the frequency and severity of floods in the Châteauguay River basin, Canada. *Canadian Journal of Civil Engineering*, 34(9), 1048-1060.

Mejía, A. I., and Niemann, J. D. (2008). Identification and characterization of dendritic, parallel, pinnate, rectangular, and trellis networks based on deviations from planform self-similarity. *Journal of Geophysical Research*, 113(F2), F02015.

Meyboom P. 1961. Groundwater resources in the City of Calgary vicinity. Bulletin 8. Research Council of Alberta, Edmonton.

National Research Council Associate Committee on Hydrology, NRCACH. 1983. *Hydrology of Floods in Canada: A Guide to Planning and Design*. National Research Council Canada.

Peel, M. C., Finlayson, B. L., and McMahon, T. A. (2007). Updated world map of the Köppen-Geiger climate classification. *Hydrology and Earth System Sciences Discussions*, 4(2), 439-473.

Pernitsky, D. J., and Guy, N. D. (2010). Closing the South Saskatchewan River Basin to New Water Licences: Effects on Municipal Water Supplies. *Canadian Water Resources Journal*, 35(1), 79-92.

Priestley, C. H. B., and Taylor, R. J. (1972). On the assessment of surface heat flux and evaporation using large-scale parameters. *Monthly Weather Review*, 100(2), 81-92.

Schindler, D. W., and Donahue, W. F. (2006). An impending water crisis in Canada's western prairie provinces. *Proceedings of the National Academy of Sciences*, 103(19), 7210-7216.

Sentelhas, P. C., Gillespie, T. J., and Santos, E. A. (2010). Evaluation of FAO Penman–Monteith and alternative methods for estimating reference evapotranspiration with missing data in Southern Ontario, Canada. *Agricultural Water Management*, 97(5), 635-644.

Singh, V. P. (1995). *Computer models of watershed hydrology*. Water Resources Publications.

Snover, A. K., Hamlet, A. F., and Lettenmaier, D. P. (2003). Climate-change scenarios for water planning studies: Pilot applications in the Pacific Northwest. *Bulletin of the American Meteorological Society*, 84(11), 1513-1518.

Sparovek, G., De Jong Van Lier, Q., and Dourado Neto, D. (2007). Computer assisted Koeppen climate classification: a case study for Brazil. *International Journal of Climatology*, 27(2), 257-266.

Valeo, C., Xiang, Z., Bouchart, F. C., Yeung, P., and Ryan, M. C. (2007). Climate change impacts in the Elbow River watershed. *Canadian Water Resources Journal*, 32(4), 285-302.

Waterline (2011). Groundwater elevation and monitoring plan Elbow River watershed sub-region TWPS 018 to 024, RGES 29W4 to 09W5 Alberta. WL10-1716, pp 100, Alberta Environment.

Wijesekara, G. N., Gupta, A., Valeo, C., Hasbani, J. G., Qiao, Y., Delaney, P., and Marceau, D. J. (2012). Assessing the impact of future land-use changes on hydrological processes in the Elbow River watershed in southern Alberta, Canada. *Journal of Hydrology*, 412, 220-232.

Wijesekara, G. N., Farjad, B., Gupta, A., Qiao, Y., Delaney, P., and Marceau, D. J. (2014). A comprehensive land-use/hydrological modeling system for scenario simulations in the Elbow River watershed, Alberta, Canada. *Environmental Management*, 53(2): 357-381.

Xu, Z. X., Zhao, F. F., and Li, J. Y. (2009). Response of streamflow to climate change in the headwater catchment of the Yellow River basin. *Quaternary International*, 208(1), 62-75.

Summary

In Chapter Two, we learned about the watershed characteristics and its hydrological regime. We also learned that there are considerable differences in the west and east sub-catchment characteristics, which may result in different hydrological responses to future climate change. In the next Chapter, we will investigate how the hydrology of the west and east sub-catchments, and the entire watershed respond to climate change, annually and seasonally.

Chapter 3 : Annual and Seasonal Variations of Hydrological Processes under Climate Change Scenarios in Two Sub-catchments of a Complex Watershed

Abstract

The Elbow River watershed, located in the rain shadow of the Rocky Mountains in western Canada, is characterized by a complex hydrological regime due to differences in climate and geomorphological settings between the west and east sub-catchments. This watershed has experienced several extreme droughts and floods in the recent decades, which might be accentuated with climate change. This study was undertaken to investigate the average annual and seasonal variations of surface and sub-surface hydrological processes in the west and east sub-catchments along with and the entire watershed under five plausible GCM-scenarios up to 2070 using the physically-based, distributed MIKE SHE/MIKE 11 model. Most of the scenarios indicate a reduction in the average annual overland flow, groundwater recharge and baseflow in the east sub-catchment, which might result in water insufficiency when considering the current and projected future water demands. The pattern of seasonal change generally exhibits a rise in overland flow, baseflow, evapotranspiration, groundwater recharge, and streamflow in winter-spring and a decline in summer-fall. The risk of flooding will enhance in mid-late spring due to an increase in rain-on-snow events coinciding with the highest increase in spring freshet. The induced changes in hydrological processes are proportionally more perceptible in the east sub-catchment compared to the west sub-catchment. However, the changes are offset by the west sub-catchment that governs the hydrology of the entire watershed. This study indicates that a greater understanding of climate change impacts on

the water balance of a watershed with differences in sub-regional settings is achieved when capturing the hydrological process responses of each sub-catchment individually.

Keywords: Hydrology, Hydrological modeling, Climate change, MIKE SHE/MIKE 11

3.1 Introduction

The latest Intergovernmental Panel on Climate Change (IPCC) report reaffirmed the strong evidence of climate change impacts on natural systems, which can threaten water security (IPCC 2014). Approximately one billion people over the world have limited access to sources of drinking water. Meanwhile, the urban population is forecasted to reach 6.3 billion people in 2050, compared to 3.4 billion in 2009, which increases the global demand for water (WWDR4 2012). In Canada, rivers discharge about 9% of the world's renewable water supply annually; however, this water is not distributed equally across the country (Whitfield and Cannon 2000). For instance, the Canada's Western Prairie Provinces (WPP) lies in the rain shadow of the Rocky Mountains under conditions of water scarcity (Schindler and Donahue 2006). This region has experienced about 30 severe droughts in the 19th and 20th centuries. The worst events occurred in the 1880s, 1890s and 1930s, the latest being referred to as the "dirty thirties", when 7.3 million hectares of agricultural land were damaged and 250,000 people were forced to leave the Canadian prairies (Gan 1998, 2000).

The Elbow River watershed, located in southern Alberta in the WPP, plays an important role as it provides water for industrial and irrigation uses and 40% of the city of Calgary's

drinking water (Wijesekara et al. 2014; Farjad et al. 2015). This watershed has experienced several extreme hydrological events such as droughts and floods in the recent decades. Insufficient water supply to fulfill increasing water demand resulted in closing the watershed to new water allocations since August 2006 (Pernitsky and Guy 2010). The fast growing city of Calgary, with a population of 1.1 M inhabitants in 2014, requires water conservation efforts to achieve a 50% reduction in water use by 2064, as compared to the current water level use (Chen et al. 2006). The watershed is also susceptible to flooding, which has occurred three times in recent years (1995, 2005, and 2013). The latest flood caused $400 million of damages along with the evacuation of 110,000 people. This context calls for a comprehensive study conducted to understand and predict the watershed hydrological responses under various climate scenarios.

Numerous studies have focused on investigating climate change impacts on water resources by translating the assumed climate changes into responses of hydrological processes (Kay et al. 2009; Prudhomme and Davies 2009; Forbes et al. 2011; Sultana and Coulibaly 2011; He et al. 2011; Tanzeeba and Gan 2012; Gan et al. 2015; Gombault et al. 2015). This investigation requires an adequate combination of appropriate climate and hydrological models along with downscaling techniques, particularly in small scale watersheds.

General circulation models (GCMs) are widely used to simulate present climate and project future climate with forcing by the continuing increase of greenhouse gas concentration in the atmosphere (Sauchyn et al. 2009; Shepherd et al. 2010; Setegn et al.

2011; Dessu and Melesse 2013). The recent generation of GCMs has considerably improved the reliability of modelling the climate compared to the GCMs used in the early 1990s. However, overreliance on a single GCM can be misleading (Wilby and Harris 2006), and it has been widely recommended to utilize a combination of as many GCM and greenhouse gas emission scenarios as possible to better cover the uncertainty associated with climate projections (Charlton et al. 2006; Minville et al. 2008; Grillakis et al. 2011). Moreover, the spatial resolution of GCMs is a key challenge for hydrologists since it is too coarse to capture subgrid-scale features such as land use and topography (Wilby and Wigley 1997; Prudhomme et al. 2002; Fowler et al. 2007); consequently, the output of GCMs is not well-suited for direct use in hydrological models at local-scale river basins (Zhang et al. 2011). Hence, various statistical (Charlton et al. 2006) and dynamical (Gonçalves et al. 2014) downscaling methods have been employed to bridge the gap between the spatial and temporal resolution of climate and hydrological modeling systems.

Assessments of statistical and dynamical downscaling methods (Xu 1999; Prudhomme et al. 2002; Fowler et al. 2007) have revealed that their performance mainly depends on the application. For instance, the delta-change or perturbation method, which applies the difference between the control and future GCM projections to observations (Goderniaux et al. 2009) can perform as well as more sophisticated statistical and dynamical methods, if reproducing the mean values (annual to monthly scale) of climate variables is the purpose (Fowler et al. 2007; Hay and McCabe 2010). Wood et al. (1997) and Prudhomme et al. (2002) went one step further and noted that sophisticated statistical and

dynamical downscaling approaches have yet to be completely satisfactory, and do not necessarily provide a sound practical alternative to the simple perturbation method. These authors suggested utilizing the perturbation method due to not only its simplicity, but also to the fact that it uses the changes of the GCMs outputs rather than absolute values.

Numerous hydrological models exist that range from lumped, conceptual models to distributed, physically-based models (Refsgaard 1997; Jothityangkoon et al. 2001; Ghanbarpour et al. 2007). Most of these models provide vital insights into the hydrological regime of a watershed, but not all of them are suitable for climate impact studies. This is highlighted when hydrological models are calibrated based on current climate conditions, and then employed to simulate projected climate scenarios that are different from those used during the calibration process. Gan and Burges (1990) found that lumped, conceptual models are climate sequence dependent. Minville et al. (2008) stated that physically-based models reduce the uncertainty linked to calibration compared to lumped models for climate impact studies. This was also indicated by Ludwig et al. (2009) in a comprehensive study conducted to compare the responses of a fully distributed, semi-distributed, and lumped hydrological model to climate change. These models respectively represent high to low model complexity, in terms of process description, parameter space, and spatial and temporal scale. The authors indicated that a model of low physical complexity that has been calibrated to current climate conditions is inadequate for application in a climate change context. In a watershed with complex terrain and geology, the impacts of climate change are not uniformly distributed spatially and temporally, even if the climate change signal may be equally distributed across the

watershed (Chang and Jung 2010). A physically-based fully distributed model is an effective tool due to its ability to capture the spatial variability of hydrological processes throughout complex watersheds (Forbes et al. 2011).

This study aims at investigating the average annual and seasonal responses of hydrological processes to climate change in the Elbow River watershed characterized by a complex hydrological regime due to the differences in climate and geomorphological characteristics between the west and east sub-catchments. To capture this complexity, the methodological approach combines three key aspects. First, following the recommendations highlighted above, a physically-based, distributed hydrological model is used to simulate hydrological processes under a range of plausible GCM-scenarios up to 2070. Second, although a majority of previous works has focused mainly on surface hydrological processes, a combination of surface and subsurface hydrological processes is investigated in this study, including overland flow, baseflow, groundwater recharge, actual evapotranspiration, and streamflow. Finally, the water balances for the west and east sub-catchments and the entire watershed were quantified separately to obtain a better understanding of the hydrology of the watershed.

3.2 Methodology

In this section, the characteristics of the Elbow River watershed are described followed by a presentation of the methodological framework.

3.2.1 Elbow River watershed characteristics

The Elbow River watershed (Fig. 3.1) drains approximately an area of 1235 km^2. The river originates at Elbow Lake in Kananaskis Country at an elevation of 2095 m above sea level and flows 120 km eastward through the alpine, subalpine, boreal foothill, and aspen parkland before discharging into the Glenmore reservoir at 1,080 m above sea level in downtown Calgary (Farjad et al. 2015). The average annual air temperature in the watershed is 2.5 °C (1961-2005) while the average maximum and minimum temperature are 13.2 °C and -9 °C in the months of July and January, respectively. The average total annual precipitation and potential evapotranspiration are 690 mm and 552.5 mm, respectively (Farjad et al., 2015). The watershed is covered by urban areas (5.9%), agricultural lands (16.7%), rangeland/parklands (6.2%), evergreen forests (34%), deciduous forests (10%), and clear-cut areas (1.8%).

The spatial heterogeneity of the land surface and geomorphological characteristics of the watershed such as shape, topography, stream patterns, density, and order varies substantially from west to east. The stream pattern of the west sub-basin is similar to a trellis pattern that is characterized by long main streams intercepted by numerous shorter right-angle tributaries. These patterns are commonly associated with folded or tilted strata regions. In comparison, the stream pattern of the east sub-catchment is dendritic, which is commonly associated with flat-lying beds of plains regions with relatively uniform lithology resistance in a horizontal direction (Frost and Woods, 1948). The average annual discharge of the river is 11.5 m^3/s at the station 05BJ010 (Fig. 3.1) with an average peak flow of 23 m^3/s in June. A large portion of the streamflow originates

upstream of the 05BJ004 station (Fig. 3.1) due to orographic precipitation and geomorphological characteristics of the watershed as well as a snowmelt-dominated regime that exhibits high flows particularly in May, June, and July (Farjad et al. 2015). The alluvial aquifer along the river results in a complex interaction between surface water and groundwater from the near headwaters to the Glenmore reservoir for about 61 km^2.

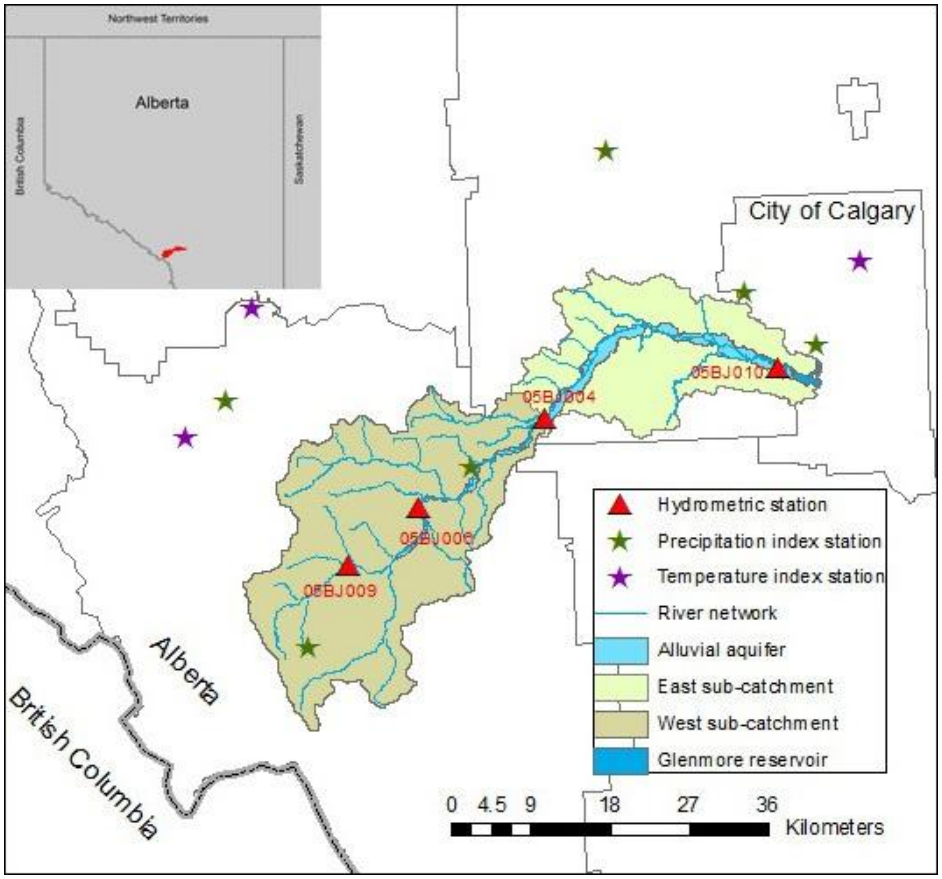

Figure 3.1 The Elbow River watershed. Locations of hydrometric and climate index stations are identified

3.2.2 Methodological framework

Figure 3.2 illustrates the methodological framework of this study, which consists of the following steps: 1) data acquisition and processing for configuring the hydrological model; 2) calculation of potential evapotranspiration (PET) rates corresponding to each

GCM-scenario, and 3) hydrological model configuration to simulate the hydrological processes in the watershed. These steps are described in details in the following sections.

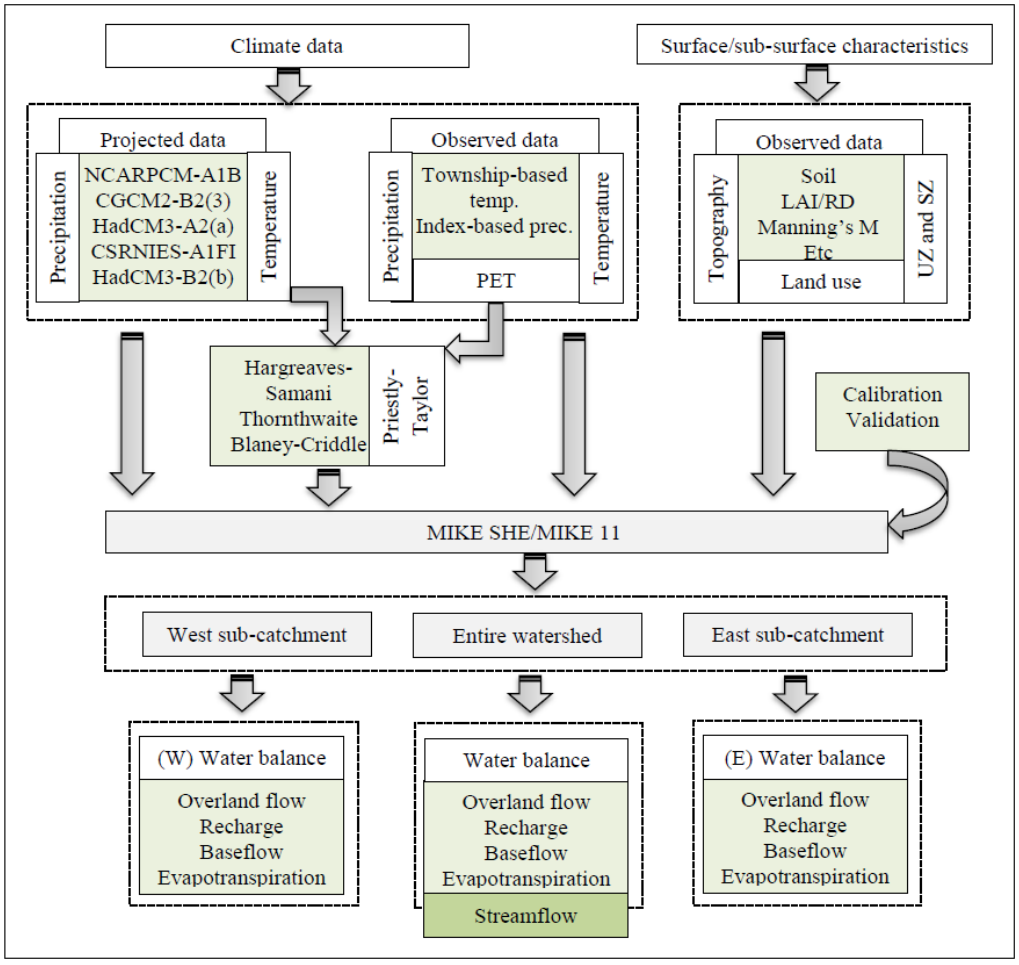

Figure 3.2 Methodological framework

3.2.2.1 Data acquisition and processing

Surface/subsurface characteristics

Historical land-use/land-cover (LULC) maps for the years 1985, 1992, 1996, 2001, and 2006 generated from Landsat Thematic Mapper (TM) imagery at the spatial resolution of

30 m (Hasbani et al. 2011) were used in this study. These maps comprise nine dominant classes: urban areas, rock, roads, water, deciduous forests, evergreen forests, agricultural land, rangeland/parklands, and forest clear-cuts. LULC maps were employed to determine land-use based parameters, including Manning's M, detention storage, paved runoff coefficient, and leakage coefficient along with the leaf area index (LAI) and root depth (RD). A soil map, obtained from the Agricultural Region of Alberta Soil Inventory Database and the Canadian Soil Information Service Data sources, was overlaid with the LULC maps to identify built-up areas and limit infiltration in these areas in the model. The ground surface topography was created using the 80 m spatial resolution DEM from GeoBase (2008) which was re-sampled at 200 m. The data related to saturated (SZ) and unsaturated zones (UZ), such as geology and groundwater information were obtained from Alberta Environment and Sustainable Resource Development (AESRD). A detailed description of these datasets can be found in Wijesekara et al. (2014).

Observed and projected climate data

Temperature data were acquired from AESRD for three climate index stations (Fig. 3.1). These data were interpolated using an areal weighting method (Jones and Hulme 1996), described in Farjad et al. (2015). Precipitation data were obtained for six climate index stations (Fig. 13) and interpolated using the Thiessen polygon method (Montenegro and Ragab 2012).

Projected temperature and precipitation were obtained from AESRD for five climate change scenarios for the 2020s and 2050s. Seven GCMs (CCSR/NIES, CGCM2,

CSIROMk2, ECHAM4, NCAR-PCM, HadCM3, and GFDL-R30) were run with six IPCC SRES emission scenarios (A1FI, A1B, A1, A2, B1, and B2) to examine changes in temperature and precipitation. Scenarios that span the range of changes over the region were then selected (Barrow and Yu, 2005). The scenarios NCARPCM-A1B, CGCM2-B2(3), HadCM3-A2(a), and CCSR/NIES-A1FI represent extreme changes in temperature and precipitation, while HadCM3-B2(b) represent median conditions.

The projected temperature and precipitation were downscaled based on the widely used delta-change method (Buytaert et al. 2010; Hay and McCabe 2010; Forbes et al. 2011; Kienzle et al. 2012). The main limitation of this method is that potential changes in the climate variability are not captured by the approach (Vano et al. 2010). However, it is easy to implement and only requires monthly time scale projected data from GCMs whereas the majority of statistical downscaling methods need data from GCMs at the daily scale, which are considered uncertain (Palutikof et al. 1997; Huth et al. 2001), and are not available for all GCMs. Furthermore, most approaches require bias correction and variance adjustment while bias correction is implicitly built into the delta-change method (Minville et al. 2008).

3.2.2.2 Calculation of potential evapotranspiration (PET)

PET is one of the primarily input variables to the MIKE SHE model that cannot be directly estimated for the future from most Global and Regional Climate Models (Kay and Davies 2008; Prudhomme and Davies 2009). Models to estimate PET generally require meteorological variable inputs such as cloud cover and vapour pressure that are

more difficult to predict from GCMs compared to a variable like temperature (Kay and Davies 2008; Thompson et al. 2014). Kay and Davies (2008) compared a temperature-based PET model suggested by Oudin et al. (2005) (25 PET models were used as input to four hydrological models for 300 catchments), with a well-known and data-intensive model, the Penman–Monteith, using climate data that were derived from GCMs. They indicated that temperature-based PET models performed better than the Penman–Monteith model, which requires a large number of climate data such as humidity, radiation, and wind speed. In fact, more variables introduced additional inherent uncertainties derived from GCM simulations into the PET model. In addition, not all of the GCMs generate the variables required in data-intensive PET models.

In this study, the available projected climate variables from GCMs were only temperature and precipitation. Therefore, a review was carried out to select the most suitable PET model based on the following criteria: 1) the model must estimate evapotranspiration based on air temperature; 2) it must have been successfully tested and used in the watershed or a similar climate, and 3) it must be widely used by the scientific community. Based on the criteria three models were compared: Hargreaves-Samani (Hargreaves and Samani 1985), Thornthwaite (Sentelhas et al. 2010), and Blaney-Criddle (Espadafor et al. 2011) (Appendix 1). Their performance was compared with the PET rates provided by AESRD for 1961–2005 that have been estimated by the well-known Priestley-Taylor model (Priestley and Taylor 1972) used by Alberta Agriculture and Food for the Elbow River watershed. The performance was assessed using linear regression analysis, Root Mean Square Error (RMSE), and Mean Bias Error (MBE). The

Hargreaves model presented the best performance (Farjad et al. 2015) and was selected for calculating PET in the watershed. This model was calibrated and validated for the periods of 1961–1990 and 1991–2005, respectively.

3.2.3 Hydrological model configuration

MIKE SHE/MIKE 11, a spatially distributed and physically-based model was used to simulate hydrological processes under the five different GCM scenarios in the watershed. This model is capable of simulating the full suite of processes occurring in the land phase of the hydrological cycle (Sultana and Coulibaly 2011).

MIKE SHE was set up to simulate overland flow using a two-dimensional diffusive wave approximation by the finite-difference method. The model domain was defined to represent the physical characteristics of the catchment horizontally by a grid-cell (200 m) network, and vertically by different layers representing the spatial variability of the surface/subsurface characteristics. Land surface features play an important role in the distribution and flux of water within the watershed. Storage depth of the land surface at each cell must be filled before overland flow is produced. The threshold of storage depth was represented by detention storage. Each LULC class was assigned a value of detention storage, which was determined through calibration. Surface roughness was represented by Manning's M for each class which was derived from the literature. A paved runoff coefficient was defined for build-up areas with a value of 1, which determines the fraction of overland flow (100%) that is directly transferred to the closest streams, lakes,

and ponds. The vegetation properties were defined using values of the leaf area index (LAI) and root depth (RD), which were also derived from the literature (Scurlock et al. 2001). A detailed description of how these values were obtained can be found in Wijesekara et al. (2014).

MIKE 11 simulates river and channel flow using a fully dynamic wave version of the Saint-Venant equations. To configure the model, a river network was defined including the Elbow River and its tributaries. The river network includes 353 cross sections that were obtained from field surveys and LiDAR generated data.

A two-layer water balance method was employed to quantify flow in the unsaturated zone (UZ). This method is based on the simple mass-balance approach and considers the interactions between components in the UZ such as: surface ponding, interception, infiltration, water content in the root zone, and evapotranspiration. An 11-class soil classification was identified in the unsaturated zone with their corresponding hydraulic conductivity. Actual evapotranspiration from the surface storage, soil surface, canopy water storage, and root zone were calculated on the basis of the relationship developed by Kristensen and Jensen (1975).

Due to the complexity of the surface-groundwater interaction, the groundwater system was modeled using a 3D groundwater flow equations solved using a numerical finite-difference scheme and simulated surface-groundwater exchange. Six hydrogeological units were defined based on the geological characteristics of the watershed. The hydraulic

properties for the geological layers were derived based on well drilling reports and pumping tests obtained from Alberta Water Well Database.

A rigorous procedure referred to as split-sample, multi-criteria, and multi-point (described in Wijesekara et al. 2013) was applied to calibrate and validate the model. The calibration was carried out for the time period 1981-1991 using the LULC map of 1985 while four time intervals (1991-1995, 1995-2000, 2000-2005, and 2005-2008) were employed for validation with their corresponding LULC maps (1992, 1996, 2001, and 2006). The model performance was evaluated by comparing the simulated results with observed streamflow using the Nash and Sutcliffe coefficient of efficiency (NSE) (Table 3.1), Ln NSE (Appendix 2), relative NSE (Appendix 3), and coefficient of determination. In addition, the simulated and observed groundwater level and snow storage were compared using the mean absolute error (MAE) and Pearson's correlation coefficient, respectively. The output of the model generally showed a good agreement between the simulated and observed streamflow, groundwater level, and snow storage.

Table 3.1 Measured vs. simulated streamflow during calibration and validation periods for the hydrometric stations, 05BJ009, 05BJ006, 05BJ004, and 05BJ010

	Calibration/validation period	NSE (daily)				NSE (monthly)			
		J009	J006	J004	J010	J009	J006	J004	J010
Calibration	Sep. 1981 to Dec. 1991	0.53	0.63	0.72	0.63	0.63	0.75	0.83	0.75
Validation	Sep. 1991 to Dec. 1995	0.38	0.66	0.74	0.73	0.41	0.71	0.87	0.87
	Sep. 1995 to Dec. 2000	N/A	N/A	0.78	0.77	N/A	N/A	0.89	0.88
	Sep. 2000 to Dec. 2005	N/A	N/A	0.74	0.71	N/A	N/A	0.85	0.84
	Sep. 2005 to Dec. 2008	N/A	N/A	0.64	0.68	N/A	N/A	0.72	0.73

The LULC map of 1985 (corresponding to the baseline period) was employed to simulate hydrological processes for the period of 1961-1990. However, in order to capture the

climate change impact on the watershed hydrology, LULC changes were assumed constant for the simulations in the 2020s and 2050s. The water balance (WB) module in the MIKE model was used to quantify the overall changes in hydrological processes in response to climate change. WB is a fundamental tool to capture the dynamic changes in storage depth based on water inputs and outputs. Hereby, storage depth was calculated (in mm) for the major WB components such as overland flow, baseflow, groundwater recharge, and actual evapotranspiration using the WB module along with streamflow (using MIKE 11) for the 2020s and 2050s, and the baseline period. In addition, the WB of the east and west sub-catchments, and the entire watershed were investigated separately to obtain a better understanding of the hydrological regime in the watershed.

3.3 Results

In this section, the annual and seasonal changes related to climate scenarios are first described, followed by the simulation results of hydrological processes and streamflow in response to climate change.

3.3.1 Annual and seasonal changes in climate scenarios

The average annual and seasonal temperature and precipitation changes for the GCM-scenarios for the 2020s and 2050s, relative to the baseline (1961-1990), are presented in Figure 3.3 and Appendix 5. The average annual temperature increases for all GCM-scenarios in the 2020s and 2050s. The changes in the 2020s remain within the range of 0.4–1.5 °C while they increase to the range of 1.9–4.1°C in the 2050s. Seasonal changes generally exhibit an increase in temperature except for the A1FI (in January and February) and A2a scenarios (in January) in the 2020s and for the scenario A2a (in

January) in the 2050s. In the 2020s, the highest increases are in winter and early spring with the largest rise with the B23 scenario in January (3.4 °C), while the largest increase in the 2050s occurs in winter and early-mid spring with the A1FI scenario in December (6.5 °C) and April (5.2 °C).

In terms of precipitation, the projected climate scenarios do not reveal a clear signal in annual and seasonal change. In the 2020s, the change in annual precipitation ranges from -4.7 to 2.8% while it varies from -2.2 to 11.1% in the 2050s. The seasonal distribution indicates that precipitation decreases with most scenarios in early-mid-summer in the 2020s while in the 2050s it decreases for most scenarios in summer and early fall, and increases in late fall, winter and spring. The A2a scenario projects a greater increase in precipitation occurring in December in both the 2020s (25.1%) and the 2050s (31.8%), while the lower decreases are projected by B2b in July (-20.6%) in the 2020s and September (-17.3%) in the 2050s.

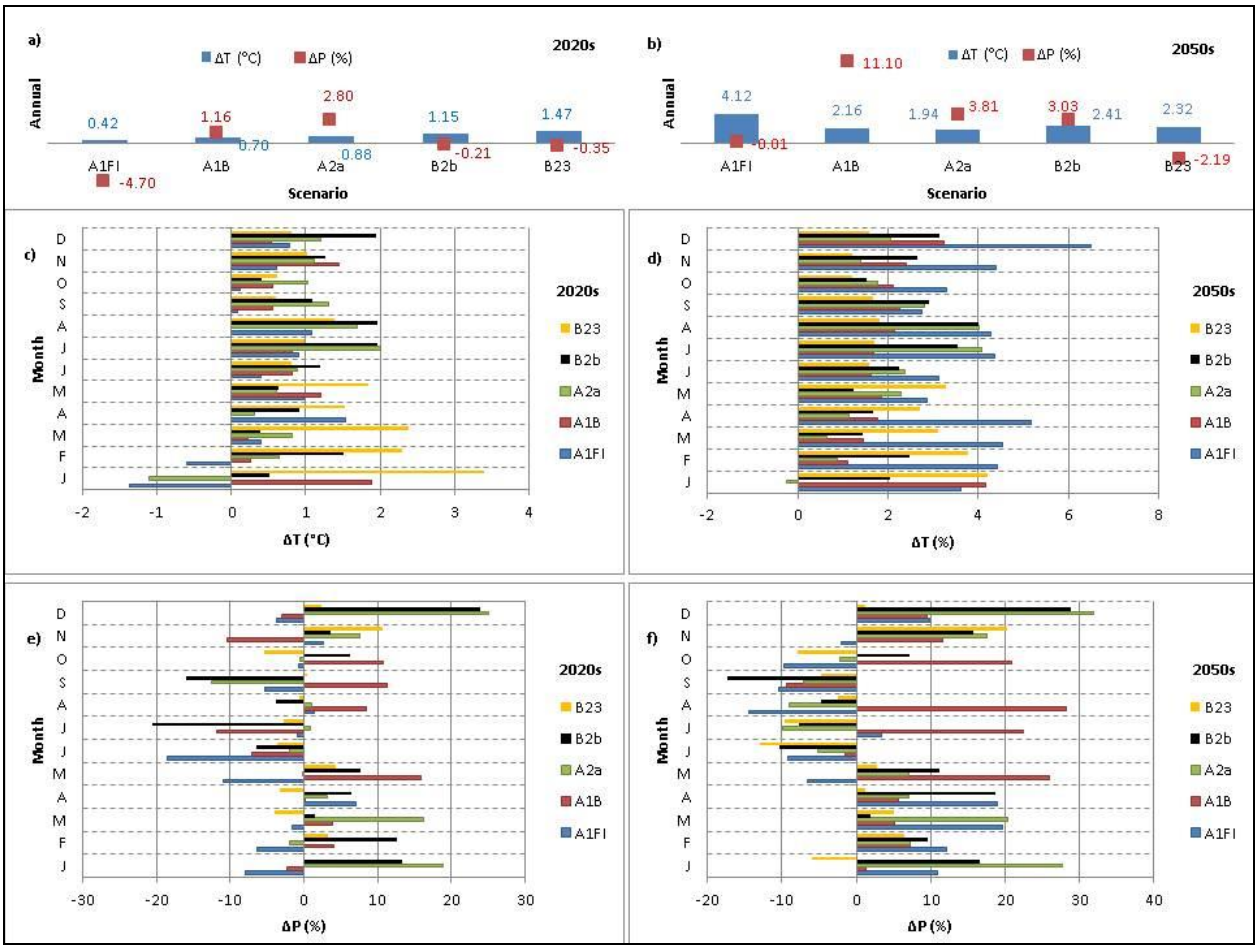

Figure 3.3 Changes in average annual and seasonal temperature and precipitation for the five scenarios in the 2020s and 2050s

3.3.2 Simulation of hydrological processes

The simulation results of hydrological processes in response to climate changes are presented below. The average annual changes related to the baseline are first described, followed by the average seasonal changes in hydrological processes for the entire watershed and the two sub-catchments.

3.3.2.1 Average annual changes

In the 2020s, overland flow decreases for A1FI (-10.5%) and B23 (-4.6%) and increases for the A1B (3.7%), A2a (6.0%), and B2b (0.6%) scenarios in the entire watershed (Fig. 3.4). The decreases in overland flow in A1FI and B23 are mostly correlated with -4.7% and -0.35% decline in precipitation whereas the increases in A1B, A2a, B2b are correlated with 1.2%, 2.8%, and 0.1% rise in precipitation. These changes in overland flow generally occur in the west sub-catchment with almost the same direction and magnitude of changes as in the entire watershed, while the changes in the east sub-catchment occur in the opposite direction (A2a and B2b) and magnitude (A1FI) compared to the entire watershed (Fig 3.4). This is due to the west sub-catchment characteristics that govern the hydrological regime of the entire watershed. For example, when overland flow increases by 6.6% for the A2a scenario in the west sub-catchment and decreases by -2.2% in the east sub-catchment, the total average overland flow in the entire watershed changes by 6.0%, which is in the same direction and almost the same magnitude as of the west sub-catchment. This also implies that changes in overland flow in the entire watershed highly depend on the spatial distribution of climate variables. In other words, overland flow may respond to the same amount of precipitation in the west and east sub-catchment differently. The relative changes in overland flow in the west and east sub-catchments range from -9.8 to 6.6% and -20.7 to 4.8%, respectively, whereas the changes in the entire watershed vary between -10.5 and 6.0%. This means that the changes in the entire watershed are similar to the ones in the west sub-catchment whereas the changes in overland flow are more substantial in the east sub-catchment. In other

words, the impact of climate change is more pronounced in the east sub-catchment; however, the changes are offset by the west sub-catchment.

In the 2050s, overland flow changes in the same direction as in the 2020s but not with the same magnitude in the entire watershed. It decreases for the A1FI (-10.6%) and B23 (-9.9%) scenarios, and increases for the A1B (17.9%), A2a (6.68%), and B2b (3.85%) scenarios. The changes are likely correlated with precipitation; however, the influence of temperature is more noticeable for A1FI and B23. Although the decline in precipitation for A1FI (-0.01) is less than B23 (-2.2%), overland flow decreases more for A1FI (-10.6%) compared to B23 (-9.9%). This is due to a larger rise in temperature for A1FI (6.6°C) compared to B23 (4.8°C). The relative changes in overland flow in the entire watershed ranges between -10.6 and 17.9%. These changes in overland flow are almost identical in the west sub-catchment, which range between -9.8 and 16.9% whereas the changes in the east sub-catchment range between -22.2 and 32.6%.

The average annual groundwater recharge varies from -6.9% to 4.1% and -5.2 to 16% in the entire watershed in the 2020s and 2050s, respectively (Fig. 4). In the 2020s, groundwater recharge increases under the A1B (3.4%) and A2a (4%) scenarios and decreases under the B23 (1.8%) and A1FI (6.9%) scenarios while the recharge variation is negligible under the B2b scenario. In the 2050s, groundwater recharge increases under the A1B (16%), A2a (4.3%), and B2b (3.7%) scenarios and decreases under A1FI (2.4%) and B23 (5.2%). The average annual changes in the west sub-catchment groundwater recharge occur with almost the same direction and magnitude as recharge variations in

the entire watershed in the 2020s and 2050s. However, groundwater recharge decreases under all scenarios expect A1B in the east sub-catchment in the 2020s and 2050s. This decline in the east sub-catchment groundwater recharge can result in groundwater depletion, which is a concern when about 90% of licensed groundwater extractions are located in the east sub-catchment.

The average annual baseflow changes in the 2020s and 2050s in the same direction as groundwater recharge for all scenarios in the entire watershed (Fig. 3.4). Change in baseflow ranges between -6.9 and 2.5% in the 2020s with a rise for the A1B (2.5%) and A2a (2.1%) scenarios and a drop for the A1FI (-6.9%), B23 (-2.3%), and B2b (-1.4%) scenarios. In the 2050s, it ranges between -5.5 and 12.7% with a rise for the A1B (12.7%), A2a (1.3%) and B2b (1.3%) scenarios and a drop for the A1FI (-3.6%) and B23 (-5.5%) scenarios. The baseflow variability in the west sub-catchment is similar to the entire watershed in the 2020s (-6.07–2.5%) and 2050s (-4.4–12.3%) while the changes occur with higher magnitude in the east sub-catchment in the 2020s (-13.0–2.67%) and 2050s (-15.4–15.6%).

Most of the GCM-scenarios indicate the same direction of change in average annual actual evapotranspiration, but not with the same magnitude (Fig. 3.4). AET increases in both the 2020s and 2050s for all GCM-scenarios: A1B (1.6% and 9.2%), A2a (2.8% and 4.8%), B2b (1.0% and 4.6%), and B23 (2.9% and 3.0%), except for the A1FI scenario where it decreases by -0.9% and increases by 6.9% in the 2020s and 2050s, respectively. The range of changes for the average annual actual evapotranspiration, in the 2020s (-

0.9–2.9%) and 2050s (3.0–9.2%), is less than both overland flow and baseflow. The relative average annual changes for AET in the east sub-catchment occur within a larger range (-3.0–2.5% and -0.3–10.5%) compared to the west sub-catchment (0.5–4.0% and 5.1–9.9%) in the 2020s and 2050s.

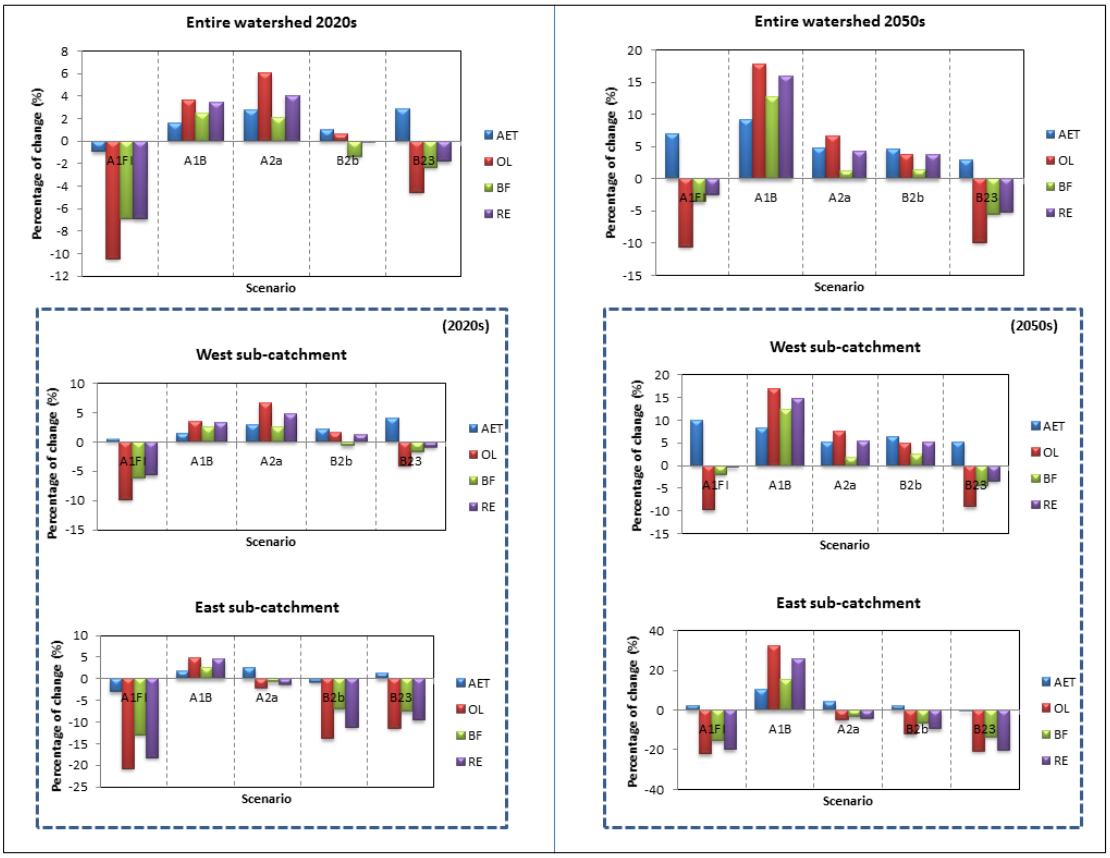

Figure 3.4 Average annual changes in overland flow (OL), groundwater recharge (RE), baseflow (BF), and actual evapotranspiration (AET) in the 2020s and 2050s

3.3.2.2 Average seasonal changes

In the 2020s and 2050s, the average monthly overland flow generally exhibits an increase in the winter months (DJF), spring (MAM), and fall (SON) and a decrease in the summer (JJA) in the entire watershed. The largest increases in overland flow occur in the early-

mid spring under all GCM-scenarios except A1F in March 2020s (Fig. 3.5). The rise in overland flow in spring is mainly due to snowmelt and a higher rain/snow ratio caused by higher temperatures. The largest increases in overland flow occur in March and April under the B23 scenario in the 2020s and under A1FI in the 2050s when a rise in temperature amplifies snowpack melting. In fact, snowmelt has a considerable contribution to overland flow (besides infiltration) since 25% of the watershed is covered with rock in highland areas in the west sub-catchment, and 6% built-up areas in the east. Furthermore, the snowmelt contribution to overland flow increases when the soil is saturated and/or frozen. Overland flow starts to decrease in summer under most GCM-scenarios, which is mostly related to a decline in precipitation and a rise in PET (caused by an increase in temperature), along with a change in timing of snowmelt which leads to decline in summer water availability. A drop occurs in June (-21%) and July (-20.7%) under the A1FI and B23 scenarios, respectively. The range of changes of overland flow in spring (-6.2–67.6%) is more than in summer (-21–6.7%). In fall, overland flow decreases for almost all GCM-scenarios in early-mid fall; however, it starts increasing in the late-fall except with the A1B scenario where it increases in all months in the fall. In the winter, all GCM-scenarios indicate an increase in overland flow, except A1FI in the 2020s. The relative changes in overland flow occur in a larger range (-11.8–32%) in the month of February compared to January (-9.6–18.0%), and December (-2.6–20.8%). The overland flow variations in the entire watershed are similar to the variations in the west sub-catchment in both magnitude and direction. In the 2020s, the peaks in the west sub-catchment overland flow occur in June. However, in the 2050, the peaks in overland flow tend to shift from June to May due to an increase in snowmelt in May and a decrease in

snowpack in June. On the other hand, snowpack melt much earlier in spring and diminish earlier in lowland areas in the east sub-catchment. This plays an important role to generate the overland flow peaks in May instead of June in the east sub-catchment in the 2020s and 2050s. Hence, the peak occurs in May for both the 2020s and 2050s due to mainly melting of the remaining spring snowpack.

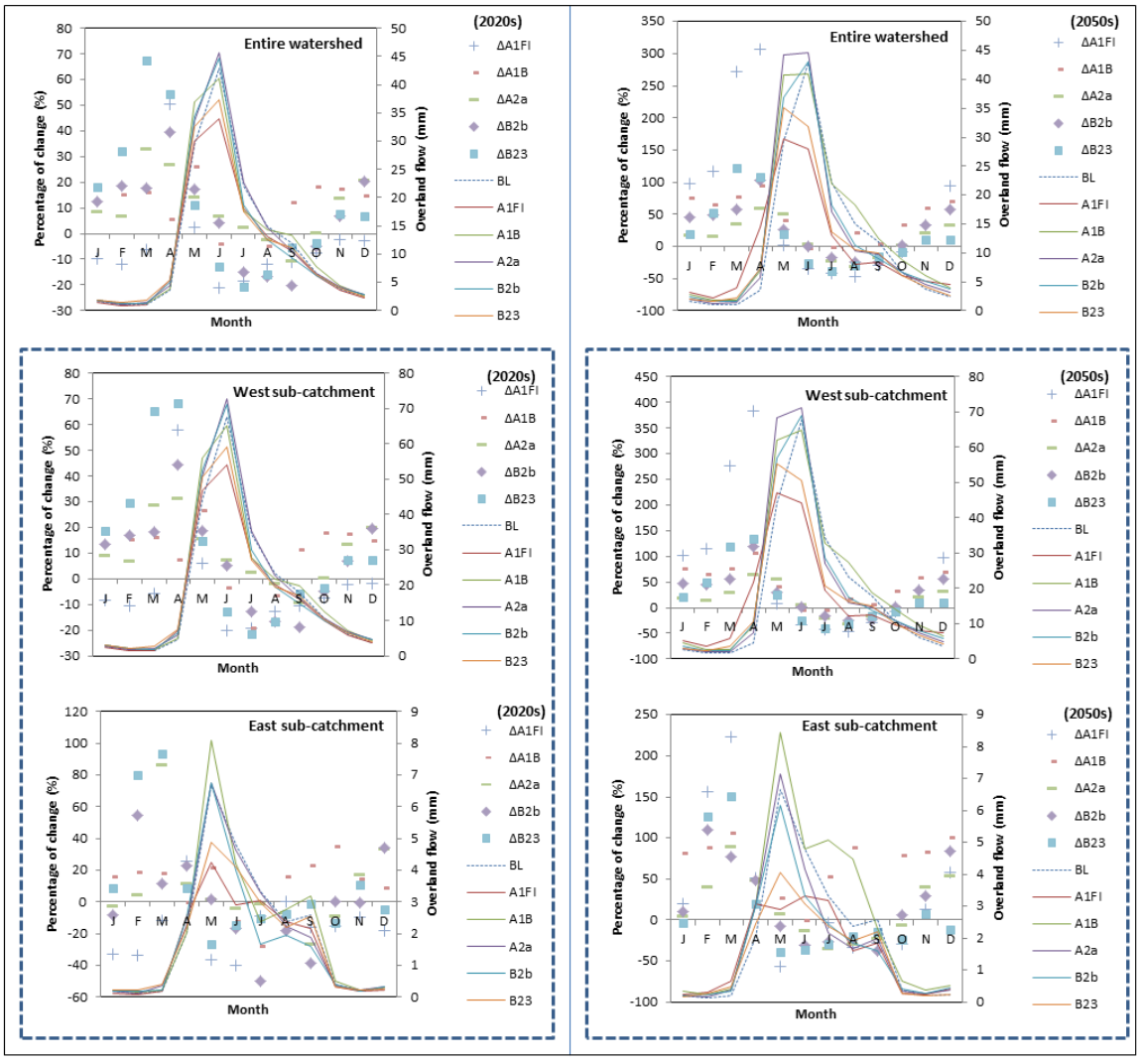

Figure 3.5 Average seasonal changes in overland flow (OL), in the 2020s and 2050s, relative to the baseline (BL)

Seasonal responses of groundwater recharge to climate change are more complex than overland flow. This is because groundwater recharge is affected not only by land surface control factors such as precipitation, temperature, and interception, it also highly depends on UZ control factors such as soil water budget, soil/geological physical properties, and transpiration process. Most of scenarios exhibit an increase in groundwater recharge in winter, early and mid-spring and late fall and a decrease in summer and early fall in the entire watershed (Fig. 3.6). The largest increase in groundwater recharge occurs in March under the B23 and A1FI scenarios in the 2020s and 2050s, respectively. This is mostly associated with a rise in temperature for the B23 (2.4 °C) and A1FI (4.5 °C) scenarios in March, which leads to higher snowmelt. Seasonal variations of groundwater recharge in the west sub-catchment are similar to the entire watershed. However, seasonal change in groundwater recharge in the east sub-catchment occurs with different patterns of variations especially for the A1FI and B23 scenarios.

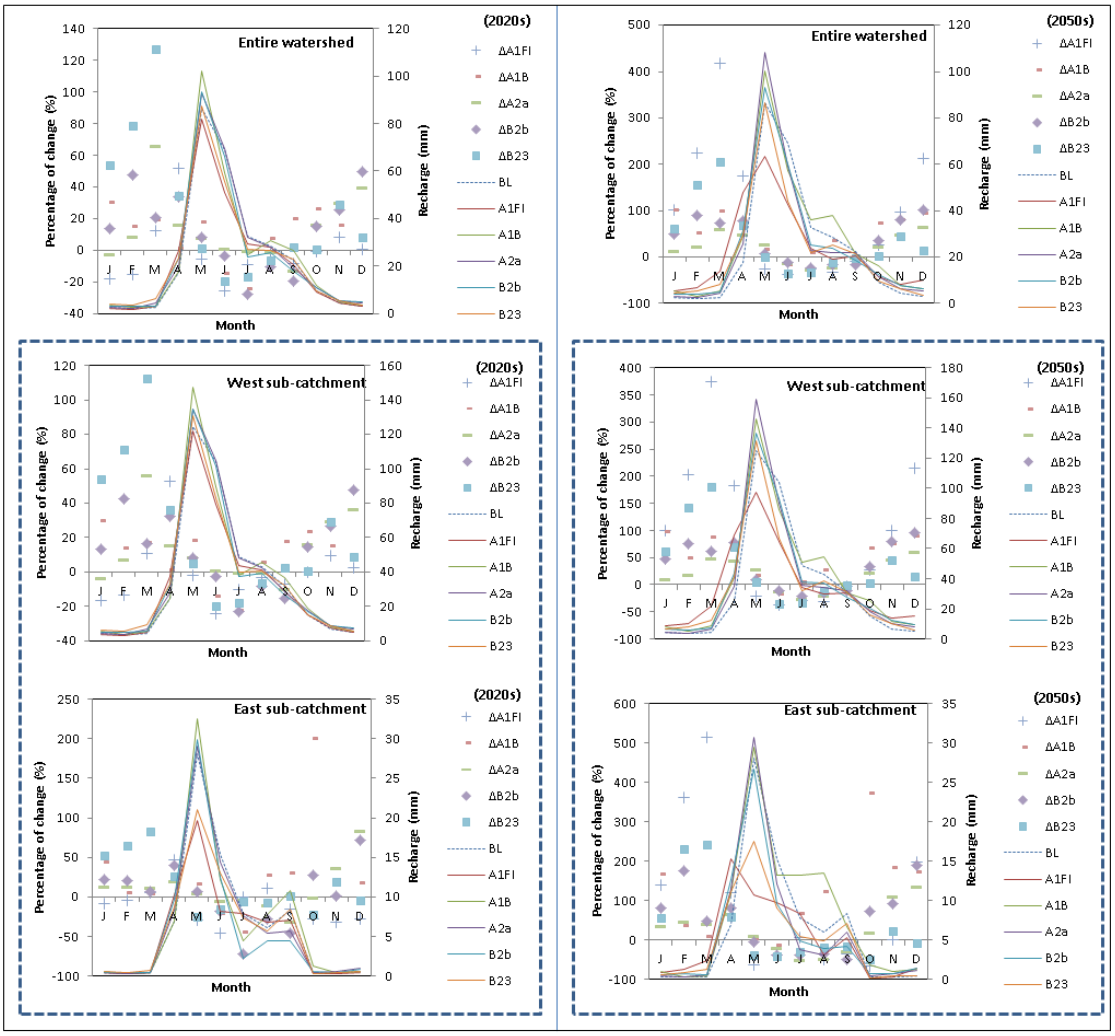

Figure 3.6 Average seasonal changes in groundwater recharge (RE), in the 2020s and 2050s, relative to the baseline (BL)

While overland flow and groundwater recharge exhibits a large range of variation particularly in winter and spring, baseflow has a smaller variability since it generally occurs through slow infiltration, flow and permeable rock (Fig. 3.7). The average monthly baseflow shows a decline in mid-late summer and early-mid fall and a rise in winter and spring under most GCM-scenarios in the 2020s and 2050s in the entire watershed. The largest increases occur in spring particularly in March and April under

B23 in the 2020s and A1FI in the 2050s. The baseflow delay in response (travel time from recharge to discharge) to variations in temperature and precipitation, and also the baseflow magnitude of changes are more complicated than for groundwater recharge and overland flow. This is because baseflow is controlled not only by factors such as land surface and soil layers characteristics, but also by hydrogeological and geological factors that either lead groundwater to channels, or storage in aquifers. The baseflow variations in the entire watershed occur almost in the same direction and magnitude of the baseflow variations in the west sub-catchment. However, baseflow in the east sub-catchment decreases under most scenarios in the 2020s and 2050s. The peaks in baseflow occur in June in the west sub-catchment when the peaks occur in July in the east sub-catchment.

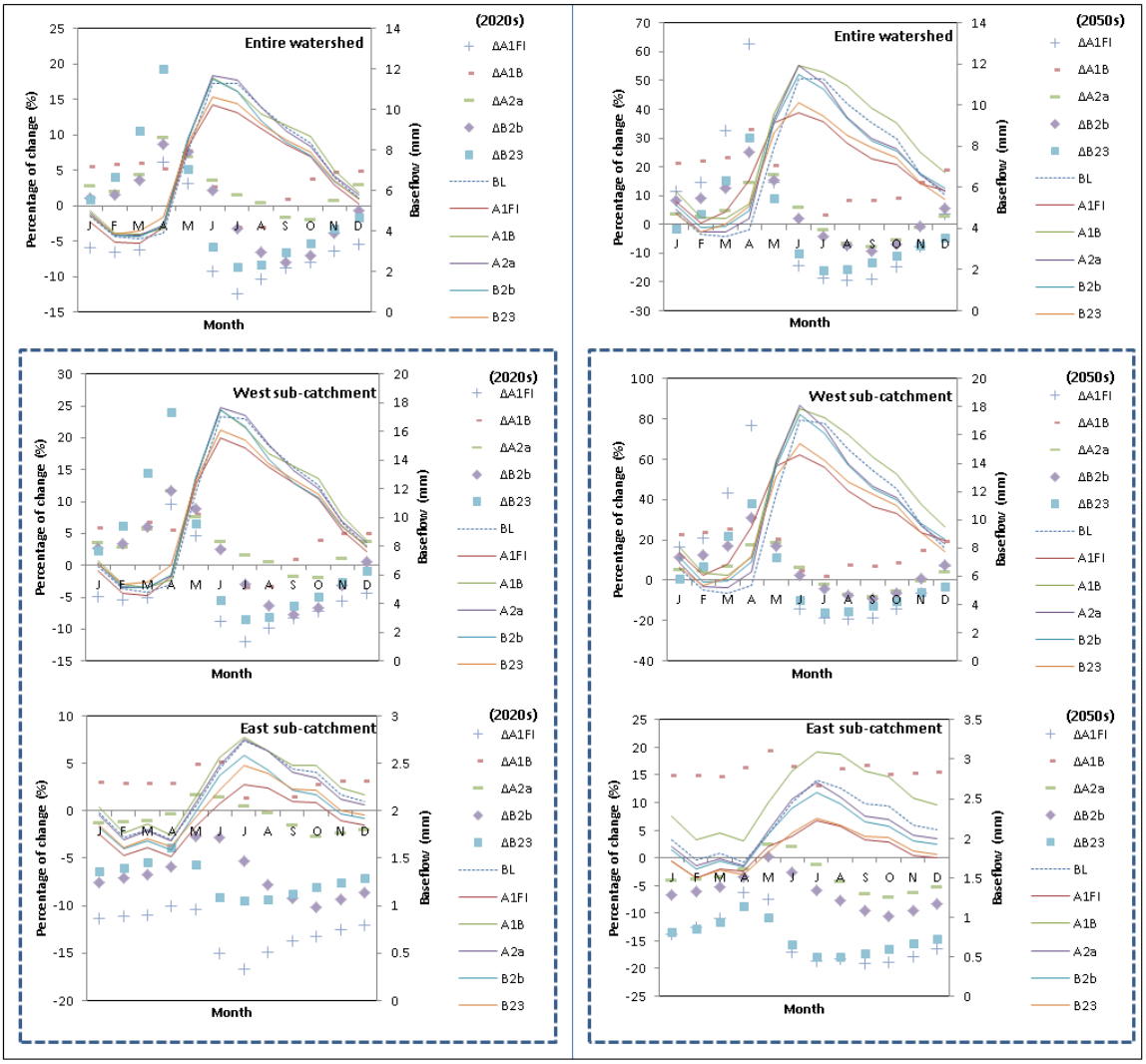

Figure 3.7 Average seasonal changes in baseflow (BF), in the 2020s and 2050s, relative to the baseline (BL)

Average monthly actual evapotranspiration (AET) tends to increase under most GCM-scenarios particularly in late fall, winter, early-mid spring in the entire watershed (Fig. 3.8). In fact, snowmelt results in increased soil moisture and ponded water, and eventually in more water available for evapotranspiration. However, there is not a substantial change in summer compared to winter and early spring; this is due to an increase in temperature and a reduction in soil water, which results in less available water

to the roots and a drop in transpiration. It should be noted that although the percentage changes in winter and fall evapotranspiration are large, there are very small values. The results show that there is more agreement in the direction of change among the scenarios in the summer. In addition, despite overland flow, recharge, and baseflow, there is more consistency between AET variations in the west and east sub-catchments. However, the west sub-catchment AET exhibits the peaks in June in the 2020s and 2050 while the peaks in the east sub-catchment can occur in May, June, and July.

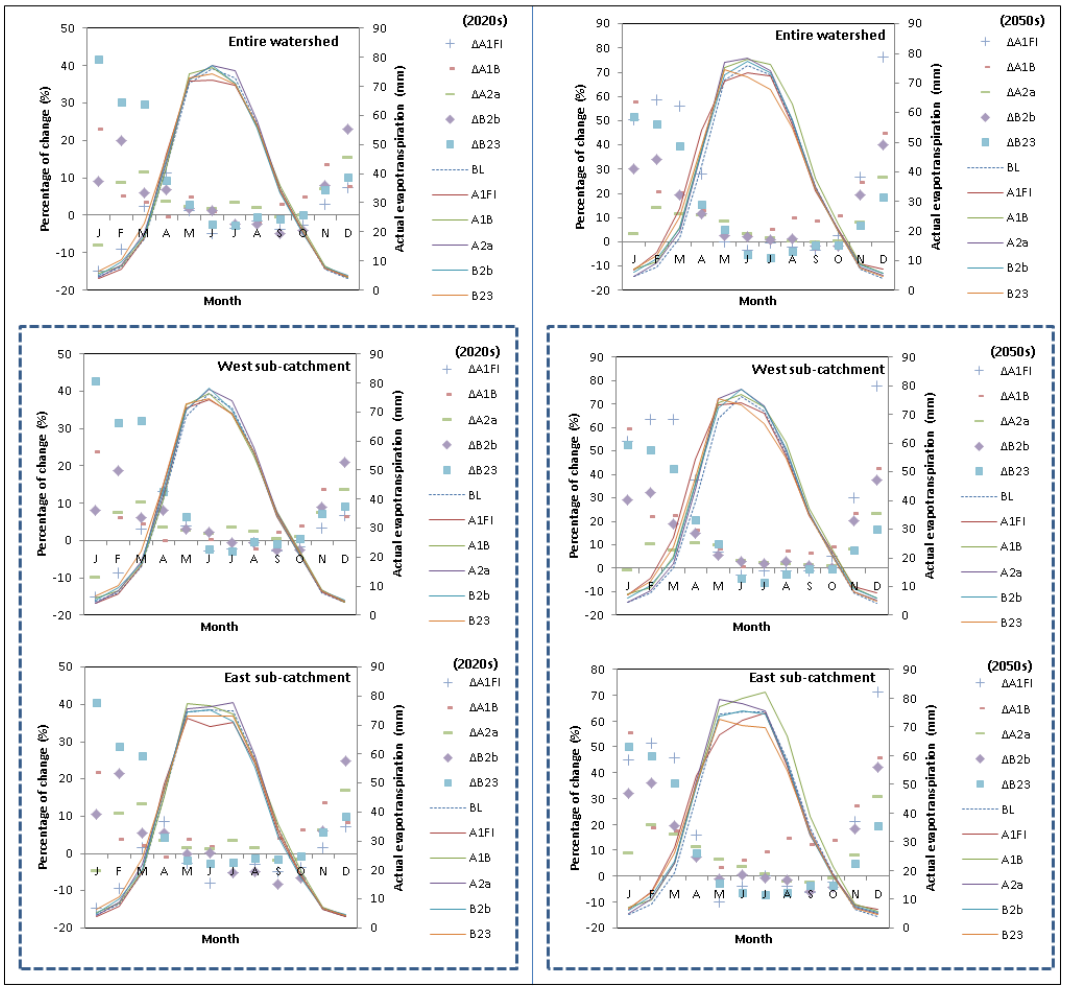

Figure 3.8 Average seasonal changes in evapotranspiration (AET), in the 2020s and 2050s, relative to the baseline (BL)

3.3.3 Simulation of annual and seasonal streamflow

Annual and seasonal variations of streamflow were estimated at the 05BJ004 and 05BJ010 stations. The 05BJ004 station measures the river discharge at the west sub-catchment outlet while the 05BJ010 station measures the discharge of the river entering the Glenmore Reservoir at the east sub-catchment and entire watershed outlets. Simulation of streamflow in the entire watershed reveals that the average annual streamflow decreases for A1FI (-8.5%), B2b (-0.1%), and B23 (-3.4%) and increases for A1B (3.0%) and A2a (4.2%) in the 2020s (Fig. 3.9). However, in the 2050s, streamflow decreases for A1FI (-7.3%), and B23 (-7.7%), and increases for A1B (14.7%), A2a (4.3%), and B2b (2.7) (Fig. 3.9). The predominant behavior of hydrological processes in the west sub-catchment (associated with its geomorphological characteristics) results in generating 94% of the average annual streamflow at the 05BJ004 station from 1961 to 1990 (considering 100% of discharge at the watershed outlet – the 05J010 station). However, this proportion of discharge varies under different scenarios in the 2020s and 2050s (Fig. 3.9).

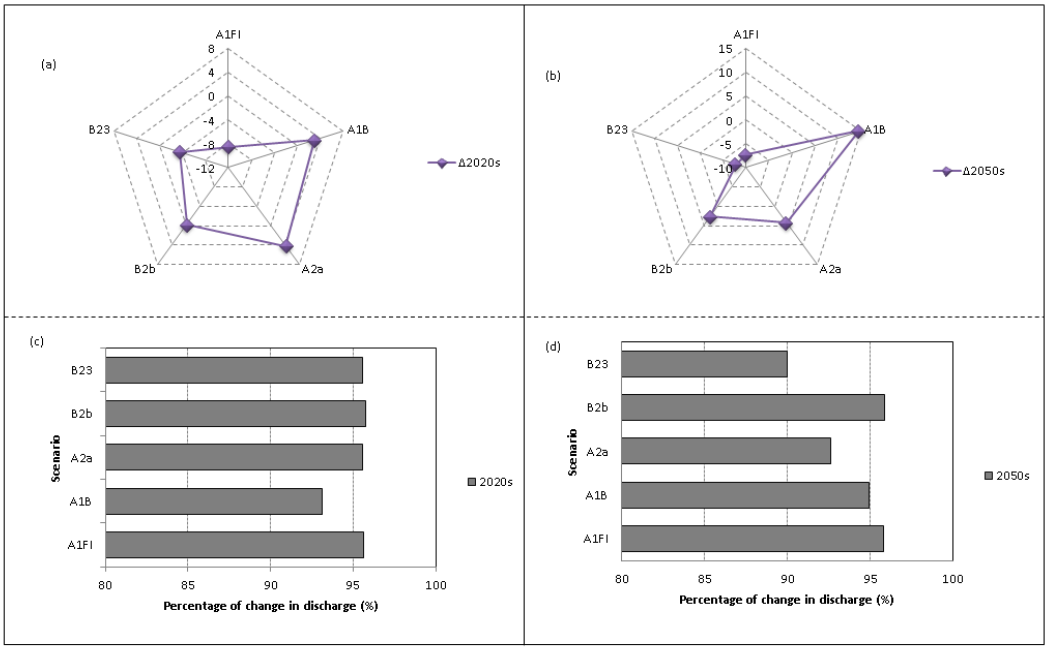

Figure 3.9 Average annual variations in streamflow in the entire watershed in the 2020s and 2050s, relative to the baseline (a and b), and percentage of streamflow that originates at the west sub-catchment outlet (c and d)

In terms of seasonal changes, streamflow tends to decrease for most of the GCM-scenarios in mid-late summer and early fall and increases in winter and spring in the entire watershed in the 2020s (Fig. 3.10). However, in the 2050s, it increases for most of the GCM-scenarios in last fall, winter, and spring, and declines in mid-late summer and early fall. High flows tend to shift from late spring-early fall to the middle of spring-summer particularly in the 2050s, which increases the possibility of spring flood mainly associated with snowmelt at an earlier date. The largest rise in discharge occurs in the month of April under the B23 and A1FI scenarios in the 2020s and 2050s, respectively. In fact, the rise in temperature in April increases rain-on-snow events and rainfall on a melting snowpack generates more overland flow and infiltration. In addition, the high

flow season becomes much shorter. Historically, river discharge exceeds 11 m^3/s during five months (May to September) of a year; however, it only lasts three months (May to July) in the 2050s except under the A1B scenario. Rising temperatures in winter increase the sublimation of snowpack before the melting occurs, and generate a reduced snowpack at lower elevations, due to an increased rain/snow fraction, which results in a reduction of water storage in winter and contribution to river flow in summer. Simulations of the average monthly streamflow at the 0B5J004 and 05BJ010 stations indicate that 90-97% and 87-97% of the average monthly streamflow originates at the 0B5J004 station in the 2020s and 2050s, respectively (Fig. 3.11).

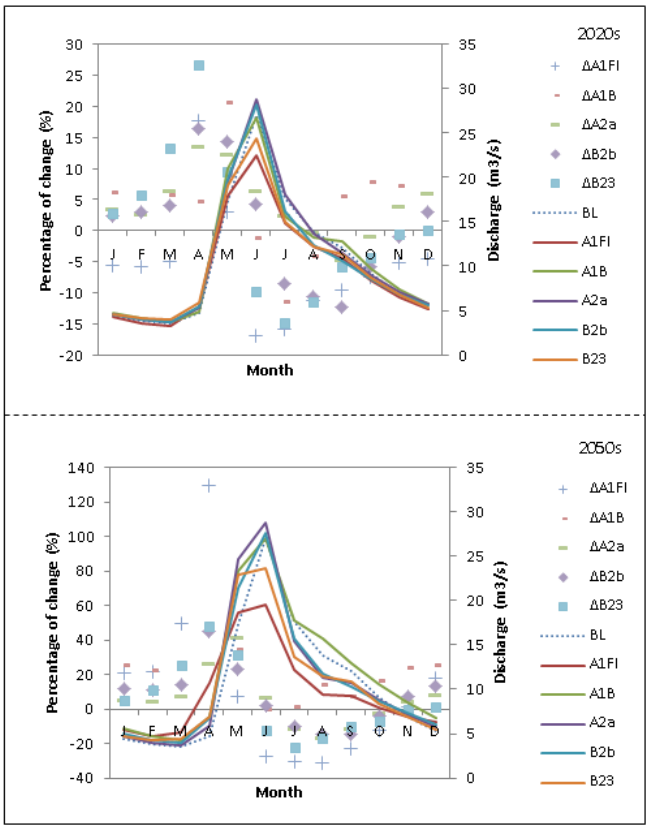

Figure 3.10 Average seasonal variations in streamflow in the entire watershed in the 2020s and 2050s, relative to the baseline

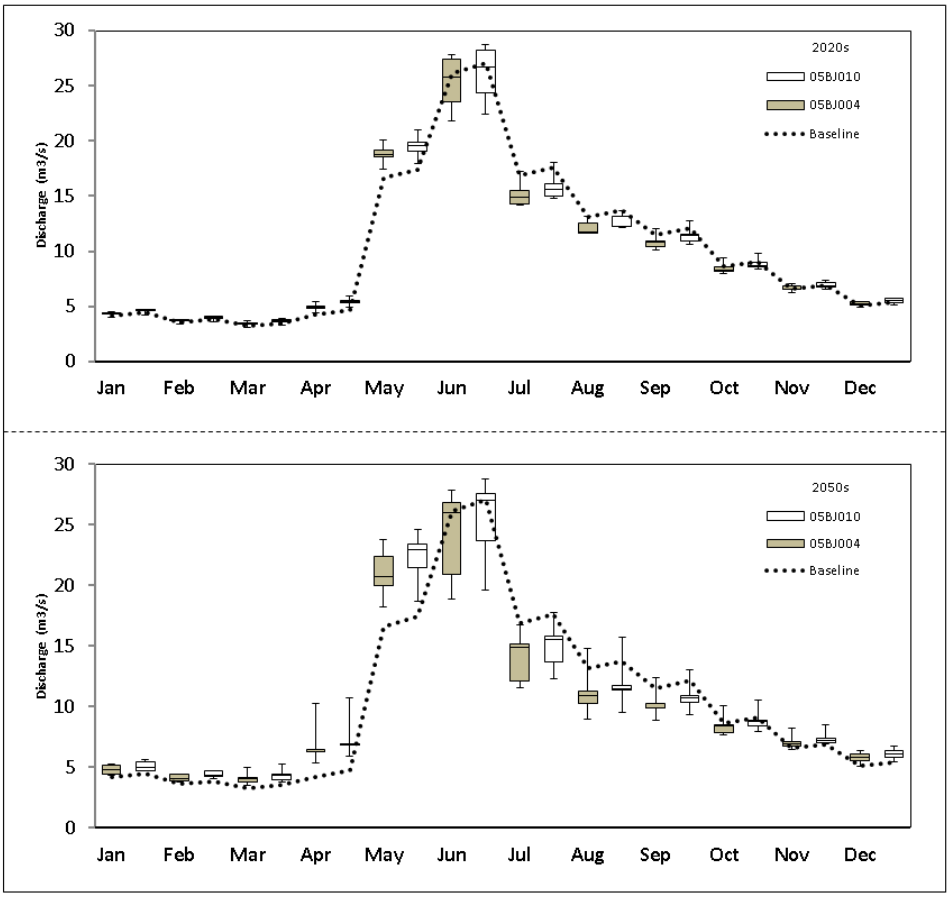

Figure 3.11 Box plot of the average monthly discharge at the west (0B5J004) and east (05BJ010) sub-catchment outlets

3.3.3.1 Flow duration curves

The impact of climate change on river flow ranging from low to peak flows can be represented by a watershed's flow duration curve (FDC). FDCs were constructed for the baseline period and each scenario in the 2020s and 2050s (Fig 3.12). Discharge of river flow were identified at the Q5, Q50, and Q90 (which represent peak, mid-range average flow inflection point, and low daily flows, respectively), related to baseline. The FDCs reveal that most scenarios show an increase in peak flows in the 2020s and 2050s while

this is not the case for low flows under all scenarios in the 2050s. This implies that flood might be more of a concern in the watershed compared to drought. Furthermore, the FDC's steep gradient reflects a flashy flow regime in the watershed.

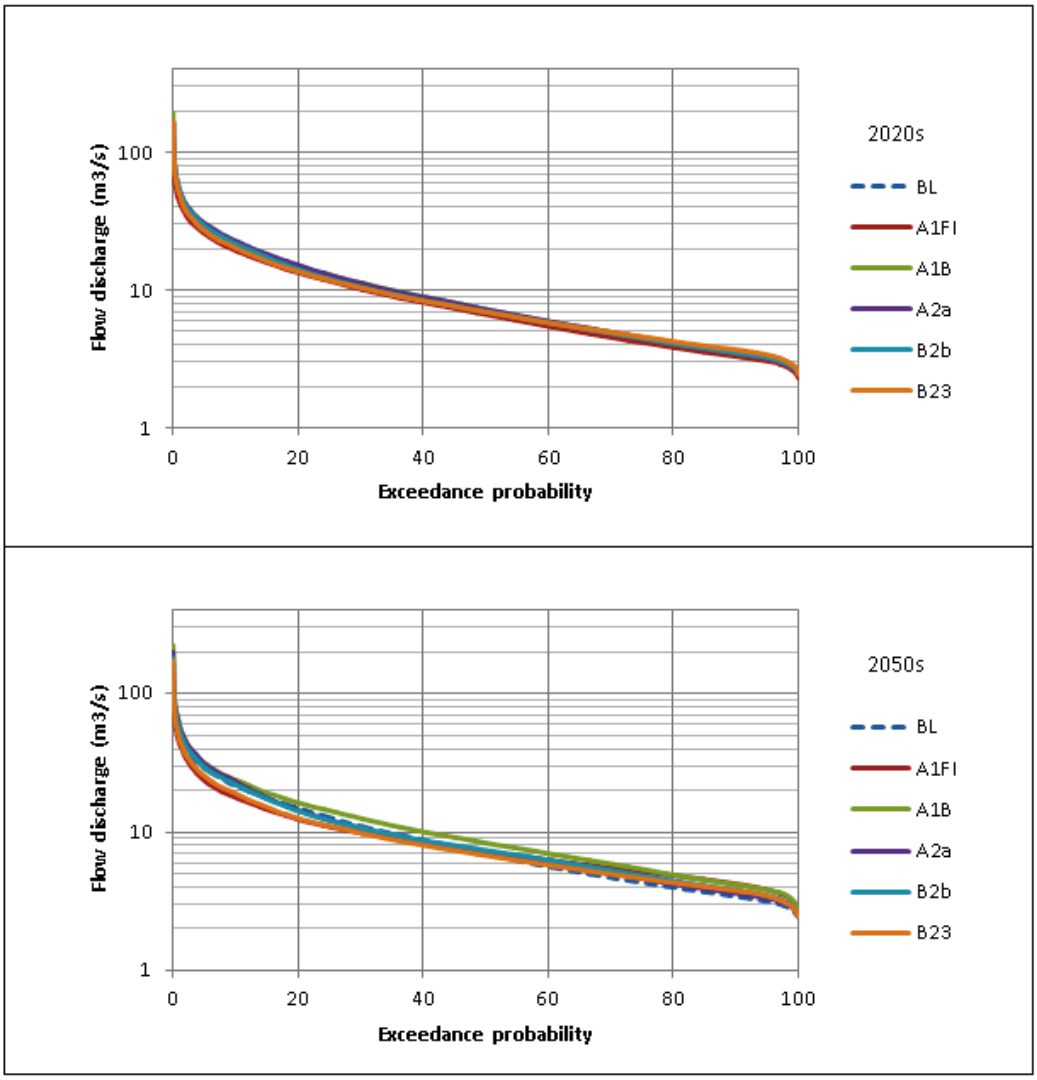

Figure 3.12 Flow duration curves for the baseline and each scenario in the 2020s and 2050s

3.4 Discussion

The results of this study indicate that projected climate changes are expected to have substantial effects on the watershed hydrology. The most critical induced modifications are the shifts in the timing of individual hydrological process that lead to shifts in the temporal patterns of river flow. Changes in seasonal patterns of streamflow can not only alter the overall annual streamflow but can also alter peak and low flows. For example, increases in spring overland flow, groundwater recharge, and baseflow, which are mainly associated with snowmelt and rain-on-snow events result in substantial rise in spring streamflow that increase the possibility of spring flood. On the other hand, a decline in summer and early fall overland flow, groundwater recharge, and baseflow can result in groundwater depletion, especially in the east sub-catchment, which has a large amount of groundwater abstraction.

The future seasonal patterns of streamflow revealed in this study are consistent with the outcomes of studies conducted in other watersheds in Alberta and snow dominated regions in Western North America. For instance, Forbes et al. (2011) investigated the seasonal patterns of streamflow in the Beaver Creek watershed in southern Alberta. They found that streamflow increases in winter and spring and decreases in summer and fall under the majority of climate scenarios. Kienzle et al. (2012) also found a shift in streamflow indicating an increase in winter and spring, and a decrease in late summer and early spring in the Cline River watershed in Alberta. The rise in winter and spring streamflow can be linked to the increase in winter and spring temperature, which results in an increase in snowmelt and in the number of rainfall events (versus snowfall). On the

other hand, an earlier snowmelt and reduced snowpack can be associated to the decline in summer and fall streamflow.

The west and east sub-catchments of the Elbow River watershed differ in terms of LULC heterogeneity, topographic and geomorphology, precipitation and temperature gradients with elevation, proportion of snow versus rain, and surface-groundwater interactions, which result in different hydrological responses to climate change in the two basins and a nonlinear relationship between climate variables and hydrological processes in the entire watershed. This means that changes in total average annual and seasonal climate variables may not necessarily translate into similar changes in hydrological processes in the entire watershed. Therefore, calculating the water balance in each individual sub-catchment, along with the entire watershed provides a better understanding of the hydrological regime in the entire watershed.

The induced hydrological modifications can ultimately influence the economic, ecological, and societal systems in the watershed. Having sufficient knowledge about the hydrological processes and their responses to climate change in each sub-catchment can help water resource management both in terms of a more rigorous assessment, and more efficient decision making processes.

3.5 Conclusions

This study investigated the response of hydrological processes to five climate change scenarios in the Elbow River watershed in southern Alberta, Canada. This response is complex, due to LULC spatial heterogeneity, and different climate and geomorphological characteristics that considerably differ in the two main sub-catchments. Future climate changes are expected to substantially modify the hydrological regime of the watershed over the next 60 years. The induced changes are proportionally more perceptible in the east sub-catchment compared to the west sub-catchment. However, the west sub-catchment governs the watershed behaviour and determines the future changes, over-riding the stronger climate change signal in the east.

Most of the scenarios indicate a reduction in the average annual overland flow, groundwater recharge and baseflow in the east sub-catchment in the 2050s, which might result in water insufficiency when considering the current and projected future water demands. In addition, the decline in the east sub-catchment groundwater recharge can result in groundwater depletion, which is a concern when about 90% of licensed groundwater extractions are located in the east sub-catchment. Although the total water balance in the west sub-catchment is less affected by climate change on an annual basis, it can offset negative water balance in the east sub-catchment. However, the west sub-catchment compensates the diminishing water balance in the east sub-catchment only in winter and spring rather than in summer and early fall when water demand is high.

The pattern of seasonal change generally exhibits a rise in overland flow, groundwater recharge, baseflow, evapotranspiration, and streamflow in the winter-spring and a decline in the summer-fall. The shift in high streamflow from late spring-early fall to the middle of spring-summer could increase the risk of flooding, particularly in the lowlands in the east sub-catchment. The risk of flooding will be enhanced in mid-late spring (April-May), due to an increase in rain-on-snow events coinciding with the highest increase in spring freshet. This might also affect the risk of flooding in the following month of June, since the soil moisture considerably increases to reach the field capacity in the previous months (April-May), resulting in more runoff from rainfall and snowmelt. The FDCs indicate an increase in peak flows under most scenarios in the 2020s and 2050s while there is a reduction in the magnitude of low flows under all scenarios in the 2050s. This implies that flood might be more of a concern in the watershed compared to drought.

This study reveals that a greater understanding of climate change impacts on the water balance of a watershed with differences in sub-regional settings is achieved when capturing the hydrological process responses of each sub-catchment individually.

ACKNOWLEDGEMENTS

This project was funded by a research grant awarded to Dr. Danielle Marceau by Tecterra and Alberta Environment and Sustainable Resource Development (AESRD), and by an Alberta Innovates Technology Futures graduate student scholarship awarded to Babak Farjad. We thank Dr. Shawn Marshall from the Department of Geography at the

University of Calgary for his careful reviews and constructive suggestions. We also thank insightful discussions with Patrick Delaney and Ying Qiao from DHI Water and Environment Canada.

3.6 References

Barrow E, Yu G (2005) *Climate Scenarios for Alberta*. Report Prepared for the Prairie Adaptation Research Collaborative (PARC) in co-operation with Alberta Environment, pp. 1–73.

Buytaert W, Vuille M, Dewulf A, Urrutia R, Karmalkar A, Celleri R (2010) Uncertainties in climate change projections and regional downscaling in the tropical Andes: implications for water resources management. *Hydrology and Earth System Sciences* 14(7): 1247-1258.

Charlton R, Fealy R, Moore S, Sweeney J, Murphy C (2006) Assessing the impact of climate change on water supply and flood hazard in Ireland using statistical downscaling and hydrological modelling techniques. *Climatic change* 74(4): 475-491

Chang H, Jung I W (2010) Spatial and temporal changes in runoff caused by climate change in a complex large river basin in Oregon. *Journal of Hydrology* 388(3): 186-207.

Chen Z, Grasby, S E, Osadetz K G, Fesko P (2006). Historical climate and stream flow trends and future water demand analysis in the Calgary region, Canada. *Water Science & Technology* 53(10): 1-11.

Dessu S B, Melesse A M (2013) Impact and uncertainties of climate change on the hydrology of the Mara River basin, Kenya/Tanzania. *Hydrological Processes* 27(20): 2973-2986.

Espadafor M, Lorite I J, Gavilán P, Berengena J (2011) An analysis of the tendency of reference evapotranspiration estimates and other climate variables during the last 45 years in Southern Spain. *Agricultural Water Management* 98(6): 1045-1061.

Farjad B, Gupta A, Marceau D J (2015) *Hydrological Regime Responses to Climate Change for the 2020s and 2050s Periods in the Elbow River Watershed in Southern Alberta, Canada*. In Environmental Management of River Basin Ecosystems, M. Ramkumar, K. Kumarasamy, and R. Mohanraj, Eds, Springer International Publishing, pp. 65-89.

Forbes K A, Kienzle S W, Coburn C A, Byrne J M, Rasmussen J (2011) Simulating the hydrological response to predicted climate change on a watershed in southern Alberta, Canada. *Climatic Change* 105(3-4): 555-576.

Fowler H J, Blenkinsop S, Tebaldi C (2007) Linking climate change modelling to impacts studies: recent advances in downscaling techniques for hydrological modelling. *International Journal of Climatology* 27(12): 1547-1578.

Frost R E, Woods K B (1948) Airphoto Patterns of Soils of the Western United States (No. TR-85). U. S. Department of Commerce Civil Aeronautics Administration. Technical report, 76 pp.

Gan T Y (1998) Hydroclimatic trends and possible climatic warming in the Canadian Prairies. *Water Resources Research* 34(11): 3009-3015.

Gan T Y (2000) Reducing vulnerability of water resources of Canadian prairies to potential droughts and possible climatic warming. *Water Resources Management* 14(2): 111-135.

Gan T Y, Burges S J (1990) An assessment of a conceptual rainfall-runoff model's ability to represent the dynamics of small hypothetical catchments: 2. Hydrologic responses for normal and extreme rainfall. *Water Resources Research* 26(7): 1605-1619.

Gan R, Luo Y, Zuo Q, Sun L (2015) Effects of projected climate change on the glacier and runoff generation in the Naryn River Basin, Central Asia. *Journal of Hydrology* 523: 240-251.

Goderniaux P, Brouyère S, Fowler H J, Blenkinsop S, Therrien R, Orban P, Dassargues A (2009) Large scale surface–subsurface hydrological model to assess climate change impacts on groundwater reserves. *Journal of Hydrology* 373(1): 122-138.

Gonçalves M, Barrera-Escoda A, Guerreiro D, Baldasano J M, Cunillera J (2014) Seasonal to yearly assessment of temperature and precipitation trends in the North Western Mediterranean Basin by dynamical downscaling of climate scenarios at high resolution (1971–2050) *Climatic Change* 122(1-2): 243-256.

Gombault C, Sottile M F, Ngwa F F, Madramootoo C A, Michaud A R, Beaudin I, Chikhaoui M (2015) Modelling climate change impacts on the hydrology of an agricultural watershed in southern Québec. *Canadian Water Resources Journal/Revue canadienne des ressources hydriques* 40 (1): 71-86.

Grillakis M G, Koutroulis A G, Tsanis I K (2011) Climate change impact on the hydrology of Spencer Creek watershed in Southern Ontario, Canada. *Journal of Hydrology* 409(1): 1-19.

Hargreaves, G. H., & Samani, Z. A. (1985). Reference crop evapotranspiration from ambient air temperature. *American Society of Agricultural Engineers* 1(2): 96-99.

Hay L E, McCabe G J (2010) Hydrologic effects of climate change in the Yukon River Basin. *Climatic change* 100(3-4): 509-523.

Hasbani J-G, Wijesekara N, Marceau DJ (2011) *An interactive method to dynamically create transition rules in a land-use cellular automata model*. In: Cellular automata simplicity behind complexity. Salcido, A. (Ed.), InTech Publisher. http://www.intechopen.com/books/cellular-automata-simplicity-behind-complexity/aninteractive-method-todynamically-create-transition-rules-in-aland- use-cellular-automata-model.

He J, Valeo C, Chu A, Neumann N. F. (2011) Stormwater quantity and quality response to climate change using artificial neural networks. *Hydrological Processes* 25(8): 1298-1312.

Huth Radan, Kysely Jan, Dubrovsky Martin (2001) Time structure of observed, GCM-simulated, downscaled, and stochastically generator daily temperature series. *Journal of Climate* 14(20): 4047–4061.

IPCC (2014) Climate change 2014: *Impacts, Adaptation, and Vulnerabilit*y. 5th assessment report (AR5): Intergovernmental Panel on Climate Change (IPCC), Working Group II.

Jones P D, Hulme M (1996) Calculating regional climatic time series for temperature and precipitation: methods and illustrations. *International Journal of Climatology* 16(4): 361-377.

Jothityangkoon C, Sivapalan M, Farmer D L (2001) Process controls of water balance variability in a large semi-arid catchment: downward approach to hydrological model development. *Journal of Hydrology* 254(1): 174-198.

Kay A L, Davies H N, Bell V A, Jones R G (2009) Comparison of uncertainty sources for climate change impacts: flood frequency in England. *Climatic Change* 92(1-2): 41-63.

Kay A L, Davies H N (2008) Calculating potential evaporation from climate model data: a source of uncertainty for hydrological climate change impacts. *Journal of Hydrology* 358(3): 221-239.

Kienzle S W, Nemeth M W, Byrne J M, MacDonald R J (2012) Simulating the hydrological impacts of climate change in the upper North Saskatchewan River basin, Alberta, Canada. *Journal of Hydrology* 412: 76-89.

Kristensen and Jensen (1975) A model for estimating actual evapotranspiration from potential evapotranspiration. *Nordic Hydrology* 6:170–188.

Ludwig R, May I, Turcotte R, Vescovi L, Braun M, Cyr J F, Fortin L G, Chaumont D, Biner S, Chartier I, Caya D, Mauser W (2009) The role of hydrological model complexity and uncertainty in climate change impact assessment. *Advances in Geosciences* 21(21): 63-71.

Minville M, Brissette F, Leconte R (2008) Uncertainty of the impact of climate change on the hydrology of a nordic watershed. *Journal of Hydrology* 358(1): 70-83.

Montenegro S, Ragab R (2012) Impact of possible climate and land use changes in the semi arid regions: A case study from North Eastern Brazil. *Journal of Hydrology* 434: 55-68.

Palutikof J P, Winkler J A, Goodess C M, Andresen J A (1997) The simulation of daily temperature time series from GCM Output. Part 1: comparison of model data with observations. *Journal of Climate* 10: 2497–2513.

Pernitsky D J, Guy N D (2010) Closing the South Saskatchewan River Basin to new water licences: effects on municipal water supplies. *Canadian Water Resources Journal* 35(1): 79-92.

Priestley C H B, Taylor R J (1972) On the assessment of surface heat flux and evaporation using large-scale parameters. *Monthly Weather Review* 100(2): 81-92.

Prudhomme C, Reynard N, Crooks S (2002) Downscaling of global climate models for flood frequency analysis: where are we now? *Hydrological Processes* 16(6): 1137-1150.

Prudhomme C, Davies H (2009) Assessing uncertainties in climate change impact analyses on the river flow regimes in the UK. Part 2: future climate. *Climatic Change* 93(1-2): 197-222.

Oudin L, Hervieu F, Michel C, Perrin C, Andréassian V, Anctil F, Loumagne C (2005) Which potential evapotranspiration input for a lumped rainfall–runoff model?: Part 2—Towards a simple and efficient potential evapotranspiration model for rainfall–runoff modelling. *Journal of Hydrology* 303(1): 290-306.

Refsgaard J C (1997) Model and data requirements for simulation of runoff and land surface processes. In Land Surface Processes in Hydrology,. Sorooshian S., Gupta H., Rodda J. (Eds.), Springer Berlin Heidelberg, pp. 423-452.

Sauchyn D, Barrow E, Fang X, Henderson N, Johnston M, Pomeroy J, ... Williams B (2009) *Saskatchewan's natural capital in a changing climate: an assessment of*

impacts and adaptation. Report to Saskatchewan Ministry of Environment from the Prairie Adaptation Research Collaborative, 162 pp.

Setegn, S. G., D. Rayner, A. M. Melesse, B. Dargahi, and R. Srinivasan (2011), Impact of climate change on the hydroclimatology of Lake Tana Basin, Ethiopia, *Water Resources Research*, 47, W04511, doi:10.1029/2010WR009248.

Scurlock JMO, Asner GP, Gower ST (2001) *Worldwide Historical estimates of Leaf Area Index, 1932–2000*, DOE Scientific and Technical Information. http://www.osti.gov/bridge/.

Schindler D W, Donahue W F (2006) An impending water crisis in Canada's western prairie provinces. *Proceedings of the National Academy of Sciences* 103(19): 7210-7216.

Sentelhas P C, Gillespie T J, Santos E A (2010) Evaluation of FAO Penman–Monteith and alternative methods for estimating reference evapotranspiration with missing data in Southern Ontario, Canada. *Agricultural Water Management* 97(5): 635-644.

Shepherd A, Gill K M, Rood S B (2010). Climate change and future flows of Rocky Mountain rivers: converging forecasts from empirical trend projection and down-scaled global circulation modelling. *Hydrological Processes* 24(26): 3864-3877.

Sultana Z, Coulibaly P (2011) Distributed modelling of future changes in hydrological processes of Spencer Creek watershed. *Hydrological Processes* 25(8): 1254-1270.

Tanzeeba S, Gan T Y (2012) Potential impact of climate change on the water availability of South Saskatchewan River Basin. *Climatic Change* 112(2): 355-386.

Thompson J R, Green A J, Kingston D G (2014) Potential evapotranspiration-related uncertainty in climate change impacts on river flow: An assessment for the Mekong River basin. *Journal of Hydrology* 510: 259-279.

Vano J A, Voisin N, Cuo L, Hamlet A F, Elsner M M, Palmer R N, Polebitski A, Lettenmaier D P (2010) Climate change impacts on water management in the Puget Sound region, Washington State, USA. *Climatic Change* 102(1-2): 261-286.

Whitfield P H, Cannon A J (2000) Recent variations in climate and hydrology in Canada. *Canadian Water Resources Journal* 25(1): 19-65.

Wilby, R. L., and I. Harris (2006), A framework for assessing uncertainties in climate change impacts: Low-flow scenarios for the River Thames, UK, *Water Resources Research*, 42, W02419, doi:10.1029/2005WR004065.

Wilby R L, Wigley T M L (1997) Downscaling general circulation model output: a review of methods and limitations. *Progress in Physical Geography* 21(4): 530-548.

Wijesekara G N, Farjad B, Gupta A, Qiao Y, Delaney P, Marceau D J (2014) A Comprehensive Land-Use/Hydrological Modeling System for Scenario Simulations in the Elbow River Watershed, Alberta, Canada. *Environmental Management* 53(2): 357-381.

Wood A W, Lettenmaier D P, Palmer R N (1997) Assessing climate change implications for water resources planning. *Climatic Change* 37(1): 203-228.

World water development report (WWDR4) (2012) *Managing Water under Uncertainty and Risk*. The United Nations World Water Development Report 4, Volume 1, Sixth World Water Forum, Marseille, France, March 12-16.

Xu C Y (1999) From GCMs to river flow: a review of downscaling methods and hydrologic modelling approaches. *Progress in Physical Geography* 23(2): 229-249.

Zhang H, Huang G H, Wang D, Zhang X (2011) Uncertainty assessment of climate change impacts on the hydrology of small prairie wetlands. *Journal of Hydrology* 396(1): 94-103.

Summary

In Chapter Three, we learned how hydrological processes respond to future climate change scenarios in the west, east, and entire watershed, annually and seasonally. The future modifications of the watershed hydrology will not only be related to climate change; LULC change may also cause modifications in the watershed hydrology. In the next Chapter, we will investigate the combined and separate impact of climate and LULC change on the hydrology of the watershed.

Chapter 4 : A Modeling Framework to Forecast Hydrological Regime under Scenarios of Climate and Land-use/cover Change

Abstract

The Elbow River watershed, located in the foothills of the Rocky Mountains, has experienced several extreme hydrological events such as droughts and floods over the last century. It is therefore critical to understand the future possible responses of the hydrological processes of the watershed to changes in climate and land-use/land-cover (LULC) since they can induce considerable stress along with economic and social costs. Very little attention has been given so far in the literature to the combined impact of climate and LULC change on hydrological processes at the watershed scale, which might result in an over- or under-estimation of the responses. This study aims at understanding the relationship between climate, LULC, and hydrology using an integrated modeling framework. The physically-based, distributed MIKE SHE/MIKE 11 model was coupled with a LULC cellular automata model to simulate hydrological processes using two extreme GCM-scenarios, NCARPCM-A1B and CGCM2-B2(3), and two LULC change scenarios in the 2020s and 2050s. Results reveal that the LULC change scenarios increase the average annual streamflow, which amplifies the magnitude of rise associated with the A1B climate scenario and compensates for the decline linked to the B2(3) climate scenario. In addition, LULC change substantially modifies the river regime in the east sub-catchment, where urbanization occurs. The separated impacts of climate and LULC change on streamflow are positively correlated in winter and spring, which intensifies their influence and leads to a rise in streamflow, which increases the vulnerability of the

watershed to floods, particularly in spring. The flow duration curves indicate that LULC change has a greater contribution to peak flows than climate change in both the 2020s and 2050s. This study highlights the importance of investigating the combined impact of climate and LULC change to avoid underestimating or overestimating the hydrological response of a watershed.

4.1 Introduction

Water stress is predicted to increase across the world as a result of population growth and climate change. In 1955, only seven countries were identified as being under water stress conditions while this number increased to 20 in 1990 and is expected to reach between 30 and 35 by 2025. Two-third of the world population is projected to be living in water-stressed countries by the year 2050 (Gosain et al. 2006).

Climate and land-use/land-cover (LULC) changes are two factors that can directly and indirectly alter water supply (Li et al. 2009; Gathenya et al. 2011). Changes in LULC can influence hydrological regimes through modifications of the infiltration rates (Weatherhead and Howden 2009), evapotranspiration losses (Dunn and Mackay 1995), and both the peak runoff and the total runoff volume (Hundecha and Bárdossy 2004). Climate change can alter the timing of high flows (Kundzewicz et al. 2008), and modify the frequency and magnitude of extreme events, such as floods and droughts (Lehner et al. 2006).

Numerous studies have been conducted to investigate hydrological responses to future climate change scenarios (Boyer et al. 2010; Grillakis et al. 2011; Barron et al. 2012). Climate models, downscaling techniques, and hydrological models serve as major tools for climate impact assessment by translating the meteorological forcing into responses of hydrological processes (Forbes et al. 2011; Kienzle et al. 2012). However, these studies do not take into account the dynamics of land surface in the hydrological system (Bronstert 2004). In other words, changes in the physical properties of the land surface are mostly neglected in both the calibration of the hydrological model and simulation conducted with this model. Neglecting changes in physical land properties introduces uncertainty in the model outcomes, especially for long-term climate impact analyses.

Other studies have focused on the impact of LULC change on hydrology (Arnold and Gibbons 1996; Thanapakpawin et al. 2007; Wijesekara et al. 2012). Changes in LULC patterns, obtained from either LULC change modeling or hypothetical scenarios, are incorporated into hydrological models. These models range from simple rainfall-runoff models such as those based on unit hydrographs (Jakeman et al. 1993) that provide limited information on the relationship between LULC patterns and hydrological components (Abbott et al. 1986), to distributed physically-based models such as MIKE SHE (Dunn and Mackay 1995) that represent the spatial variability of the surface and subsurface along with their interactions in a watershed (Wijesekara et al. 2014). In these studies, it is assumed that the climate remains constant, an assumption that conflicts with the inherent complex behaviour of the system. For instance, the evapotranspiration (ET) process (which is a major component of water balance) is fully controlled by both climate

factors, such as temperature, net radiation, turbulent transport, and LULC factors, such as leaf area and root depth. However, their relative importance varies with different conditions. For instance, leaf area, net radiation, and turbulent transport are the factors controlling ET in a wet climate, which may not be the case in a dry climate (Zhang et al. 2001). Hendriks (2010) showed that change from forest to grassland can affect ET differently according to climate conditions. In a dry climate, a conversion from forest to grassland caused an increase in actual ET while it did not necessarily increase ET in wet climate conditions. This is because the aerodynamic resistance and surface resistance respond differently to different climatic conditions.

Overall, an evaluation of the response of a hydrological regime based solely on climate or LULC change may not provide a reliable conclusion since the hydrological regime is tied to these two controlling factors. In other words, a clear understanding of hydrological processes can be difficult to ascertain from LULC or climate change alone when a complex dynamical and physical interaction exists between those components (Notebaert et al. 2011).

Despite the need for an integrated framework to investigate the combined effects of future climate and LULC changes on hydrology, to date, not only few studies have been conducted, but they also have limitations in the way they address the complexity of some major physical processes. For instance, Tu (2009) and Antonellini et al. (2014) employed a lumped, conceptual hydrological model to simulate hydrological processes under climate and LULC change. However, these models are climate sequence dependent and

increase the uncertainty linked to calibration compared to physically-based model employed for climate impact assessment (Gan and Burges 1990). Khoi and Suetsugi (2014) employed the semi-distributed SWAT model to evaluate responses of hydrological processes to climate and LULC change in the Be River Catchment, in Vietnam. The SWAT model uses a number of empirical equations that were developed in the US climate conditions, which may not be suitable for different climate conditions. For instance, the SCS (Soil Conservation Service) curve number equation was developed based on rainfall-runoff relationships in small rural watersheds across the U.S over 20 years (Neitsch et al. 2011).

Overall, a physically-based fully distributed model is an effective tool to capture the spatial variability of climate, LULC, and hydrology in an integrated modeling framework especially when the dynamics of land surface is considered during the calibration and validation processes. Montenegro and Ragab (2012) used the physically-based distributed DiCaSM model to assess the combined impact of climate and LULC in the Ipanema catchment in Brazil. However, they calibrated and validated the model based on constant LULC conditions and changing climate rather than applying different LULC maps corresponding to different climate time intervals specified for the model simulation periods.

Other limitations are associated with the way LULC changes are predicted. Some studies set up hypothetical LULC change scenarios (e.g., catinga forest replaced with castor beans in Montenegro and Ragab' study, 2012) while others generate only one LULC map

for a specific year corresponding to long-term projections of climate change (Tong et al. 2012; Wang et al. 2014). For example, Wang et al. (2014) employed a LULC map generated for the year 2030 corresponding to projected climate scenarios for the period of 2016–2040. The LULC map of the 2030 was applied into the SWAT model to simulate hydrological processes under different climate scenarios over 25 years in the Wolf Bay watershed in Alabama, USA that is expected to experience considerable urbanization. This may result in overestimating run-off in the earlier half of the simulation period and underestimating it in the second half of the period. An integrated modeling system requires a rigorous LULC prediction method to replicate spatial patterns and real-world dynamics. Prediction of LULC changes should be done at different time intervals in a spatially explicit context, especially for long-term climate and LULC impact assessment in an urban watershed.

Finally, limitations associated with projection of climate change scenarios also exist. For example, Tong et al. (2012) employed hypothetical values to define future climate conditions rather than using GCMs, which are required to adequately represent physical processes in the atmosphere, ocean, land surface, and cryosphere, along with geophysical climate feedbacks (changes in water vapor, clouds, and sea ice albedo) and biogeochemieal feedbacks (changes in sources of greenhouse gases and vegetation albedo).

Addressing the limitations of the previous studies, this research aims at understanding the relationship between climate, LULC, and hydrology using an integrated modeling

framework which consists of three major components: (i) a LULC change cellular automata (CA) model, (ii) the distributed physically-based, MIKE SHE/MIKE 11 model, and (iii) GCM scenarios from the Intergovernmental Panel on Climate Change. The framework is applied to the Elbow River watershed in southern Alberta, Canada to understand how hydrological processes respond to both LULC and climate change.

4.2 Method

In this section, the study area is first described, followed by the methodological framework.

4.2.1 The Elbow River watershed

The Elbow River watershed (Fig. 4.1) lies between 50^{o} 30' and 51^{o} 20' north latitude and 114^{o} 00' and 115^{o} 00' west longitude with a drainage area of 1235 km^2. The river originates in the eastern slopes of the Rocky Mountains and flows eastward, before entering the Glenmore reservoir and the Bow River in the City of Calgary. Elevations of the watershed range from a high of over 3,000 m above sea level to a low of 1,080 m. The watershed is characterized by a complex hydrological regime due to variations in climate, geomorphology, and topography in the west and east sub-catchments, along with complex surface and groundwater interactions along the river. In addition, the hydrology of the watershed is influenced by heterogeneous LULC that includes evergreen forest (34%), agricultural land (16.7%), deciduous forest (10%), rangeland/parkland (6.2%), urban area (5.9%), and forest clear-cut (1.8%) (Wijesekara et al., 2014).

Long-term historical climate data (1961–2005), obtained from Alberta Environment and Sustainable Resource Development (AESRD), indicate that the mean annual temperature is 2.5 °C with the warmest month being July (13.2 °C) and the coldest month being January (-9 °C). The mean annual precipitation is 690 mm with a high spatial variability due to the large differences in elevation. The largest amount of precipitation occurs in June (99.6 mm). The mean annual discharge varies from a low of 3.33 m^3/s at the 05BJ009 hydrometric station in the front ranges of the Rocky Mountains in the west sub-catchment to a high of 10 m^3/s at the 05BJ010 station upstream of the outlet of the watershed (Fig. 4.1).

The hydrology and ecosystem balance of the watershed are under great pressure due to the rapid population growth and land development in the east portion of the watershed, included and adjacent to the City of Calgary. The population of Calgary has increased by 71% between 1985 and 2010 (The City of Calgary 2010), and is expected to rise on average by 1.6% annually in the next 25 years (Alberta Treasury Board and Finance, 2014). The watershed has experienced several droughts (Gan 1998) and floods over the past decades (The City of Calgary 2013). It is therefore critical to understand the future possible responses of the hydrological processes to changes in climate and LULC since they can induce considerable stress in addition to economic and social costs.

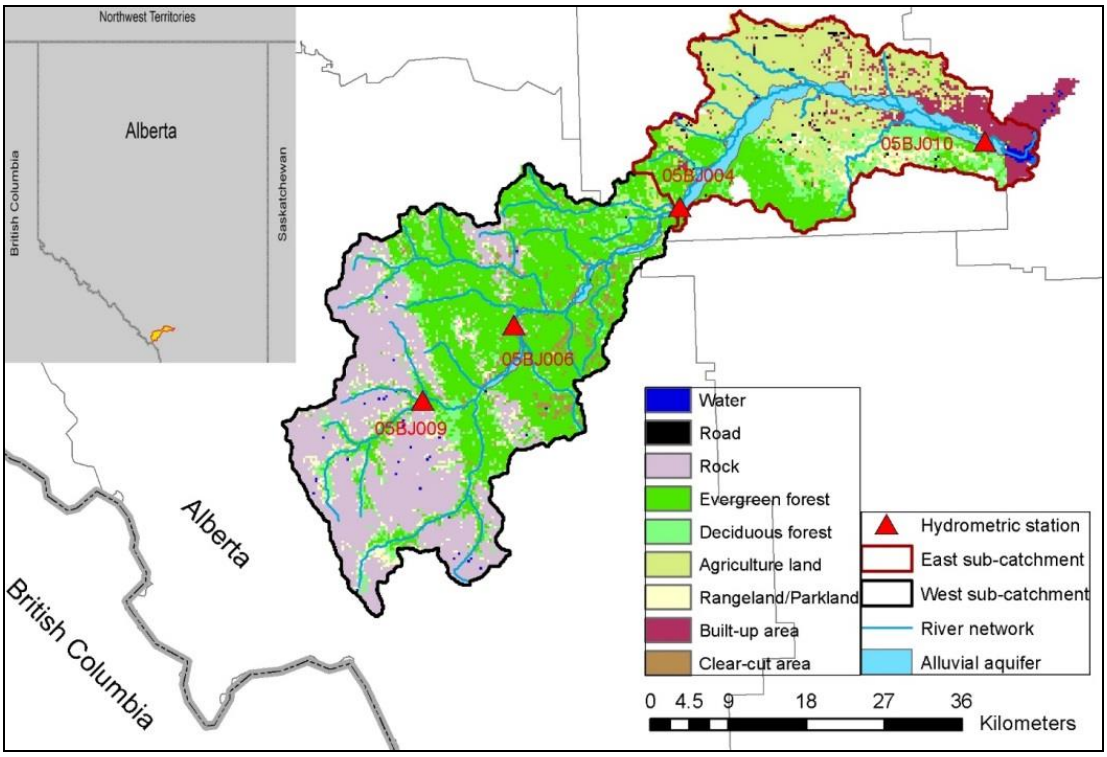

Figure 4.1 Location and land-use/cover of the watershed for the year 2010

4.2.2 Methodological framework

The methodological framework includes four main components: 1) gathering of observed LULC and climate data, 2) GCMs-scenarios, 3) LULC change modeling with a cellular automata, and 4) hydrological modeling using MIKE SHE/MIKE 11 (Fig. 4.2).

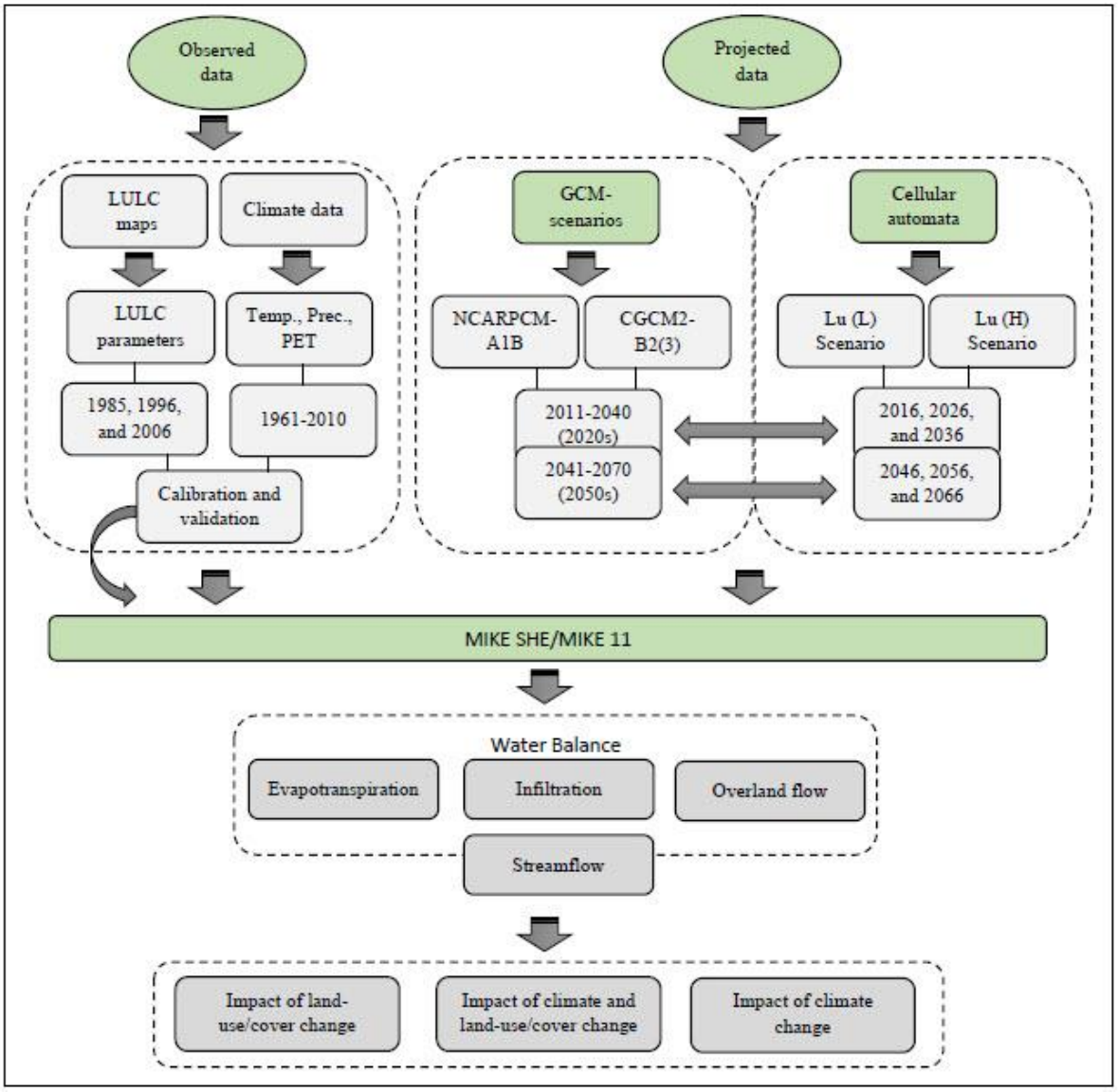

Figure 4.2 Methodological framework of the study

4.2.2.1 Observed climate and LULC data

Temperature and precipitation data were obtained from AESRD for the period of 1961-2010. Temperature data were acquired for three climate index stations, and were interpolated using an areal weighting method (Jones and Hulme 1996). The spatial

distribution of precipitation over the watershed was generated based on six climate index stations using the Thiessen polygon method (He and Hogue 2012).

Soil information was retrieved for the watershed from two databases: the Agricultural Region of Alberta Soil Inventory Database and the Canadian Soil Information Service Data sources. This information was used to create the soil layer for the MIKE SHE/MIKE 11 model. The topography layer was derived from the 80 m spatial resolution digital elevation model from GeoBase (2008). Physical land properties such as leaf area index (LAI) and root depth (RD) were derived from historical LULC maps generated from Landsat Thematic Mapper images at 30 m resolution, acquired for the years 1985, 1992, 1996, 2001, 2006, and 2010. Time series of LAI and RD were created for each LULC class based on values obtained from the literature (Scurlock et al. 2001).

Daily discharge was acquired from AESRD for the period of 1961-2010 for four hydrometric stations: 05BJ009, 05BJ006, 05BJ004, and 05BJ010 (Fig. 4.1), while cross-section information was obtained from field surveys and LiDAR generated data. Detailed information about these datasets can be found in Wijesekara et al. (2014).

4.2.2.2 GCMs-scenarios

The output of two climate models: the CGCM2 (Canadian Centre for Climate Modelling and Analysis) and the NCARPCM (National Centre for Atmospheric Research), forced by two climate scenarios: A1B (Tu 2009; Zhang et al. 2012) and B2 (Boyer et al. 2010; Zhang et al. 2011), were used to construct time series climate variables for the periods of

2020s (2011-2040) and 2050s (2041-2070). The A1B scenario assumes a world of very rapid global economic and population growth with peaks in mid-century, whereas B2 describes lower growth rates of the global economic and population (IPCC 2001).

The climate variables associated with these scenarios include temperature and precipitation over two periods (2020s and 2050s) relative to 1961–1990. The widely used delta change method was utilized for downscaling climate model outputs into hydrological model inputs (Snover et al. 2003; Hay and McCabe 2010; Forbes et al. 2011; Kienzle et al. 2012). This method is easy to employ, but it has the limitation of retaining the temporal structure of the baseline data (Arnell and Reynard 1996). To overcome this limitation, only changes in annual and seasonal responses of hydrological processes to climate scenarios were taken into account in this study (Köplin et al. 2013).

PET, another required climate variable, was calculated using the Hargreaves and Samani's temperature-based model (Hargreaves and Samani 1985). This model was selected using a rigorous procedure based on a comprehensive literature review and a comparison of the Hargreaves-Samani (Hargreaves and Samani 1985), Thornthwaite (Sentelhas et al. 2010), and Blaney-Criddle (Espadafor et al. 2011) models against the PET rates obtained from AESRD as reference, which were calculated using the Priestley-Taylor model (Farjad et al. 2015).

4.2.2.3 LULC change modeling and scenarios

IPCC has not provided sufficient information related to future land-use change corresponding to SRES climate scenarios, which makes linking global and local scale for land-use projection difficult (Wilbanks and Kates 1999; Strengers et al. 2004; Sleeter et al. 2012). Although, a few efforts have been undertaken to downscale land use from coarse scales to finer scales based on IPCC-SRES (Kankaanpää and Carter 2004; Verburg et al. 2006; Sleeter et al. 2012), they have been limited to either downscaling from global scale to continental scale (Abildtrup et al. 2006; Rounsevell et al. 2006) or to sub-continental scale, which only provides a narrow range of land-use types (Solecki and Oliveri 2004). To overcome the challenges that constrain the connection of global scale and local scale land-use projection, a number of studies have used modeling to predict future LULC change at the local scale independent from IPCC-SRES (Tong et al. 2012; Wang et al. 2014). This approach not only overcomes the uncertainty related to downscaling from global scale to local scale, but also allows a user to take into account the local regulations and plans of future land development in a region.

In this study, a cellular automata (CA) model was employed to simulate future LULC change in the watershed. CA allows the characterization of complex spatial systems through a bottom up simulation of local interactions between neighboring cells. A typical CA consists of five main elements: i) geographic space that is represented by a grid of cells, ii) cell states that define the set of possible values associated to the cells, iii) a neighborhood of adjacent cells that can influence the central cell, iv) transition rules that define the next state of the central cells according to their states, the states of the adjacent

cells in the neighborhood, and some external factors, and v) discrete time step that allows all cells to change state simultaneously (Moreno et al. 2009).

Based on a comprehensive sensitivity analysis conducted by Hasbani et al. (2011), four factors driving LULC changes in the watershed were considered: distance to Calgary city center, distance to a main road, distance to a main river, and the ground slope. The neighborhood configuration was designed to approximate a circle around a center cell containing three concentric neighborhood rings. The influence of neighboring cells within each ring on the central cell was constant, but varies between rings.

Historical LULC maps for the years 1985, 1992, 1996, 2001 and 2006, which include the following classes: water, rock, road, deciduous forest, agriculture land, rangeland/parkland, built-up areas, and clear-cut areas were used to calibrate the CA model. The extraction of the transition rules was done as follow. First, the number of cells in each LULC class and their transitions from one state to another as observed in the historical maps were computed. Then, for each LULC transition that occurred in the past, frequency histograms were built to identify the neighborhood configuration, state of the cells within the neighborhood, and external driving factor that best represent the conditions associated to these transitions. These values were used to construct the transition rules. The validation was conducted through a comparison of the simulated and reference LULC map of 2010 using a set of landscape metrics. A detailed description of this developed in-house CA model can be found in Hasbani et al. (2011) and Wijesekara et al. (2014).

In order to consider the uncertainty related to long-term prediction, two opposite scenarios of LULC change, Lu-(PL) and Lu-(PH), were identified to cover a plausible range of change in the watershed. These scenarios represent alternative futures under different sets of assumptions to explore possible future developments in complex systems with high levels of uncertainty (Sleeter et al. 2012). The Lu-(PL) scenario captures the possibility of lower growth in economy and immigration and consequently in population, while higher growth is projected under the Lu-(PH) scenario. The long-term projected data and information for these scenarios were obtained from the Alberta Treasury Board and Finance (Alberta Treasury Board and Finance 2014, Appendix 4). The LULC changes were simulated up to 2070 at a 10-year interval. The CA model was then run to obtain simulated LULC maps for the years 2016, 2026, 2036, 2046, 2056, and 2066. Spatial distribution of LULC parameters such as root depth (RD), surface roughness, and leaf area index (LAI) were extracted from these LULC maps and employed as inputs into the hydrological model MIKE SHE/MIKE 11.

4.2.2.4 Hydrological modeling

MIKE SHE/MIKE 11 is a distributed, physically-based model that includes all the major hydrological components and their interactions such as overland flow, saturated and unsaturated flow, channel flow, and evapotranspiration. The model discretizes the watershed by horizontal-grid square networks for surface and groundwater flow components, which are connected to the unsaturated zone through vertical columns of nodes at each grid. In this study, a finite difference approximation of the St. Venant

equation was used to solve two-dimensional overland flow along with one-dimensional channel flow. In addition, the two-layer water balance method was employed to divide the unsaturated zone (UZ) into a root zone, from which water can be taken by plants, and a zone below the root zone, where water can be recharged into the saturated zone.

Saturation zone (SZ) computations were accomplished using the 3D Darcy equation and solved using a numerical finite-difference scheme. The 3D finite difference method relates the unsaturated zone model to a dynamic water table. The saturation zone was configured using six geologic layers. For each geological layer, four hydrogeologic parameters were assigned, namely vertical hydraulic conductivity, horizontal hydraulic conductivity, specific storage, and specific yield.

ET was simulated by the coupled Kristensen and Jensen model (1975) and the two-layer water balance UZ/ET method (Yan and Smith 1994). This approach considers parameters that are involved in the processes of interception, plant transpiration, and soil evaporation. The parameters can be grouped into characterisation of the vegetation cover such as LAI and RD, and the physical soil properties, such as the soil moisture contents at the wilting point, field capacity, and a constant infiltration capacity. The interception process was modeled based on an interception storage that must be filled before adding water to the soil moisture and ponded water on the ground surface. The process of soil evaporation occurs from the upper UZ layer, and also from excess soil water when the soil reaches field capacity, while transpiration only decreases the water content in the root zone (it does not occur below the root zone). On the other hand, when the plant roots

reach the capillary zone, water is extracted directly from the SZ. However, this process does not reduce the soil moisture content, whereas any water deficit can be replaced by water carried from the SZ up through capillary action. In addition, an ET surface depth parameter was defined at which evapotranspiration extracts water directly from the water table if capillary zone reaches the ground surface at the defined ET surface depth.

Snowmelt was calculated based on the simple degree-day method using air temperature, degree-day factor (mm snow/day/^{o}C), and threshold melting temperature (the temperature at which snow begins to melt). Therefore, if the air temperature is above the threshold temperature then the snow starts to melt; otherwise, the precipitation accumulates as snow.

For the MIKE 11 model, a river network was created for the Elbow River and its tributaries with 353 cross sections, obtained from field surveys and LiDAR generated data. Furthermore, in the boundary condition, a water stage-discharge relationship was applied downstream at the end of the main river stream.

A comprehensive calibration and validation procedure was conducted using the split-sample, multi-criteria, and multi-point method (Wijesekara et al. 2014). The time period 1981-1991 with the LULC map of 1985 was used for calibration while the time periods of 1991-2000 and 2001-2010 with their corresponding LULC maps of 1996 and 2006 were used for validation. A comparison of simulated data against snow storage, streamflow, and groundwater level was performed, which indicated a satisfactory

agreement between the simulated and observed values. Table 4.1 shows the model performance by comparing the simulated results with observed streamflow during calibration and validation periods for different hydrometric stations.

Table 4.1. Measured vs. simulated streamflow during calibration and validation periods for the hydrometric stations 05BJ009, 05BJ006, 05BJ004, and 05BJ010

	Calibration/validation period	NSE (daily)				NSE (monthly)			
		J009	J006	J004	J010	J009	J006	J004	J010
Calibration	Sep. 1981 to Dec. 1991	0.53	0.63	0.72	0.63	0.63	0.75	0.83	0.75
Validation	Sep. 1991 to Dec. 2000	N/A	N/A	0.73	0.71	N/A	N/A	0.87	0.86
	Sep. 2001 to Dec. 2010	N/A	N/A	0.61	0.63	N/A	N/A	0.70	0.71

4.2.2.5 Simulated scenarios

In order to investigate changes in the water balance of the watershed, a base case scenario (BL) was defined to represent the hydrological responses to the baseline climate from 1961 to 1990 with the LULC map of 1985. Then, the water balance was calculated for the following three scenarios over different time periods, relative to the BL scenario:

1) Impact of LULC change on hydrological processes:

a) LU-H scenario: this scenario assumes constant baseline climate (1961-1990) while LULC changes for the 2020s and 2050s under the Lu-(PH) scenario.

b) LU-L scenario: this scenario assumes constant baseline climate (1961-1990) while LULC changes for the 2020s and 2050s under the Lu-(PL) scenario.

2) Impact of climate change on hydrological process:

a) A1B scenario: this scenario considers the A1B climate scenario while LULC is constant.

b) B2(3) scenario: this scenario considers the B2(3) climate scenario while LULC is constant.

3) Impact of climate and LULC change on hydrological processes:

a) LU(H)-A1B scenario: this scenario considers the A1B climate scenario with the LU- PH scenario.

b) LU(L)-A1B scenario: this scenario considers the A1B climate scenario with the LU- PL scenario.

c) LU(H)-B23 scenario: this scenario considers the B2(3) climate scenario with the LU- PH scenario.

d) LU(L)-B23 scenario: this scenario considers the B2(3) climate scenario with the LU- PL scenario.

The hydrological processes considered in the water balance of the watershed are evapotranspiration, infiltration, and overland flow. Ten-year intervals were considered for the simulation of hydrological processes. Climate data for three periods, namely 2011-2020, 2021-2030, and 2031-2040 with the corresponding predicted LULC maps of 2016, 2026, and 2036 were used for the simulation in the 2020s (Fig. 4.3). For the simulation of hydrological processes in the 2050s, climate data for three periods, namely 2041-2050, 2051-2060, and 2061-2070 with the corresponding predicted LULC maps of 2046, 2056, and 2066 were used. These simulations were iterated for each individual scenario.

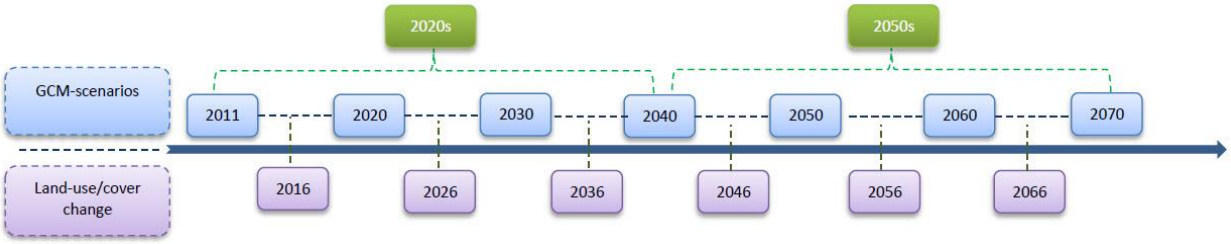

Figure 4.3 Time periods used for the simulation of future climate change and their respective land use/cover

4.3 Results

In this section, the annual and seasonal changes in climate scenarios are described, followed by the simulation results of hydrological processes in response to climate and LULC change.

4.3.1 Annual and seasonal changes in climate scenarios

A rise in the average annual temperature occurs for both the A1B (0.7 °C and 2.2 °C) and B2(3) (1.5 °C and 2.3 °C) scenarios in the 2020s and 2050s, respectively (Fig. 4.4). In comparison, the average annual precipitation increases for A1B (1.2% and 11.1%) and decreases for B23 (−0.4% and −2.2%) in the 2020s and 2050s, respectively (Fig. 4.4).

The average seasonal changes in the air temperature indicate an increase for both A1B and B2(3) scenarios in all seasons in the 2020s and 2050s (Fig. 4.4). Winter temperature exhibits the largest change under the A1B (0.9 °C and 2.8 °C) and B2(3) (2.2 °C and 3.2

°C) scenarios in the 2020s and 2050s. The seasonal rise in temperature under the A1B scenario varies in the range of 0.5-0.9% and 1.7-2.8% while it varies in the range of 0.7-2.2% and 1.4-3.2% under B2(3) in the 2020s and 2050s, respectively. Although these changes occur in the same direction, even a small magnitude of change in temperature with a different temporal pattern may influence hydrological components differently depending on the season. For instance, an increase in air temperature during winter, spring, and early summer may result in a rise in water yield when snow is the dominant factor in the watershed water balance. On the other hand, an increase in air temperature during fall and late summer may result in water losses when there is a reduction in the snow storage and evapotranspiration is the dominant factor in the water balance.

The complexity of interactions between the climate and the hydrology regime in the watershed can be enhanced when precipitation and temperature tend to offset each other's influence differently in different seasons. In other words, the dominant climate variable in a season may differ depending on the season. Changes in seasonal precipitation show that fall precipitation increases under both the A1B (5.6% and 4.4%) and B2(3) (1.5% and 0.9%) scenarios in the 2020s and 2050s, respectively. Meanwhile, summer precipitation decreases under the A1B (-3.9%) in the 2020s and B2(3) (-2.5% and -8.9%) scenarios in the 2020s and 2050s, except in A1B in the 2050s where a rise (14.5%) in precipitation occurs. In the 2020s, changes in precipitation occur in different directions in winter (-0.6% and 1.9%) and spring (7.6% and -0.2) under the A1B and B2(3) scenarios, respectively. However, in the 2050s, both the A1B and B2(3) scenarios indicate an increase in precipitation in winter (6% and 0.4%) and spring (14.2% and 2.7%).

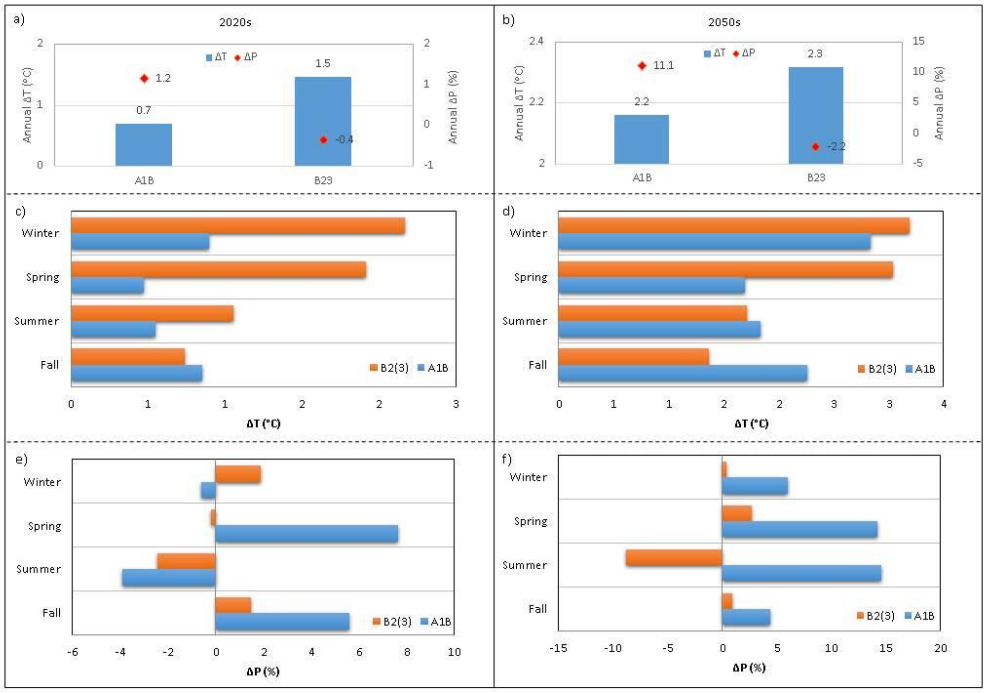

Figure 4.4 Average annual and seasonal changes in temperature and precipitation in the 2020s (a, c, and e) and 2050s (b, d, and f), relative to the baseline (1961-1990)

4.3.2 Impact of LULC and climate change on water balance

4.3.2.1 Average seasonal changes in water balance

Seasonal variation of evapotranspiration, infiltration, and overland flow in response to climate and LULC change in the 2020s and 2050s are described in the following sections.

4.3.2.1.1 Evapotranspiration

ET is a complex process that depends on several factors such as rainfall interception, leaf area, root depth, and soil water. The estimation of ET can be complicated by environmental conditions such as climate and LULC change. In this study, evapotranspiration was forced by climate change, which likely affects atmospheric

demand as well as LULC change, which mainly affects the plant-water transpiration. The estimation of evapotranspiration was further complicated when these factors interacted differently in different seasons.

Simulation results (Fig. 4.5) indicate that, in winter, the dominant driver of the ET process is climate change rather than LULC change in both the 2020s and 2050s. During this season, a rise in temperature under the two climate scenarios results in more snowmelt, which in turn creates more water available for evaporation and transpiration from soil and vegetation, respectively. The magnitude of changes is greater under the B2(3) scenario (28.6–42.2%) compared to the A1B (10.8–36.9%) scenario, in the 2020s and 2050s, respectively. On the other hand, the two LULC change scenarios, LU-H and LU-L, induce not only less modification (-4.8–7.7% and -4.4–7.3%) to ET compared to climate change scenarios in the 2020s and 2050s, but the changes occur in different directions. In spring, the impact of climate change is greater than the influence of LULC change in the 2020s and 2050s, except under the A1B scenario in the 2020s. The largest variation in ET occurs in the summer as a result of two factors: first, a higher atmospheric demand due to higher average air temperature in this season; second, an increase in the leaf area, which plays an important role for evapotranspiration especially in the summer when the key control is rainfall interception considering that the highest amount of rainfall occurs during this season. The second factor is mostly attributed to LULC characteristics, meaning that a change in LULC can cause considerable variation in ET in summer compared to other seasons. For instance, a conversion from forest to urban areas results in less canopy and root density, and in turn, more paved areas, which causes a

reduction in ET. Figure 4.5 illustrates that variations in ET in summer due to climate change occur in the same direction as LULC change, which amplifies the combined impact of climate and LULC change. However, this is not the case for the A1B scenario in the 2050, which compensates the impact of LULC change scenarios.

In the fall, the induced changes in ET under the A1B scenario occur in the opposite direction and with almost the same magnitude of changes caused by the LU-H and LU-L scenarios in the 2020s and 2050s. On the other hand, there is a slight change in ET due to the B2(3) climate scenario indicating that LULC change scenarios are the dominant drivers for the changes in ET in response to combined climate and LULC change scenarios in the 2020s and 2050s. The peak in the watershed ET occurs in June in the baseline period. However, the ET peaks under the B2(3), LU(H)-B23, and LU(L)-B23 scenarios tend to shift from June to May in the 2050s.

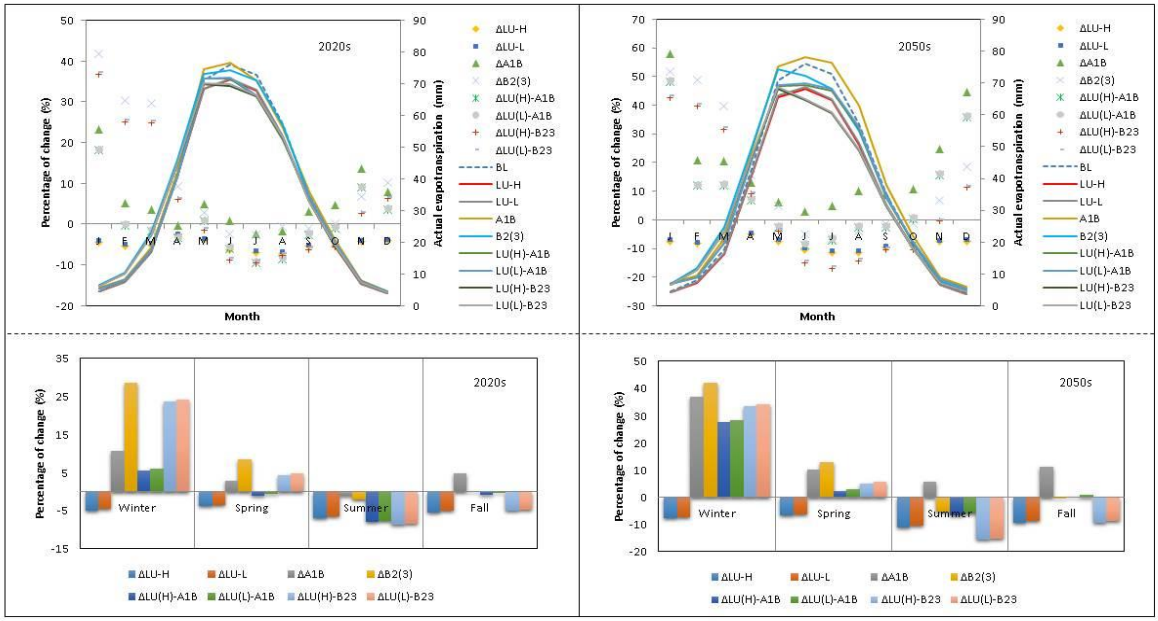

Figure 4.5 Average seasonal changes in evapotranspiration for the period of 2020s and 2050s, relative to the baseline (1961-1990)

4.3.2.1.2 Infiltration

Rainfall and/or snowmelt can enter into the soil through infiltration. In this process, a complex and dynamic interaction occurs at the interface between unsaturated zone properties such as soil texture, structure and moisture content, and physical surface properties such as vegetation, detention storage, and ponded water. These parameters can be affected by both LULC and climate change, spatially and temporally. For instance, an increase in the soil moisture content due to wet climate conditions may gradually lower the infiltration rate. The infiltration rate can also be affected by an increase in impervious surface areas related to urban development.

The impact of climate change on infiltration is more pronounced in the winter and spring, whereas the impact of LULC change is more dominant in the summer in the 2020s and 2050s (Fig. 4.6). The greatest change in infiltration occurs in winter under the A1B and B2(3) scenarios in the 2020s (21.2% and 47.4%) and 2050s (85.3% and 76.1%), respectively. This is mostly attributed to snowmelt due to a rise in temperature. In addition, less saturated soil tends to intensify the infiltration rate in this season. This was also found by Huntington et al. (2007) when they investigated the impact of climate change on winter snow regime and infiltration in the northeastern US. The influence of LULC change scenarios on winter infiltration is minimal compared to the impact of climate change.

The response of infiltration to climate change in spring is less pronounced than the response in winter. The soil is more saturated in the spring compared to winter due to higher rates of snow melt. This increases the possibility of reaching the steady-state infiltration rate, which results in a reduction in spring infiltration rates. On the other hand, the influence of LULC change on infiltration increases in the spring, though climate change is still the dominant driver in this season. In the 2020s and 2050s, summer infiltration decreases under both climate and LULC scenarios, except for the A1B scenario in 2050s. The decline under climate change scenarios is associated mostly with a reduction in precipitation, except with the A1B scenario in 2050s that results in an increase in infiltration, likely linked to a rise in precipitation. On the other hand, the decline in infiltration under LULC change scenarios is associated with an increase in impervious surface areas, which is highlighted in the summer when the highest rainfall events occur. This means the more surface areas are impervious, the less infiltration per unit of rainfall occurs in the watershed. In the fall, the impact of LULC change scenarios compensates the influence of the B2(3) climate scenario in the 2020s and 2050s; however, this is not the case for the A1B scenario.

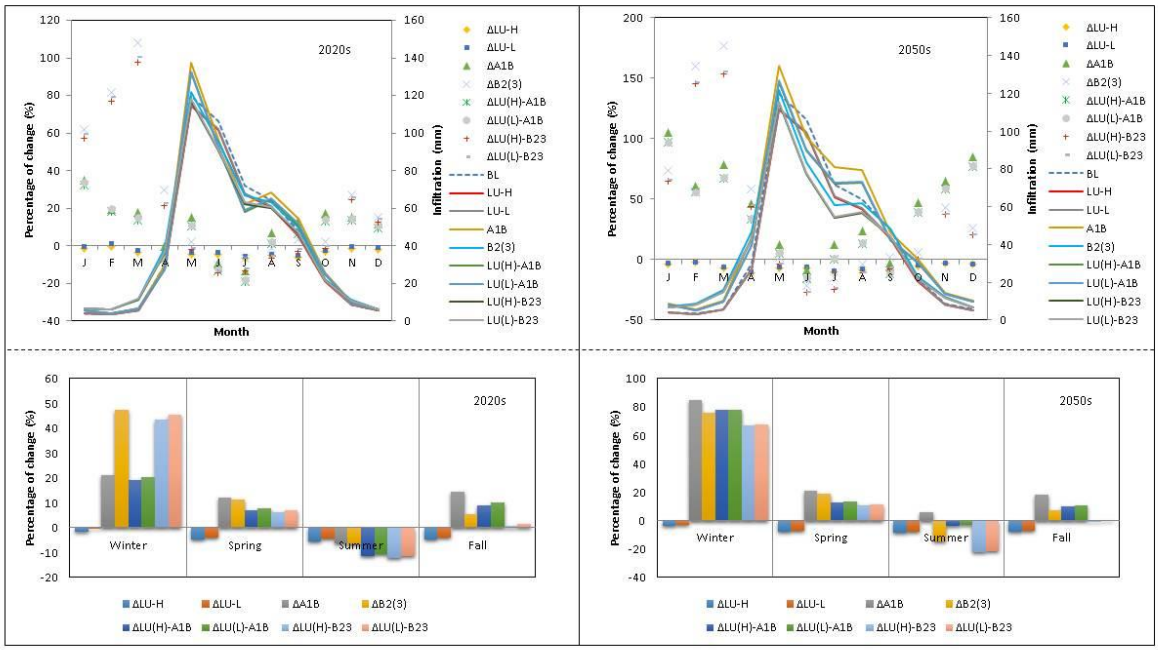

Figure 4.6 Average seasonal changes in infiltration for the period of 2020s and 2050s, relative to the baseline (1961-1990)

4.3.2.2.3 Overland flow

Overland flow is generally controlled by the surface roughness and topography, and is highly affected by infiltration and evapotranspiration. The overland flow process occurs across land surfaces when: a) the amount of water (usually as rainfall or snowmelt) exceeds infiltration capability, b) the depression storage is filled or the soil is saturated, and c) the groundwater flows to the surface.

In winter, overland flow increases under both, the climate and LULC scenarios in the 2020s and 2050s, the more pronounced impact being driven by climate change (Fig. 4.7). Spring overland flow also increases under all climate and LULC scenarios in the 2020s

and 2050s with a greater contribution from LULC changes. Contributions from climate and LULC scenarios to summer overland flow occur in opposite directions, which results in a decline in the magnitude of changes in overland flow under the combined climate and LULC change scenarios. In fall, overland flow increases under all scenarios in the 2020s and 2050s except with the B2(3) climate scenario. The peaks in overland flow occur in June under the LULC scenarios (similar to the baseline scenario) but tend to shift from June to May under the climate and combined climate and LULC scenarios, especially in the 2050s. The largest increase in overland flow occurs in March and April under the LU(H)-B23 scenario in the 2020s and 2050s.

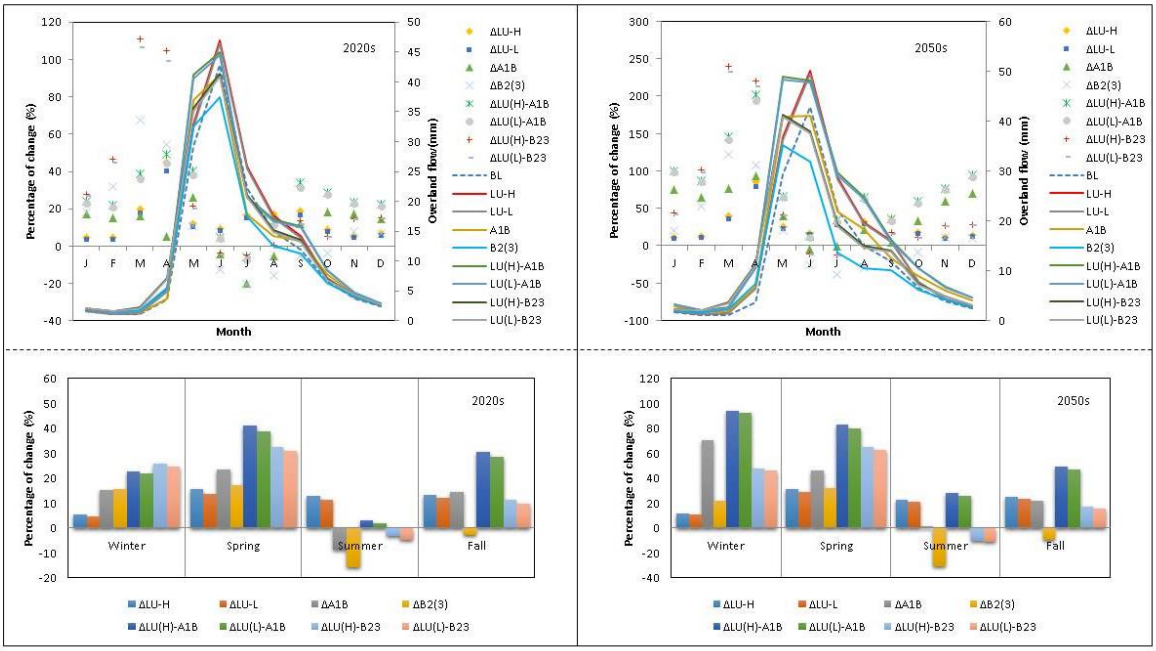

Figure 4.7 Average seasonal changes in overland flow for the period of 2020s and 2050s, relative to the baseline (1961-1990)

4.3.2.2 Average annual changes in water balance

Results reveal that LULC change is the dominant factor effecting the average annual changes in ET (Fig. 4.8). The negative changes (decreases) in ET occur under the LULC change scenarios, LU-H (-5.5% and -9.2%) and LU-L (-5.1% and -8.6%), which compensate the positive changes under the climate scenarios, A1B (1.6 and 9.2%) and B2(3) (2.9% and 3.1%) in the 2020s and 2050s, respectively. This leads to a negative change in ET under all combined climate and LULC change scenarios, ranging from -2.3% to -4.1% and -0.6% to -6.2% in the 2020s and 2050s, respectively.

LULC change is also the dominant factor affecting infiltration in the 2020s and 2050s, except with the A1B climate scenario in the 2050s. A decrease in the watershed infiltration under LULC change scenarios, LU-H (-4.9% and -7.7%) and LU-L (-4% and -7.2%), compensates the increase observed with the B2(3) climate scenario (2.4% and 2.1%) in the 2020s and 2050s, respectively. This results in a decline in combined impact of climate and LULC change scenarios, LU(H)-B23 (-2.7% and -5.8%) and LU(L)-B23 (-1.8% and -5.2%), in the 2020s and 2050s, respectively. On the other hand, the impact of LULC change offsets the rise (3.8%) in infiltration under the A1B scenario in the 2020s, resulting in a decline in infiltration under the combined LU(H)-A1B (-1.3%) and LU(L)-A1B (-0.4%) scenarios. However, a rise (15%) in infiltration leads to an increase (6.3% and 6.9%) in infiltration under the LU(H)-A1B and LU(L)-A1B scenarios, respectively.

The impact of LULC change on overland flow is more pronounced compared to the impact of climate change in the 2020s and 2050s. The responses of overland flow to the

LULC change scenarios (LU-H and LU-L) and the A1B climate scenario occur in the same direction. Therefore, the conjunction of the LULC change scenarios with the A1B climate scenario amplifies the magnitude of the rise in overland flow by 17.4% and 15.9% under the LU(H)-A1B and LU(L)-A1B scenarios, respectively. On the other hand, the responses of overland flow to LULC change scenarios (LU-H and LU-L) occur in the opposite direction of changes in overland flow affected by the B2(3) climate scenario. This leads to a reduction in the magnitude of change in overland flow by 8.7% and 7.3% under the LU(H)-B23 and LU(L)-B23 scenarios, respectively. In the 2050s, changes in overland flow occur with the same directions of the 2020s, but with a higher magnitude.

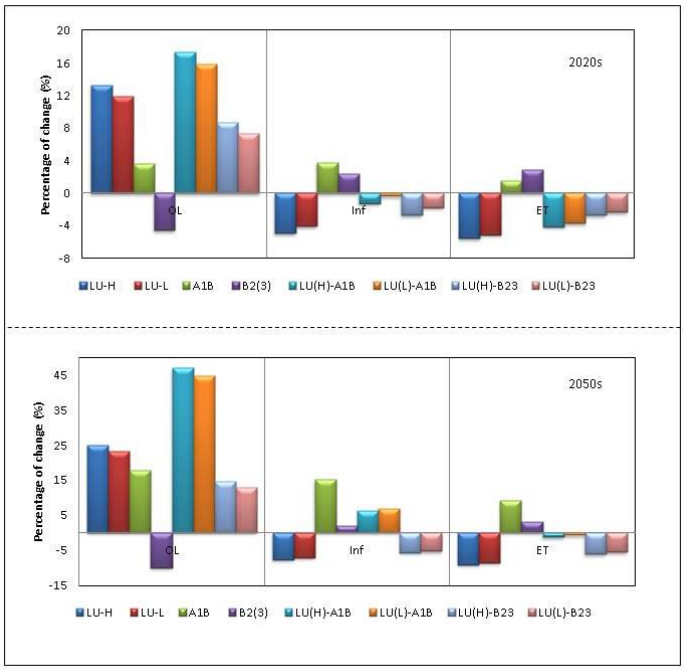

Figure 4.8 Average annual changes in overland flow (OL), infiltration (Inf), and evapotranspiration (ET) for the period of 2020s and 2050s, relative to the baseline (1961-1990)

4.3.2.3 Streamflow

In the 2020s and 2050s, the impact of LULC change on average annual streamflow is more important than the influence of climate change, except with the A1B climate scenario in the 2050s (Fig. 4.9). The LULC change scenarios increase streamflow in the 2020s (8.1% and 7.5%) and 2050s (13.7% and 12.7%). Changes in streamflow under the A1B climate scenario occur in the same direction as with the LULC scenarios, which result in an increase in streamflow under the LU(H)-A1B and LU(L)-A1B scenarios in the 2020s and 2050s. On the other hand, LULC scenarios compensate the decline in streamflow under the B2(3) scenarios in the 2020s and 2050s.

Historical data indicate that a large portion of the average annual discharge (~93%) is generated at the 05BJ004 station, considering 100% of discharge at the 05J010 station (Fig. 4.9). Simulation shows that this proportion of discharge at the 05BJ004 station increases under the climate scenarios, A1B and B2(3), while it decreases under the LULC scenarios in the 2020s and 2050s. In addition, LULC change compensates the influence of climate change, which results in a decline in the proportion of streamflow generated at the 05BJ004 station due to the combined climate and LULC scenarios in the 2020s and 2050s.

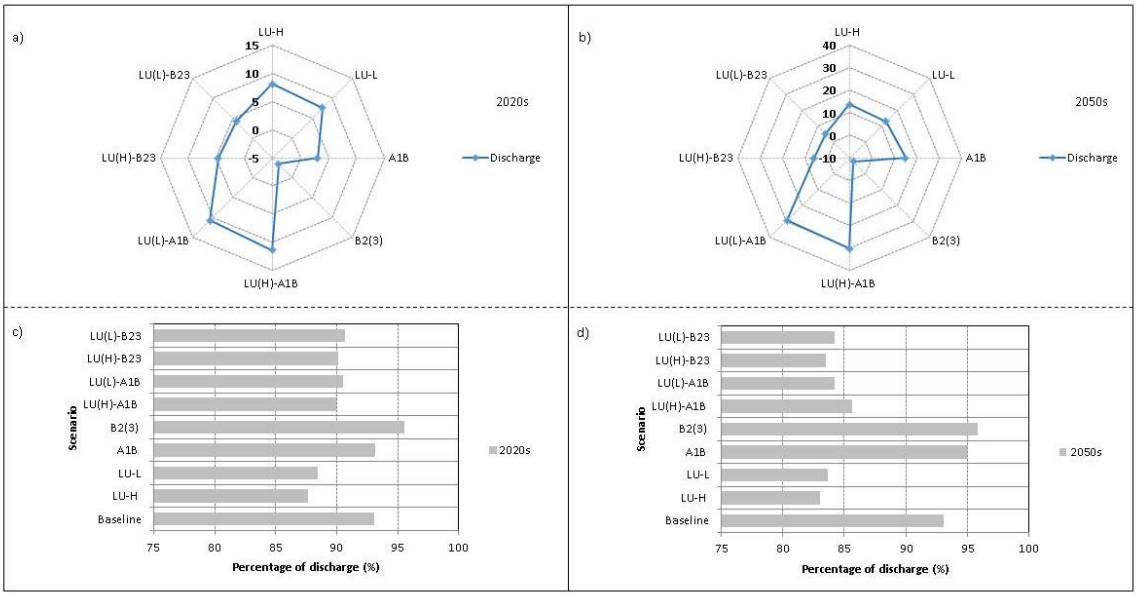

Figure 4.9 Average annual variations in streamflow in the 2020s and 2050s relative to the baseline (a and b) and percentage of streamflow that originates at the 05BJ004 station (c and d)

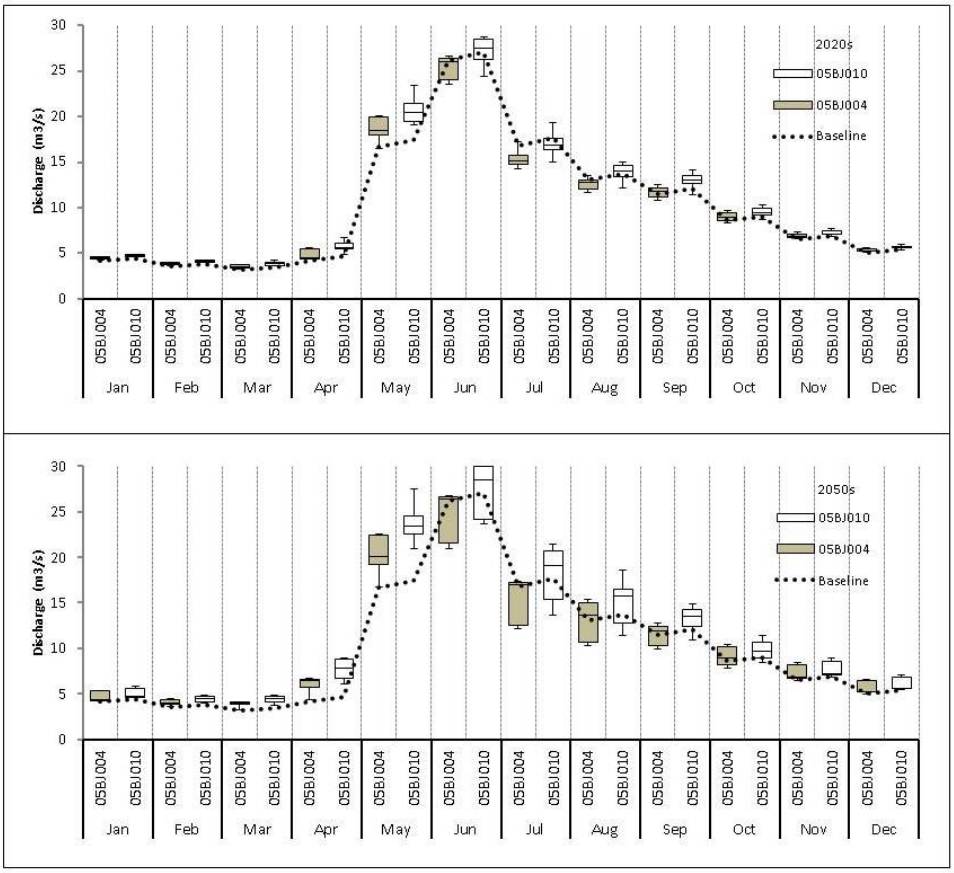

Figure 4.10 Box plot of the average monthly discharge at the 0B5J004 and 05BJ010 stations

The average seasonal streamflow increases under the combined and individual climate and LULC change scenarios in the winter and spring of the 2020s and 2050s. During these seasons, streamflow is strongly attributed to snowmelt, which in turn is more controlled by variations in temperature than precipitation. At high elevations in the watershed, precipitation falls predominantly as snow in the winter and accumulates in storage until spring melt, although snowmelt occurs in winter especially at low elevations when temperatures are above freezing, which results in a low flow through winter and early spring. In 2020s, winter streamflow increases under the A1B and B2(3) climate change scenarios by 5.9% and 2.5%, respectively, while it also increases under the LULC

change scenarios by 3.4%. The direction of the change in streamflow affected by LULC change-alone and climate change-alone is the same; therefore, the rise in streamflow is enhanced in response to the combined climate and LULC scenarios. In the 2050s, the magnitude of change in winter streamflow under the A1B scenario (24.6%) is considerably larger than under the B2(3) scenario (1.6%); this can be associated with a rise in precipitation. This results in greater streamflow under the combined climate and LULC change scenarios, LU(H)-A1B and LU(L)-A1B, compared to the LU(H)-B23 and LU(L)-B23 scenarios. On the other hand, streamflow increases by 3.8-4% under the LULC scenarios, which is not a considerable change compared to A1B (24.6%); however it is greater than the increase under the B2(3) scenario (1.6%).

In spring, streamflow exhibits the largest variations in both the 2020s and 2050s. The greatest changes in spring occur under the LU(H)-A1B and LU(L)-A1B scenarios in the 2020s (28.3-29.4%) and 2050s (58.2-59.8%), respectively. This is mostly associated with the A1B climate scenario, which is the dominant driver compared to the LULC change scenarios and the B2(3) climate scenario. Streamflow increases considerably in the late spring for both climate scenarios due to a considerable rise in precipitation along with an intensified snowmelt. High flows can be even further amplified especially in the late spring when an increase in temperature can lead to a rise in a number of rain-on-snow events and eventually enhance the risk of flooding. Although there is a decline in precipitation under the B2(3) scenario in the 2020s, streamflow exhibits a increase in this season, which implies an intensified snowmelt.

In the summer, the climate change scenarios generate a decline in streamflow in the 2020s and 2050s, except with the A1B scenario in the 2050s when a slight increase can be observed. On the other hand, LULC change results in an increase in summer streamflow. Increasing streamflow in many watersheds has been attributed to LULC change (Troendle and Olsen 1994; Costa et al. 2003; Zhang and Schilling 2006; Peña-Arancibia et al. 2012). A change in LULC due to urbanization and deforestation can result in a decline in rainfall interception loss, canopy evapotranspiration, and a rise in converted units of rainfall to runoff and snowpack water equivalent. These changes are more pronounced in the summer when streamflow tends to respond directly and quickly to the precipitation that falls on the ground, mainly as rain. Simulation of summer streamflow indicates a rise under the LULC change scenarios, LU-H (8.1%) and LU-L (7.4%), in the 2020s. A rise in streamflow under the LU-H (8.1%) and LU-L (7.4%) scenarios creates a buffering effect on declining streamflow under the A1B (-5%) climate scenario, and eventually results in an increased streamflow under the LU(H)-A1B (2.4%) and LU(L)-A1B (1.8%) scenarios. However, the rise in streamflow affected by the LULC change scenarios cannot offset the decline in streamflow affected by the B2(3) (-11.8%) climate scenario, which results in a decrease in streamflow under the combined LU(L)-B2(3) (-4.1%) and LU(H)-B3(3) (-4.7%), scenarios. In the 2050s, the direction of changes in streamflow in the summer is the same as the 2020s, but with a higher magnitude, except for the A1B climate scenario, which causes a rise (3.7%) in streamflow in the 2050s and enhances the increase in LU(H)-A1B (19.9%) and LU(L)-A1B (18.8%).

In the fall, an increase in temperature can result in more water losses by evapotranspiration from the watershed, rather than a rise in the snowmelt when snowpack reaches a lower volume. Simulation shows that an increase in streamflow due to the LULC change scenarios and the A1B climate change scenario amplifies the rise in streamflow under the combined LU(H)-A1B (14.3–25.4%) and LU(L)-A1B (13.9–24.7%) scenarios in the 2020s and 2050s, respectively. However, the B2(3) scenario compensates the LULC change impact and results in a small rise in streamflow in the LU(H)-B23 and LU(L)-B23 scenarios.

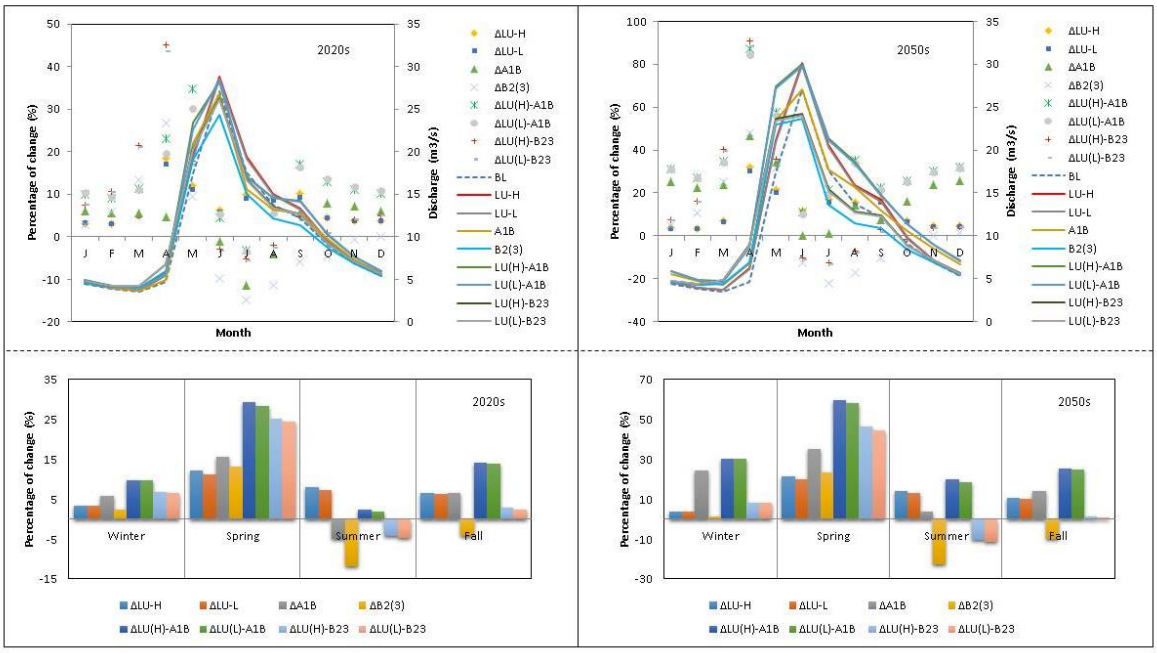

Figure 4.11 Average seasonal changes in streamflow for the period of 2020s and 2050s relative to the baseline (1961-1990)

4.3.2.3.1 Flow duration curve

A flow duration curve (FDC) is a widely-used method to represent the relationship between the magnitude and frequency of river flow in a watershed over a period of time. FDCs estimate the percentage of time a given stream discharge is likely to equal or exceed some identified value of interest that can be used as a general indicator of hydrologic conditions such as floods and droughts. FDCs were generated for each scenario and the baseline in the 2020s and 2050s (Fig. 4.12). They were evaluated at the Q5 (representing peak flows), Q50 (representing mid-range average flow inflection point), and Q90 (representing low flows) discharges, related to baseline in the 2020s and 2050s. Discharge values at Q5 reveal that the LULC contribution to peak flows is more

important than the contribution of climate change in the watershed for both 2020s and 2050s, which is not the case for the average (Q50) and low (Q95) discharge flows. In other words, LULC change may have more effects on floods rather than droughts and normal discharge flows in the watershed. The influence of LULC change on the peak flow magnitude can be intensified when it occurs in the same direction as climate change impacts.

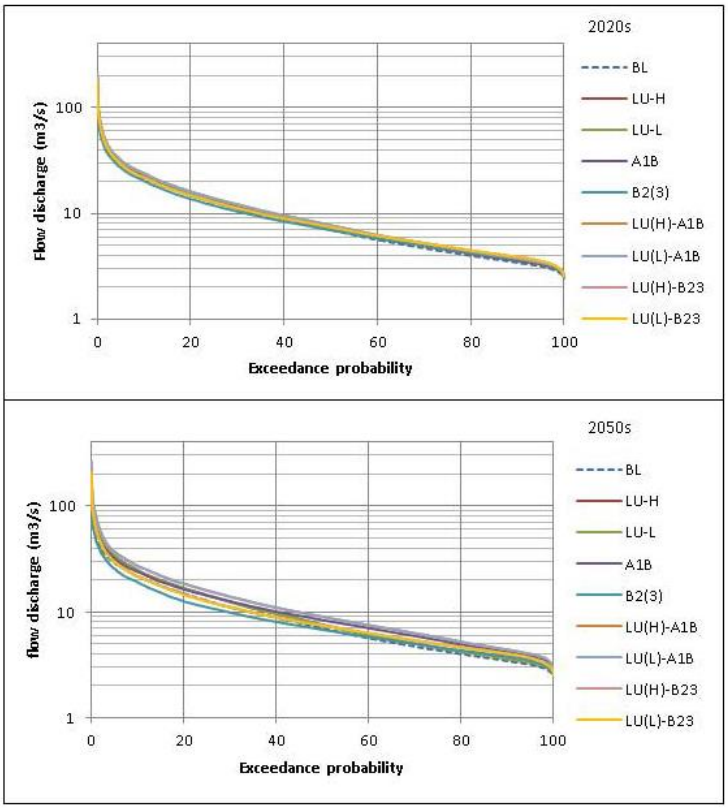

Figure 4.12 Flow duration curves for the baseline and each scenario in the 2020s and 2050s

4.4 Discussion and Conclusion

The hydrological processes in the Elbow River watershed exhibit a complex behaviour due to the seasonal and spatial patterns of snow and rainfall along with other factors such

as temperature, climatic gradients associated with altitude, heterogeneity of the land surface, and geomorphology. This complexity can be further enhanced due to projected changes in climate and LULC.

This paper describes the hydrological responses of the watershed under two extreme climate and LULC scenarios over the next 60 years using an integrated modeling system that incorporates the major components of climate, LULC, and hydrology. Results indicate that both LULC and climate change introduce considerable modifications to the hydrological processes, annually and seasonally. Simulations reveal that the LULC change scenarios increase the average annual streamflow, which amplifies the magnitude of rise associated with the A1B climate scenario and compensates for the decline linked to the B2(3) climate scenario. In addition, changes in LULC substantially modify the river regime in the east sub-catchment, in which urbanization occurs.

Seasonal patterns reveal that the largest rise in streamflow occurs in spring under both the climate and LULC scenarios. The flow duration curves indicate that LULC change has a greater contribution to peak flows than climate change in both the 2020s and 2050s, which creates favorable conditions for spring flooding. In addition, the separated impacts of climate and LULC change on streamflow are positively correlated in winter and spring, which intensifies their combined influence and may also increase the vulnerability of the watershed to floods in spring. LULC change results in a decline in evapotranspiration and infiltration and a rise in overland flow and streamflow in all

seasons. Climate change leads to an increase in all hydrological processes in winter and spring, and fluctuations of the responses in summer and fall.

Our findings highlight the fact that LULC and climate changes can amplify or offset each other's impact on hydrological processes based on the direction and magnitude of their influence. Investigating the hydrological responses to climate change-alone or LULC change-alone may lead to an underestimation or overestimation of the hydrological response of a watershed. This uncertainty has been mentioned in previous studies, especially those that linked variations in streamflow primarily to climate change without considering the influence of LULC. For instance, Fleming and Moore (2008) indicated that some meteorological signals such as the Pacific Decadal Oscillation may be obfuscated by long-term LULC change in a watershed. Mortsch et al. (2015) reviewed challenges of climate- and hydrology-based indicators for estimating water availability in Canada. They mentioned that changes in LULC confound the detection process of indicators that consider a sole relationship between trends/patterns of climate variables and hydrological processes. We therefore advocate that water resources management and adaptation policies should incorporate the impact of both climate and LULC factors on hydrological responses, particularly in urban watersheds.

Acknowledgements

This project was funded by a research grant awarded to Dr. Danielle Marceau by Tecterra and Alberta Environment and Sustainable Resource Development (AESRD), and by an Alberta Innovates Technology Futures graduate student scholarship awarded to Babak

Farjad. We thank Patrick Delaney and Ying Qiao from DHI Water and Environment Canada for their insightful support.

4.5 References

Abbott M B, Bathurst J C, Cunge J A, O'Connell P E, Rasmussen J (1986) An introduction to the European Hydrological System—Système Hydrologique Européen,"SHE", 1: History and philosophy of a physically-based, distributed modelling system. *Journal of Hydrology* 87(1): 45–59.

Abildtrup J, Audsley E, Fekete-Farkas M, Giupponi C, Gylling M, Rosato P, Rounsevell M (2006) Socio-economic scenario development for the assessment of climate change impacts on agricultural land use: a pairwise comparison approach. *Environmental Science & Policy* 9(2):101–115.

Alberta Treasury Board and Finance, (2014). Alberta Population Projections, by Census Division. http://finance.alberta.ca/aboutalberta/population-projections/index.html

Antonellini M, Dentinho T, Khattabi A, Masson E, Mollema P N, Silva V, Silveira P (2014) An integrated methodology to assess future water resources under land use and climate change: an application to the Tahadart drainage basin (Morocco) *Environmental Earth Sciences* 71(4): 1839–1853.

Arnell N W, Reynard N S (1996) The effects of climate change due to global warming on river flows in Great Britain *Journal of Hydrology* 183(3): 397–424.

Barron O, Silberstein R, Ali R, Donohue R, McFarlane D J, Davies P, Donn M (2012) Climate change effects on water-dependent ecosystems in south-western Australia. *Journal of Hydrology* 434: 95–109.

Boyer C, Chaumont D, Chartier I, Roy A G (2010) Impact of climate change on the hydrology of St. Lawrence tributaries. *Journal of Hydrology* 384(1): 65–83.

Bronstert A (2004) Rainfall-runoff modelling for assessing impacts of climate and land-use change. *Hydrological Processes* 18(3): 567–570.

Costa M H, Botta A, Cardille J A (2003) Effects of large-scale changes in land cover on the discharge of the Tocantins River, Southeastern Amazonia. *Journal of Hydrology* 283(1): 206–217.

Dunn S M, Mackay R (1995) Spatial variation in evapotranspiration and the influence of land use on catchment hydrology. *Journal of Hydrology* 171(1): 49–73.

Espadafor M, Lorite I J, Gavilán P, Berengena J (2011) An analysis of the tendency of reference evapotranspiration estimates and other climate variables during the last 45 years in Southern Spain. *Agricultural Water Management*, 98(6):1045–1061.

Fleming S W, Moore R D (2008) Local-scale controls on hydrologic responses to climatic variability. *CMOS Bulletin*, 36:15–19.

Forbes K A, Kienzle S W, Coburn C A, Byrne J M, Rasmussen J (2011) Simulating the hydrological response to predicted climate change on a watershed in southern Alberta, Canada. *Climatic Change* 105(3-4): 555–576.

Gan T Y (1998) Hydroclimatic trends and possible climatic warming in the Canadian Prairies. *Water Resources Research* 34(11): 3009–3015.

Gan T Y, Burges S J (1990) An assessment of a conceptual rainfall- runoff model's ability to represent the dynamics of small hypothetical catchments: 2. Hydrologic responses for normal and extreme rainfall. *Water Resources Research* 26(7): 1605–1619.

Gathenya M, Mwangi H, Coe R, Sang J (2011) Climate-and land use-induced risks to watershed services in the Nyando River Basin, Kenya. *Experimental Agriculture* 47(02): 339–356.

Gosain A K, Rao S, Basuray D (2006) Climate change impact assessment on hydrology of Indian River basins. *Current Science* 90(3): 346–353.

Hargreaves, G. H., & Samani, Z. A. (1985). Reference crop evapotranspiration from ambient air temperature. *American Society of Agricultural Engineers* 1(2): 96-99.

Hasbani J G, Wijesekara N, Marceau D J (2011) *An interactive method to dynamically create transition rules in a land-use Cellular Automata model, Cellular Automata - Simplicity Behind Complexity*, Alejandro Salcido (Ed.), ISBN: 978-953-307-230-2, InTech Publisher, Available from: http://www.intechopen.com/articles/show/title/an-interactive-method-to-dynamically-create-transition-rules-in-a-land-use-cellular-automata.

Hay L E, McCabe G J (2010) Hydrologic effects of climate change in the Yukon River Basin. *Climatic Change* 100(3-4): 509–523.

He M, Hogue T S (2012) Integrating hydrologic modeling and land use projections for evaluation of hydrologic response and regional water supply impacts in semi-arid environments. *Environmental Earth Sciences* 65(6): 1671–1685.

Hendriks M (2010) *Introduction to physical hydrology*. Oxford University Press, 331 pp.

Hundecha Y, Bárdossy A (2004) Modeling of the effect of land use changes on the runoff generation of a river basin through parameter regionalization of a watershed model. *Journal of Hydrology* 292(1): 281–295.

Huntington T G, Sheffield J, Hayhoe K (2007, May) Impacts of climate change on wintertime precipitation, snowmelt regime, surface runoff, and infiltration in the northeastern USA during the 21st century. *Proceedings of the 64th Eastern Snow Conference,* St. Johns, Newfoundland, Canada 29:181–189.

IPCC (2001) Intergovernmental Panel on Climate Change [IPCC] 2001 *Climate change 2001, the scientific basis*. Houghton J T, Ding Y, Griggs D J, Noyuer M, van der Linden P J, Xiaosu D (Editors) Contribution of Working Group I to the Third Assessment Report of the Intergovernmental Panel on Climate Change Cambridge University Press, 941 pp.

Jakeman A J, Littlewood I G, Whitehead P G (1993) An assessment of the dynamic response characteristics of streamflow in the Balquhidder catchments. *Journal of Hydrology* 145(3): 337–355.

Kankaanpää S, Carter T R (2004) *Construction of European forest land use scenarios for the 21st century*. In: The Finnish Environment 707, Finnish Environment Institute Helsinki, 57 pp.

Khoi D N, Suetsugi T (2014) The responses of hydrological processes and sediment yield to land-use and climate change in the Be River Catchment, Vietnam. *Hydrological Processes* 28(3): 640–652.

Kienzle S W, Nemeth M W, Byrne J M, MacDonald R J (2012) Simulating the hydrological impacts of climate change in the upper North Saskatchewan River basin, Alberta, Canada. *Journal of Hydrology* 412:76–89.

Köplin N, Schädler B, Viviroli D, Weingartner R (2013) The importance of glacier and forest change in hydrological climate-impact studies. *Hydrology and Earth System Sciences* 17(2): 619–635.

Kristensen K J, Jensen S E (1975) A model for estimating actual evapotranspiration from potential evapotranspiration. *Nordic Hydrology* 6:170–188.

Kundzewicz Z W, Mata L J, Arnell N W, Döll P, Jimenez B, Miller K, Oki T, Şen Z, Shiklomanov I (2008) The implications of projected climate change for freshwater resources and their management. Hydrological Sciences Journal 53(1): 3–10.

Lehner B, Döll P, Alcamo J, Henrichs T, Kaspar F (2006) Estimating the impact of global change on flood and drought risks in Europe: a continental, integrated analysis. *Climatic Change* 75(3): 273–299.

Li Z, Liu W Z, Zhang X C, Zheng F L (2009) Impacts of land use change and climate variability on hydrology in an agricultural catchment on the Loess Plateau of China. *Journal of Hydrology* 377(1): 35–42.

Montenegro S, Ragab R (2012) Impact of possible climate and land use changes in the semi arid regions: A case study from North Eastern Brazil. *Journal of Hydrology* 434: 55–68.

Mortsch L, Cohen S, Koshida G (2015) Climate and water availability indicators in Canada: Challenges and a way forward. Part II–Historic trends. *Canadian Water Resources Journal/Revue canadienne des ressources hydriques* 40(2):146–159.

Neitsch S L., Arnold J G, Kiniry J R, Williams J R (2011) *Soil and Water Assessment Tool.* Theoretical Documentation Version 2009, Technical report no. 406, Texas Water Resources Institute, 618 pp.

Notebaert B, Verstraeten G, Ward P, Renssen H, Van Rompaey A (2011) Modeling the sensitivity of sediment and water runoff dynamics to Holocene climate and land use changes at the catchment scale. *Geomorphology* 126(1): 18–31.

Peña-Arancibia J L, van Dijk A I, Guerschman J P, Mulligan M, Bruijnzeel L A, McVicar T R (2012) Detecting changes in streamflow after partial woodland clearing in two large catchments in the seasonal tropics. *Journal of Hydrology* 416: 60–71.

Rounsevell M D A, Reginster I, Araújo M B, Carter T R, Dendoncker N, Ewert F, Tuck G (2006) A coherent set of future land use change scenarios for Europe. *Agriculture, Ecosystems & Environment* 114(1): 57–68.

Sentelhas P C, Gillespie T J, Santos E A, (2010) Evaluation of FAO Penman–Monteith and alternative methods for estimating reference evapotranspiration with missing data in Southern Ontario, Canada. *Agricultural Water Management* 97(5): 635–644.

Scurlock J M O, Asner G P, Gower S T (2001) *Worldwide Historical estimates of Leaf Area Index, 1932–2000*, DOE Scientific and Technical Information http://www.osti.gov/bridge/.

Sleeter B M, Sohl T L, Bouchard M A, Reker R R, Soulard C E, Acevedo W, ... Zhu Z (2012) Scenarios of land use and land cover change in the conterminous United States: utilizing the special report on emission scenarios at ecoregional scales. *Global Environmental Change* 22(4): 896–914.

Snover A K, Hamlet A F, Lettenmaier D P (2003) Climate-change scenarios for water planning studies: Pilot applications in the Pacific Northwest. *Bulletin of the American Meteorological Society* 84(11): 1513–1518.

Solecki W D, Oliveri C (2004) Downscaling climate change scenarios in an urban land use change model. *Journal of Environmental Management* 72(1):105–115.

Strengers B, Leemans R, Eickhout B, Vries D, B, Bouwman L (2004) The land-use projections and resulting emissions in the IPCC SRES scenarios as simulated by the IMAGE 2.2 model. *GeoJournal* 61(4): 381–393.

Thanapakpawin P, Richey J, Thomas D, Rodda S, Campbell B, Logsdon M (2007) Effects of landuse change on the hydrologic regime of the Mae Chaem river basin, NW Thailand. *Journal of Hydrology* 334(1): 215–230.

The City of Calgary (2010) *2010 civic census results*. http://www.calgary.ca/CA/city-clerks/Documents/Election-and-informationservices/Census/2010_census_result_book.pdf.

The City of Calgary (2013), *Calgary flood 2013 infographic*. http://www.calgary.ca/General/flood-recovery/Pages/Calgary-flood-2013-infographic-recap.aspx.

Tong S T, Sun Y, Ranatunga T, He J, Yang Y J (2012) Predicting plausible impacts of sets of climate and land use change scenarios on water resources. *Applied Geography* 32(2): 477–489.

Troendle C A, Olsen W K (1994) *Potential effects of timber harvest and water management on streamflow dynamics and sediment transport*. Sustainable Ecological Systems: Implementing an Ecological Approach to Land Management. USDA Forest Service General Technical Report RM–247, Fort Collins Co, pp. 34–41.

Tu J (2009) Combined impact of climate and land use changes on streamflow and water quality in eastern Massachusetts, USA. *Journal of Hydrology* 379(3): 268–283.

Verburg P H, Schulp C J E, Witte N, Veldkamp A (2006) Downscaling of land use change scenarios to assess the dynamics of European landscapes. *Agriculture, Ecosystems & Environment* 114(1): 39–56.

Wang R, Kalin L, Kuang W, Tian H (2014) Individual and combined effects of land use/cover and climate change on Wolf Bay watershed streamflow in southern Alabama. *Hydrological Processes* 28(22): 5530–5546.

Weatherhead E K, Howden N J K (2009) The relationship between land use and surface water resources in the UK. *Land Use Policy* 26: S243–S250.

Wilbanks T J, Kates R W (1999) Global change in local places: how scale matters. *Climatic Change* 43(3): 601–628.

Wijesekara G N, Gupta A, Valeo C, Hasbani J G, Qiao Y, Delaney P, Marceau D J (2012) Assessing the impact of future land-use changes on hydrological processes in the Elbow River watershed in southern Alberta, Canada. *Journal of Hydrology* 412: 220–232.

Wijesekara G N, Farjad B, Gupta A, Qiao Y, Delaney P, Marceau D J (2014) A Comprehensive Land-Use/Hydrological Modeling System for Scenario Simulations in the Elbow River Watershed, Alberta, Canada. *Environmental Management* 53(2): 357–381.

Yan J, Smith K R (1994) Simulation of integrated surface water and ground water system-model formulation. *JAWRA Journal of the American Water Resources Association* 30(5): 879–890.

Zhang X C, Liu W Z, Li Z, Chen J (2011) Trend and uncertainty analysis of simulated climate change impacts with multiple GCMs and emission scenarios. *Agricultural and Forest Meteorology* 151(10): 1297–1304.

Zhang Y K, Schilling K E (2006) Increasing streamflow and baseflow in Mississippi River since the 1940s: Effect of land use change. *Journal of Hydrology* 324(1): 412–422.

Zhang L, Dawes W R, Walker G R (2001) Response of mean annual evapotranspiration to vegetation changes at catchment scale. *Water Resources Research* 37(3): 701–708.

Zhang S, Gao X, Zhang X, Hagemann S (2012) Projection of glacier runoff in Yarkant River basin and Beida River basin, Western China. *Hydrological Processes* 26(18): 2773–2781.

Chapter 5 : Conclusions and Future Work

The objective of this research was to investigate the impact of climate and LULC change on the hydrology of the Elbow River watershed in southern Alberta in the 2020s and 2050s using an integrated modeling system able to capture the complexity of these three components. After presenting the main characteristics of the watershed, a twofold investigation was conducted. First, the influence of climate change on hydrology of the watershed was investigated in order to understand responses of hydrological processes to a range of future possible climate scenarios up to 2070. Second, two climate change scenarios (which were selected based on assessing the prominent climate change signals and their associated GCM-scenarios in the first study), along with two opposite scenarios of LULC change (which were identified to cover a plausible range of LULC change in the watershed) were employed into an integrated modeling framework consisting of MIKE SHE/MIKE 11, a CA model, and GCMs to investigate the separate and the combined impact of climate and LULC changes on hydrological processes in the watershed.

The characteristics of the Elbow River watershed create a complex hydrological regime. Different geomorphological characteristics in the west and east sub-catchments such as the drainage area, slope steepness, basin shape and drainage network configuration result in different hydrological behaviours in the two sub-catchments. The west sub-catchment is larger, steeper, with a more compact pear-shaped and higher drainage density compared to the east sub-catchment. Water is delivered from all parts of this sub-catchment to the outlet more quickly than in the east sub-catchment, which tends to do so

over a prolonged period of time. Moreover, the same amount of precipitation can result in different hydrological responses in the west and east sub-catchments. For example, storms in the west sub-catchment tend to concentrate the flow at the sub-catchment outlet whereas storms in the east sub-catchment tend to spread the resulting runoff out over time.

In addition to the inherent complexity of the watershed, a change in climate and LULC, which exerts a control over hydrological processes, can modify the watershed hydrological regime. For example, rapid urbanization can affect how water is delivered to the outlet from a slow flow to one in which water from a single storm arrives in an abrupt pulse of flow. In this study, it was found that the contribution of the east sub-catchment to flood magnitude can increase considerably in the 2050s due to urbanization. The coupling of MIKE SHE/MIKE 11 with a CA model, and different GCM-scenarios allowed capturing the dynamical, physical, and distributed nature of the changes in the hydrological regime, which reduced the uncertainty in the projection of hydrological processes in the 2020s and 2050.

The key findings of this study can be summarized as follows.

- Both LULC and climate change are expected to substantially modify the hydrological regime of the watershed over the next 60 years, annually and seasonally.
- The induced changes in hydrological processes under the climate scenarios are proportionally more perceptible in the east sub-catchment compared to the west

sub-catchment. However, the west sub-catchment governs the watershed behaviour and determines the future changes, over-riding the stronger climate change signal in the east sub-basin.

- The average annual overland flow and baseflow decrease in the east sub-basin that is adjacent to the fast growing City of Calgary, which might result in water scarcity.
- The shift in high streamflow from late spring-early fall to the middle of spring-summer could increase the risk of flooding, particularly in the lowlands in the east sub-catchment.
- The risk of flooding will enhance in mid-late spring, due to an increase in rain-on-snow events coinciding with the highest increase in spring freshet.
- The decline in the east sub-catchment groundwater recharge can result in groundwater depletion, which is a concern when about 90% of licensed groundwater extractions are located in the east sub-catchment.
- The separated impacts of climate and LULC change on streamflow are positively correlated in winter and spring, which intensifies their combined influence.

5.1 Uncertainty

There are different dimensions of uncertainty in climate and LULC change impact studies that are associated with future emission scenarios, downscaling approaches, GCM, LULC, and hydrological model structure and parameters. Some of these uncertainties might be removed or minimized through an improvement in approach and/or modelling exercise whereas some of them cannot be reduced. However, understanding the source of

uncertainty can help with water resource management and planning for the decision-making process.

One of the largest sources of uncertainty arises from GCMs (Prudhomme and Davies, 2008) that can simulate quite different climate changes even under the same future greenhouse-gas emission scenarios (Giorgi and Francisco 2000). Therefore, overreliance on a single GCM can be misleading, and there is a need to employ a combination of as many GCMs as possible to better cover the uncertainty associated with climate projections. In this sense, emerging patterns of changes in hydrological processes due to climate change can be determined by identifying the consistency of changes in hydrological processes in both direction and magnitude under a wide range of GCMs. For instance, Kienzle et al., (2012) determined future patterns of hydrological processes based on the consistency of changes in direction and magnitude of hydrological processes under different GCMs in the upper North Saskatchewan River basin, Alberta. Similarly, greenhouse-gas emission scenarios can increase uncertainty; however, Prudhomme et al., (2003) found that the uncertainty in impact studies due to greenhouse-gas emission scenarios is less than the uncertainty due to GCMs. In addition, uncertainties of the emission scenarios are less pronounced for shorter time horizons such as the 2020s and 2050s, compared to the 2080s.

Downscaling approaches also add uncertainty to climate data due to the limitations that are inherent in each technique. There are two broad classes of downscaling techniques; dynamical and statistical. Their assessment has revealed that their performance mainly

depends on the application (Xu 1999; Prudhomme et al. 2002; Fowler et al. 2007). The main drawback of dynamical downscaling is that their outputs are too coarse for small watershed studies, while the main limitation of statistical downscaling is the probable lack of a stable relationship between observed local climatic variables (predictands) and large-scale GCM outputs (predictors) (Wilby and Wigley, 1997).

Hydrological models can also be a source of uncertainty due to model parameters and model structural errors (Vázquez et al., 2008). Physically-based models can reduce the uncertainty linked to calibration compared to lumped models for climate impact studies while lumped, conceptual models are climate-sequence dependent (Minville et al. 2008). Previous researches utilized sensitivity analyses to reduce uncertainties that arise from model parameters (Refsgaard and Storm, 1995; Wijesekara et al., 2014). Some of these uncertainties, especially those that are related to the model structure, are not easy to remove. For example, the majority of hydrological models do not take into account frozen soil conditions, which can introduce uncertainty to the model results especially for the infiltration process. However, infiltration rates are generally small in the winter and in this case the associated uncertainty can be small.

Incorporating future LULC changes in the modeling framework can also introduce additional uncertainties. Some studies downscaled future LULC from coarse scales to finer scales based on IPCC-SRES (Kankaanpää and Carter 2004; Verburg et al. 2006; Sleeter et al. 2012). These studies have been limited to downscaling from a global scale to continental and/or sub-continental scales, which only provides a narrow range of

LULC types (Solecki and Oliveri 2004). To overcome the challenges that constrain the connection of global scale and local scale LULC projection, a number of studies have used modeling to predict future LULC change at the local scale, independent from IPCC-SRES (Tong et al. 2012; Wang et al. 2014). This approach not only overcomes the uncertainty related to downscaling from global scale to local scale, but also allows a user to take into account the local regulations and plans of future land development in a region. However, the uncertainties still exist related to the LULC modeling exercise, especially for longer time horizons such as 2050s and 2080s, compared to 2020s. These uncertainties are mainly associated with model structure, and lack of future local information e.g., socio-economical information.

5.2 Thesis contribution

The first part of this research, described in Chapter 3, is the first of this nature that enhances our understanding of the potential impact of climate and LULC change on the hydrology of the Elbow River watershed. It also addresses the limitation of a previous study on the influence of climate change in the watershed (Valeo et al., 2007). These authors used the output of the Canadian Regional Climate Model CRCM-II (V3.5) as input to the SSARR (Streamflow Synthesis and Reservoir Regulation) hydrological model to evaluate the future river discharge in the watershed. This study has several limitations. First, the CRCM-II model was run for current and doubled CO2 scenarios, and simulated a steady-state CO2 concentration while it ignored the gradually changing CO2 concentrations over time. Second, not only the use of the SSARR as a lumped model is questionable for application in a climate change context, but also the model has

some inherent limitations: a) it is unable to adequately quantify the complex interactions between groundwater and surface water, due to the representation of the groundwater system as one reservoir, b) it does not sufficiently take into account the spatial heterogeneity of the watershed, and c) the depletion-curve mode of SSARR, which divides the watershed into snow covered and snow free areas, cannot calculate snowpack accumulation, while it can only calculate depletion in an existing snowpack (Kite, 1978).

The second part of the research, described in Chapter 4, is the first of this nature that employed a comprehensive integrated modeling framework to address the gaps and challenges in the literature discussed in Section 4.1. This modeling system encompasses the following powerful models. The first one is MIKE SHE/MIKE 11, which is based on physical principles and provides a detailed description of the processes that occur in a watershed, and which considers the catchment as finite geo-referenced computational units with different responses to forcing inputs. The second model is the CA that provides several advantages to the integrated modeling framework. First, as a spatially explicit model, it provides detailed spatial characteristics of the land surface that are required in a distributed hydrological model; second, the dynamic nature of CA makes possible the prediction of LULC changes at different time intervals, which makes it highly compatible with the different time intervals of hydrological simulations; and third, the rule-based nature of the CA allows the consideration of external (e.g., socio-economical) and internal (e.g., distance from river, city center) driving factors. Finally, the use of a combination of GCMs forced by IPCC SRES emission scenarios covers the uncertainty associated with future climate projections.

5.3 Recommendations for future work

Several avenues for future work could be investigated. An important one is modeling groundwater flooding defined as the emergence of water from sub-surface at the surface or into basement or structures. Sub-surface water emerges from either point or diffuse locations, and it often occurs away from flood plains. During the 2005 flood, over 80% of the damage was associated with groundwater flooding whereas over 500 homes were damaged during the 2013 flood due to groundwater flooding (Hugo, 2015). At present, there is no extensive groundwater monitoring or modelling technology to identify groundwater flood-risk areas in Alberta (Alberta WaterPortal, 2014). The mechanisms associated with groundwater flooding are inherently complex and poorly understood. This is especially the case in the Elbow River watershed due to its characteristics.

Our modeling system is well suited to study groundwater flooding in the watershed. This is because a coupled surface- and subsurface-flow process model such as MIKE SHE/MIKE 11 is essential for groundwater assessment in the Elbow River watershed due to complex surface/subsurface interactions. In addition, even when it is possible to employ a groundwater model such as MODFLOW, the calculation of recharge (as one of the primary input data for groundwater models) is still a challenge. Recharge is the most difficult component of water balance to calculate (Cherkauer, 2004), and the existing simple methods such as groundwater budget may not be applicable for the watershed hydrological system. A dynamic spatially explicit LULC model needs to be considered in the watershed groundwater flooding assessment when rapid urbanization can

substantially modify infiltration and recharge processes. Finally, future groundwater flooding can be predicted under a range of scenarios.

Another area for future work is to apply additional downscaling approaches, such as dynamic downscaling and/or weather generator, to deliver better predictions of dry and wet climate variability in order to better quantify the occurrence of extreme hydrological events for the future. Dynamic downscaling considers the inter-variability of climate variables whereas weather generator does not replicate observed sequences of events but simulate the sequence of wet and dry weather events and the transition from one to another that can result in a better evaluation of future extreme hydrological events.

Finally, further efforts are required to provide and organize the data resources that will enhance modeling performances. For example, having access to more accurate and up-to-date groundwater data (e.g., groundwater level) will enhance the quality of the calibration and validation of the MIKE SHE/MIKE 11 groundwater related hydrological fluxes, and as a result can increase the capability of the model to predict groundwater components.

5.4 References

Alberta WaterPortal, (2014). *Understanding groundwater flooding*. http://albertawater.com/flood-mitigation/understanding-groundwater-flooding#footnote3.

Cherkauer, D. S., (2004). Quantifying ground water recharge at multiple scales using PRMS and GIS. *Groundwater*, 42(1): 97-110.

Fowler, H. J., Blenkinsop, S., & Tebaldi, C. (2007). Linking climate change modelling to impacts studies: recent advances in downscaling techniques for hydrological modelling. *International journal of climatology*, 27(12), 1547-1578.

Giorgi, F., & Francisco, R. (2000). Evaluating uncertainties in the prediction of regional climate change. *Geophysical Research Letters*, 27(9), 1295-1298.

Hugo, K., (2015) *Bow River floods and groundwater*. http://www.esaa.org/

Jiang, C., Xiong, L., Wang, D., Liu, P., Guo, S., & Xu, C. Y. (2015). Separating the impacts of climate change and human activities on runoff using the Budyko-type equations with time-varying parameters. *Journal of Hydrology*, 522, 326-338.

Jones, R. N., Chiew, F. H., Boughton, W. C., & Zhang, L. (2006). Estimating the sensitivity of mean annual runoff to climate change using selected hydrological models. *Advances in Water Resources*, 29(10), 1419-1429.

Kankaanpää, S., Carter, T. R. (2004) *Construction of European forest land use scenarios for the 21st century*. In: The Finnish Environment 707, Finnish Environment Institute Helsinki, 57 pp.

Kienzle, S. W., Nemeth, M. W., Byrne, J. M., & MacDonald, R. J. (2012). Simulating the hydrological impacts of climate change in the upper North Saskatchewan River basin, Alberta, Canada. *Journal of Hydrology*, 412, 76-89.

Lashof, D. A. (1989). The dynamic greenhouse: feedback processes that may influence future concentrations of atmospheric trace gases and climatic change. *Climatic Change*, 14(3), 213-242.

Minville M, Brissette F, Leconte R (2008) Uncertainty of the impact of climate change on the hydrology of a nordic watershed. *Journal of Hydrology* 358(1): 70-83.

Prudhomme, C., Jakob, D., & Svensson, C. (2003). Uncertainty and climate change impact on the flood regime of small UK catchments. *Journal of hydrology*, 277(1), 1-23.

Prudhomme, C., Davies, HN. (2008) Assessing uncertainties in climate change impact analyses on river flow regimes in the UK. Part 2: future climate. *Climatic Change*. doi:10.1007/s10584-008-9461-6.

Sleeter, B. M., Sohl, T. L., Bouchard, M. A., Reker, R. R., Soulard, C. E., Acevedo, W, ... Zhu, Z. (2012) Scenarios of land use and land cover change in the conterminous United States: utilizing the special report on emission scenarios at ecoregional scales. *Global Environmental Change* 22(4): 896–914.

Solecki, W. D., Oliveri, C. (2004) Downscaling climate change scenarios in an urban land use change model. *Journal of Environmental Management* 72(1):105–115.

Tong S T, Sun Y, Ranatunga T, He J, Yang Y J (2012) Predicting plausible impacts of sets of climate and land use change scenarios on water resources. *Applied Geography* 32(2), 477–489.

Valeo, C., Xiang, Z., Bouchart, F. C., Yeung, P., and Ryan, M. C. (2007). Climate change impacts in the Elbow River watershed. *Canadian Water Resources Journal*, 32(4), 285-302.

Verburg, P.H., Schulp, C.J.E., Witte, N., Veldkamp, A. (2006) Downscaling of land use change scenarios to assess the dynamics of European landscapes. *Agriculture, Ecosystems & Environment* 114(1): 39–56.

Wang R, Kalin L, Kuang W, Tian H (2014) Individual and combined effects of land use/cover and climate change on Wolf Bay watershed streamflow in southern Alabama. *Hydrological Processes,* 28(22), 5530–5546.

Wilby, R.L., Wigley, T.M.L., (1997). Downscaling general circulation model output: a review of methods and limitations. *Progress in Physical Geography* 214, 530–548.

Wijesekara, G.N., Farjad, B., Gupta, A., Qiao, Y., Delaney, P., Marceau, D.J. (2014) A Comprehensive Land-Use/Hydrological Modeling System for Scenario Simulations in the Elbow River Watershed, Alberta, Canada. *Environmental Management* 53(2): 357-381.

Xu C Y (1999) From GCMs to river flow: a review of downscaling methods and hydrologic modelling approaches. *Progress in Physical Geography* 23(2): 229-249.

Appendix 1. Evapotranspiration models

Priestley-Taylor model

The Priestley-Taylor model is a shortened version and modification of the Penman's theoretical equation (Priestley and Taylor 1972). This model is a physically-based model that can be used as a reference model to evaluate the quality of the empirical ET models (Weib and Menzel, 2008). The model has been used and validated by Alberta Agriculture and Food for the Elbow River watershed. It estimates ET using air temperature and solar radiation data (Priestley and Taylor 1972, Jensen et al. 1990, McAneney and Itier 1996). The following Priestley-Taylor equation was developed by Jensen et al. (1990):

$$ET = \alpha \frac{\Delta}{\Delta + \gamma}(R_n - G)$$

where ET is the rate of evapotranspiration (mm day^{-1}), R_n is net radiation (MJ m^{-2} day^{-1}), Δ is the slope of the saturation vapor pressure-temperature curve (Pa K^{-1}), G is soil heat flux (MJ $m^{-2}day^{-1}$), γ is the psychrometric constant (kPa $°C^{-1}$), and α is a coefficient, 1.26. This value (1.26) of α is suitable for the most climate regimes (McAneney and Itier 1996), but it could be modified for different wind and humidity climates.

Hargreaves-Samani model

Hargreaves-Samani (1985) introduced an evapotranspiration model that is based on air temperature data. The model is as follow:

$$ET = \alpha\,(T_m + 17.8)\,(\sqrt{T_{max} - T_{min}})\,R_a$$

where α is an empirical coefficient (0.0023 is the original coefficient suggested by Hargreaves and Samani 1985). T_m (°C) is the mean air temperature, calculated by averaging T_{max} and T_{min}. Ra is the extraterrestrial radiation [mm day^{-1}], that can be calculated for a specific location and time. Mathematical formulas for calculating extraterrestrial radiation are as follows:

$$R_a = \frac{1}{\pi} E_o\, d_r\, [\omega_s \sin(\varphi)\sin(\delta) + \cos(\varphi)\cos(\delta)\sin(\omega_s)]$$

$$d_r = 1 + 0.033\cos\left(\frac{2\pi}{365} DOY\right)$$

$$\delta = 0.409\sin\left(\frac{2\pi}{365} DOY - 1.39\right)$$

$$Radians = \frac{\pi}{180}[decimal\ degrees]$$

$$\omega_s = arccos\,[-\tan(\varphi)\tan(\delta)]$$

where R_a is the extraterrestrial radiation, [Wm^{-2}], E_o is solar constant, 1353 Wm^{-2} [1], dr is the inverse relative distance between earth and sun, δ is the solar declination angle

[radians], φ is the latitude [radians], ωs is the sunset hour angle [radians], and DOY is the number of the day in the year.

Thornthwaite model

Thornthwaite (1948) developed a model that calculates ET based on the air temperature and day length. The Thornthwaite equation is as follow:

$$E = 16\,(N/360)(10T_a/I)^t$$

where N is the number of days in the month, and T_a (°C) is the average daily temperature. I and t could be calculated as follows:

$$I = \sum_{1}^{12} \left(\frac{T_m}{5}\right)^{1.514}$$

$$\text{and } t = (6.7510^{-7})I^3 - (7.71 * 10^{-5})I^2 + (1.79*10^{-2})I + 0.49$$

where T_m (°C) is the monthly average temperature.

Blaney and Criddle model

Blaney and Criddle (1950) proposed a simple method that uses air temperature data for estimating ET:

$$ET = P\ (0.46\ T_{mean} + 8)$$

where T_{mean} is the mean temperature and P is the mean daily percentage of annual daytime hours. This model is simple due to using only air temperature for estimating ET.

Appendix 2. Calibration/validation of MIKE SHE/MIKE 11 using Ln NSE

Calibration/validation of MIKE SHE/MIKE 11 using daily and monthly (streamflow) values of Ln NSE. J004, J006, J009, and J010 correspond to the 05BJ004, 05BJ006, 05BJ009, and 05BJ010 hydrometric stations, respectively.

	Calibration/validation period	Ln NSE (daily)				Ln NSE (monthly)			
		J009	J006	J004	J010	J009	J006	J004	J010
Calibration	Sep. 1981 to Dec. 1991	0.62	0.80	0.73	0.53	0.70	0.86	0.78	0.77
Validation	Sep. 1991 to Dec. 1995	0.42	0.71	0.76	0.87	0.49	0.78	0.89	0.91
	Sep. 1995 to Dec. 2000	N/A	N/A	0.74	0.79	N/A	N/A	0.83	0.93
	Sep. 2000 to Dec. 2005	N/A	N/A	0.73	0.69	N/A	N/A	0.81	0.90
	Sep. 2005 to Dec. 2008	N/A	N/A	0.68	0.65	N/A	N/A	0.72	0.70

Appendix 3. Calibration/validation of MIKE SHE/MIKE 11 using rel NSE

Calibration/validation of MIKE SHE/MIKE 11 using daily and monthly (streamflow) values of relative NSE. J004, J006, J009, and J010 correspond to the 05BJ004, 05BJ006, 05BJ009, and 05BJ010 hydrometric stations, respectively.

	Calibration/validation period	rel NSE (daily)				rel NSE (monthly)			
		J009	J006	J004	J010	J009	J006	J004	J010
Calibration	Sep. 1981 to Dec. 1991	0.84	0.89	0.82	0.85	0.83	0.90	0.82	0.88
Validation	Sep. 1991 to Dec. 1995	0.62	0.78	0.92	0.96	0.68	0.79	0.88	0.95
	Sep. 1995 to Dec. 2000	N/A	N/A	0.89	0.92	N/A	N/A	0.83	0.91
	Sep. 2000 to Dec. 2005	N/A	N/A	0.87	0.91	N/A	N/A	0.81	0.93
	Sep. 2005 to Dec. 2008	N/A	N/A	0.79	0.89	N/A	N/A	0.74	0.78

Appendix 4. Population projection

Population projection (Alberta Treasury Board and Finance)

Year	Population (lower growth scenario)	Population (high growth scenario)
1996	904,049	904,049
1997	934,326	934,326
1998	968,502	968,502
1999	995,780	995,780
2000	1,021,989	1,021,989
2001	1,049,059	1,049,059
2002	1,081,450	1,081,450
2003	1,105,613	1,105,613
2004	1,131,524	1,131,524
2005	1,169,252	1,169,252
2006	1,208,763	1,208,763
2007	1,242,201	1,242,201
2008	1,277,147	1,277,147
2009	1,313,916	1,313,916
2010	1,338,030	1,338,030
2011	1,363,607	1,363,607
2012	1,409,076	1,409,076
2013	1,468,701	1,468,701
2014	1,508,750	1,530,845
2015	1,545,250	1,587,925
2016	1,576,940	1,640,215
2017	1,606,595	1,690,565
2018	1,634,450	1,739,960
2019	1,660,520	1,786,860
2020	1,685,890	1,833,505
2021	1,711,095	1,881,570

2022	1,735,885	1,929,735
2023	1,760,205	1,977,945
2024	1,784,540	2,027,035
2025	1,807,595	2,074,190
2026	1,830,345	2,121,700
2027	1,852,585	2,169,160
2028	1,874,545	2,216,945
2029	1,896,050	2,264,760
2030	1,917,300	2,312,860
2031	1,938,085	2,360,980
2032	1,958,460	2,409,145
2033	1,978,485	2,457,585
2034	1,998,240	2,506,405
2035	2,017,830	2,555,720
2036	2,036,945	2,605,185
2037	2,055,805	2,655,140
2038	2,074,235	2,705,240
2039	2,092,335	2,755,800
2040	2,110,085	2,806,595
2041	2,127,600	2,857,830

Appendix 5. Changes in average annual and seasonal temperature and precipitation

	Scenario (2020s)					Scenario (2050s)				
	A1FI	A1B	A2a	B2b	B23	A1FI	A1B	A2a	B2b	B23
Annual Temp.	0.4	0.7	0.9	1.2	1.5	4.12	2.2	1.9	2.4	2.32
Annual Prec.	-4.7	1.2	2.8	1.0	-0.4	0.0	11.1	3.8	3.0	-2.2
	Temperature (°C)									
J	-1.4	1.9	-1.1	0.5	3.4	3.6	4.2	-0.3	2.0	4.2
F	-0.6	0.3	0.6	1.5	2.3	4.4	1.1	0.9	2.5	3.8
M	0.4	0.2	0.8	0.4	2.4	4.5	1.5	0.7	1.5	3.1
A	1.5	0.0	0.3	0.9	1.5	5.2	1.8	1.1	1.7	2.7
M	1.0	1.2	0.6	0.6	1.8	2.9	1.9	2.3	1.3	3.3
J	0.4	0.8	0.9	1.2	0.8	3.1	1.6	2.4	2.3	1.6
J	0.9	0.8	2.0	2.0	1.0	4.4	1.7	4.1	3.6	1.7
A	1.1	0.0	1.7	2.0	1.4	4.3	2.2	4.0	4.0	1.8
S	0.1	0.6	1.3	1.1	0.6	2.8	2.3	2.8	2.9	1.7
O	0.1	0.6	1.0	0.4	0.6	3.3	2.1	1.8	1.5	1.2
N	0.6	1.5	1.1	1.3	1.0	4.4	2.4	1.4	2.6	1.2
D	0.8	0.5	1.2	2.0	0.8	6.5	3.2	2.1	3.1	1.6
	Precipitation (%)									
J	-7.9	-2.3	18.9	13.3	0.0	10.9	1.3	27.8	16.6	-6.0
F	-6.4	4.0	-1.9	12.6	3.3	12.1	7.2	7.3	9.6	6.4
M	-1.7	3.9	16.3	1.5	-3.9	19.7	5.1	20.3	1.9	5.1
A	7.0	0.1	3.2	6.5	-3.3	19.0	5.7	7.1	18.6	1.2
M	-11.0	15.9	-0.1	7.7	4.3	-6.6	26.0	7.1	11.1	2.7
J	-18.5	-7.0	-1.9	-6.5	-3.6	-9.2	-1.6	-5.2	-10.3	-13.0
J	-0.9	-11.9	0.8	-20.6	-2.7	3.3	22.4	-9.9	-7.8	-9.6
A	1.4	8.4	1.1	-3.8	-0.6	-14.5	28.3	-9.0	-4.8	-2.5
S	-5.3	11.4	-12.6	-16.0	0.5	-10.4	-9.3	-7.2	-17.3	-4.7
O	-0.8	10.8	-0.6	6.3	-5.5	-9.8	20.9	-2.2	7.1	-7.8
N	2.7	-10.4	7.6	3.6	10.6	-2.0	11.5	17.5	15.7	20.2
D	-3.7	-3.1	25.1	23.9	2.4	9.9	9.5	31.9	28.7	1.2